UNIVERSITI TEKNOLOGI MARA

PHYSICO-MECHANICAL PROPERTIES AND REACTION KINETICS OF H_2CO_3 INCORPORATED CEMENTITIOUS BINDERS VIA AQUEOUS CARBON DIOXIDE CO_2 INTEGRATION

ZULHAZIQ KHAN BIN ZULJAR

MSc

July 2026

UNIVERSITI TEKNOLOGI MARA

PHYSICO-MECHANICAL PROPERTIES AND REACTION KINETICS OF H_2CO_3 INCORPORATED CEMENTITIOUS BINDERS VIA AQUEOUS CARBON DIOXIDE CO_2 INTEGRATION

ZULHAZIQ KHAN BIN ZULJAR

Thesis submitted in fulfillment
of the requirements for the degree of
Master of Science
(Civil Engineering)

Faculty of Civil Engineering

July 2026

CONFIRMATION BY PANEL OF EXAMINERS

I certify that a Panel of Examiners has met on 11 March 2026 to conduct the final examination of Zulhaziq Khan Bin Zuljar in his Master of Science thesis entitled "Physico-Mechanical Properties and Reaction Kinetics of H_2CO_3 Incorporated Cementitious Binders Via Aqueous CO_2 Integration" in accordance with Universiti Teknologi MARA Act 1976 (Akta 173). The Panel of Examiner recommends that the student be awarded the relevant degree. The Panel of Examiners was as follows:

Mohd Khairul Kamarudin, PhD
Assoc Professor
Faculty of Civil Engineering
Universiti Teknologi MARA
(Chairman)

Mohd Raizamzamani Bin Md Zain, PhD
Senior Lecturer
Faculty of Civil Engineering
Universiti Teknologi MARA
(Internal Examiner)

Meor Ahmad Faris Meor Ahmad Tajudin, PhD
Senior Lecturer
Faculty of Mechanical Engineering
Universiti Malaysia Perlis
(External Examiner)

PROF DR HJH ZURAEDA IBRAHIM
Dean
Institute of Postgraduate Studies
Universiti Teknologi MARA
Date: 27 July 2026

AUTHOR'S DECLARATION

I declare that the work in this thesis was carried out in accordance with the regulations of Universiti Teknologi MARA. It is original and is the results of my own work, unless otherwise indicated or acknowledged as referenced work. This thesis has not been submitted to any other academic institution or non-academic institution for any degree or qualification.

I, hereby, acknowledge that I have been supplied with the Academic Rules and Regulations for Postgraduate, Universiti Teknologi MARA, regulating the conduct of my study and research.

Name of Student	:	Zulhaziq Khan Bin Zuljar
Student I.D. No.	:	2023589797
Programme	:	Master of Science (Civil Engineering) – CEEC750
Faculty	:	Civil Engineering
Thesis Title	:	Physico-Mechanical Properties and Reaction Kinetics of H2CO3 Incorporated Cementitious Binders Via Aqueous Carbon Dioxide CO2 Integration
Signature of Student	:	
Date	:	July 2026

ABSTRACT

This study addresses the need to reduce the carbon footprint of cement while maintaining structural performance by evaluating an early carbon dioxide treatment pathway in ordinary Portland cement (OPC) paste. Conventional hydration alone does not utilise CO_2, and unoptimised carbonate incorporation can either retard setting excessively or fail to improve strength. The novelty of this work is the systematic integration of carbonic-acid-rich mixing water with calcium-bearing carbonate precursors to identify a practical parameter window for aqueous CO_2 incorporation under ambient curing. Unlike studies that focus mainly on chamber-based carbonation curing, this study evaluates the mixing-water route by linking batching pH, precursor type, precursor replacement level, setting behaviour, compressive strength, water absorption and hydration-carbonation indicators within the same OPC paste system. The objectives of the study were to evaluate the effect of aqueous CO_2-conditioned mixing water on early batching behaviour, determine the influence of $CaCO_3$ and $CaMg(CO_3)_2$ replacement on the physico-mechanical performance of OPC paste, and relate the observed behaviour to chemical, thermal and microstructural evidence. The reference binder consisted of 100% OPC, while modified binders were prepared by partially replacing OPC with calcium carbonate ($CaCO_3$) or dolomite, $CaMg(CO_3)_2$, by binder mass. Carbonic-acid-rich solutions were used as mixing water within selected pH bands, with pH 3.5 to 4.0 representing the principal low-pH aqueous CO_2 batching condition. Setting behaviour was measured using the Vicat method, while compressive strength was determined on 50 mm cube specimens in accordance with ASTM C109/C109M at selected curing ages under ambient curing. Water absorption, XRF, SEM-EDX, XRD and TGA were used to support the interpretation of physical performance, chemical composition, microstructure, and carbonate-related reaction behaviour. The results showed that aqueous CO_2-conditioned mixing water influenced both setting behaviour and strength development. $CaCO_3$-bearing systems showed a dosage- and age-dependent response, where moderate replacement improved early-age strength, while higher replacement influenced later-age densification within the tested range. This indicates that $CaCO_3$ should be interpreted through a performance window rather than as a single universal optimum. $CaMg(CO_3)_2$ showed a narrower beneficial range, with higher replacement levels reducing strength due to dilution and weaker paste continuity. Thermal and microstructural observations supported the presence of carbonate-related reactions and matrix densification, although greater carbonate formation did not automatically produce higher compressive strength because strength also depends on hydrate continuity, pore refinement, particle distribution and matrix compactness. The findings indicate that aqueous CO_2 integration can modify OPC paste performance when mixing-water pH and carbonate precursor dosage are controlled. However, the study is limited to cement paste rather than mortar or concrete, short-term mechanical evaluation and selected microstructural characterisation. Direct CO_2 uptake, long-term durability, broader statistical replication and scale-up validation are recommended for future work before the method is treated as a verified carbon-reduction technology.

ACKNOWLEDGEMENT

In the name of Allah, the Most Gracious and the Most Merciful

First and foremost, all praise to Allah SWT for granting me the strength, health, and perseverance to complete this thesis. I would like to express my deepest appreciation and sincere gratitude to Dr. Warid Wazien Ahmad Zailani for his invaluable guidance, patience, and encouragement throughout this research. His clear direction, constructive criticism, and meticulous review of both technical and non-technical aspects were instrumental in shaping the quality of this work. I also extend heartfelt thanks to Dr. Nazirah binti Mohd Apandi for her thoughtful input, timely advice, and continuous support, which strengthened the experimental design and the clarity of my writing.

My deepest gratitude goes to my parents, Zuljar bin Jaafar and [redacted] for their prayers, patience, sacrifices, guidance, and unwavering emotional and financial support from the first day of this journey. This period has been a challenging phase of my life, and I am truly fortunate to have their understanding and love. To my wife, Tuan Ruzainie, thank you for your patience, encouragement, and motivation during long days of experiments and writing; your support has been a constant source of strength.

I am grateful to the Faculty of Civil Engineering, Universiti Teknologi MARA (UiTM), for providing an enabling academic environment and access to laboratory facilities. My appreciation goes to the technical staff of the Concrete and Materials Laboratory and the analytical units for Thermogravimetric Analysis (TGA) and Scanning Electron Microscopy (SEM) for their assistance with specimen preparation, instrument scheduling, and laboratory safety. Their professionalism helped ensure consistent procedures and reliable data acquisition throughout the study.

I would also like to thank my colleagues and friends in the research team; Najmudin Helmi, Khairul Nazhan, and Alia Sofea, for their companionship, feedback, and practical help during testing and drafting. The discussions we shared, whether formal or informal, often clarified ideas and improved the presentation of results. I am likewise grateful to friends and peers who contributed indirectly through moral support, shared resources, or helpful suggestions; your kindness is sincerely appreciated.

Finally, I am thankful for the institutional support that facilitated access to facilities and materials during this project. Any remaining errors are entirely my own, and I welcome constructive correction. This thesis is dedicated to everyone who contributed time, expertise, and goodwill to the journey from the first idea to the final page.

TABLE OF CONTENTS

		Page
CONFIRMATION BY PANEL OF EXAMINERS		**ii**
AUTHOR'S DECLARATION		**iii**
ABSTRACT		**iv**
ACKNOWLEDGEMENT		**v**
TABLE OF CONTENTS		**vi**
LIST OF TABLES		**x**
LIST OF FIGURES		**xii**
LIST OF ABBREVIATIONS		**xvii**
LIST OF NOMENCLATURE		**xviii**
CHAPTER 1 INTRODUCTION		**1**
1.1	Research Background	1
1.2	Problem Statement	4
	1.2.1 General Problem	4
	1.2.2 Specific Problem	5
1.3	Objectives of Study	6
1.4	Significance of Study	7
	1.4.1 Technical Contribution	8
	1.4.2 Materials Insight	8
	1.4.3 Practical Relevance	8
1.5	Scope of Works	8
1.6	Limitations of Study	9
1.7	Thesis Layout	10
CHAPTER 2 LITERATURE REVIEW		**11**
2.1	Introduction	11

2.2 Trend Analysis on CO_2 Sequestered Cement 12
2.2.1 Search String Utilized 12
2.2.2 Bibliometric Analysis 14
2.3 CO_2 Utilisation Methods & Mechanism in Cementitious Systems 17
2.3.1 Mineral Carbonation 18
2.3.2 Applications of Carbonated Solids 33
2.3.3 Accelerated Carbonation Curing (ACC) 38
2.3.4 CO_2 as Supersaturated Aqueous Solutions 46
2.3.5 Carbonation Curing 52
2.4 CO_2 Carbonated Cured Concrete 57
2.4.1 Compressive Strength of Carbonated Cured Concrete Specimen 57
2.4.2 Densification of Carbonated Cured Concrete Specimen 59
2.5 Mechanical Alteration of Calcium Precursor Integration 60
2.6 Carbonated Concrete Parameter Analysis 62
2.7 Concluding Remarks 64

CHAPTER 3 RESEARCH METHODOLOGY 66
3.1 Introduction 66
3.2 Research Framework 67
3.3 Raw Materials 68
3.3.1 OPC 69
3.3.2 $CaMg(CO_3)_2$ & $CaCO_3$ Powder 69
3.4 Preparation of Aqueous H_2CO_3 Solution 70
3.4.1 Atomization Rig, Sensors, and Operating set-points 70
3.4.2 pH Calibration and Short-Term Stability 72
3.4.3 Mix Design and Batching Protocol 74
3.5 Specimen Preparation and Curing 75
3.6 Test Methods 76
3.6.1 Setting Time Test 77

3.6.2 Compressive Strength 78

3.6.3 Water Absorption 79

3.6.4 Microstructure Overview 81

3.6.5 Chemical Composition 82

3.6.6 Phase Analysis 84

3.6.7 Thermal Properties 85

CHAPTER 4 RESULTS AND DISCUSSION 87

4.1 Batching pH and Early-Age Behaviour 87

4.2 Setting Behaviour of of H_2CO_3 Mixed OPC Paste with Carbonate Precursor Replacement 90

4.3 Compressive Strength 92

4.3.1 Effect of CO_2 Conditioned Batching pH on Compressive Strength 93

4.3.2 $CaCO_3$ Bearing Systems Under Aqueous CO_2 Solution 95

4.3.3 Compressive Strength Response of $CaCO_3$ Bearing Systems under the Aqueous CO_2 Solution 97

4.4 Water Absorption 99

4.5 Bulk Chemical Composition by XRF 101

4.6 Microstructural and Elemental Characterisation 103

4.6.1 SEM Microstructure 103

4.6.2 EDX Elemental Composition 106

4.6.3 SEM-EDX Synthesis 109

4.7 Thermogravimetric Analysis (TGA) 110

4.8 Correlation of Degree of Reaction with Physico-Mechanical Performance 113

CHAPTER 5 CONCLUSIONS 117

5.1 Summary of Study 117

5.2 Limitations 119

5.3 Recommendations for Future Works 121

REFERENCES **123**

AUTHOR'S PROFILE **142**

LIST OF TABLES

Tables	Title	Page
Table 1.1	Previous Research on The Implications of Global CO2 Emissions	5
Table 2.1	Variation of Cementitous Materials Integrated Into CO_2 Fused Concrete and Findings	23
Table 2.2	Applications of Carbonated Solids in Cementitious Systems	33
Table 2.3	Compact Ranges & Efect of $CaCO_3$ Family Additives in OPC	37
Table 2.4	Reported Operating Ranges for Supersaturated CO_2 Mixing Water (0 to 3 Evidence Rubric)	50
Table 2.5	Compiled Research on the CO_2 Concrete Testing Parameters	54
Table 2.6	Chemical Composition of Dolomite and Limestone (wt/%)	62
Table 3.1	Experimental Design Summary	66
Table 3.2	Chemical Composition and Particle-Related Information of Raw Materials	70
Table 3.3	Mix-Design Matrix for OPC Pastes with Aqueous H_2CO_3 Mixed with $CaCO_3$ & $CaMg(CO_3)_2$	74
Table 3.4	Methods and Durations of Compressive Strength Testing From Other Research	76
Table 4.1	pH Evolution (0 to 8 min) of Aqueous CO_2 Solution Under Combined CO_2 Gas Flow (5, 10, 15 L/min) and Water Flow (10, 15, 20 L/h) Operating Conditions	89
Table 4.2	Setting Times Measured Through Vicat Testing	92
Table 4.3	Compressive Strength by Mixing-Water pH Band (ASTM C109; 50 mm Cubes)	93

Table 4.4 Average Compressive Strength of $CaMg(CO_3)_2$ by Age of Curing 98

Table 4.5 Final Specimen Mass After 14-day Water Immersion for OPC Paste Prepared with Selected Aqueous CO_2 Mixing-Water pH Ranges 100

Table 4.6 Bulk Oxide Composition (wt%) of Selected Binders and $CaMg(CO_3)_2$ Precursor by XRF (SiO_2, Al_2O_3, Fe_2O_3, CaO, MgO, SO_3, Na_2O, K_2O, TiO_2, and LOI) 102

Table 4.7 EDX Elemental Composition (wt%) of Selected Area Analyses of Selected Samples 107

Table 4.8 Summary of TG Residual Mass and Mass-Loss Partition by Temperature Windows 112

LIST OF FIGURES

Figures	Title	Page
Figure 2.1	Direct CO Intensity of Cement Production and The NZE Pathway to 2030 IEA (2024).	12
Figure 2.2	Workflow for The Systematic literature review (SLR)	13
Figure 2.3	Overview of Publications on CO2-Cement (Scopus, 1981–2023): (a) The Annual Trend, (b) Countries with The Largest Number of Publications, and (c) Network Map Showing The Co-Authorship Between Countries	15
Figure 2.4	Overview of Keywords in Publication Related to Topic of Interest: (a) Pie Chart Depicting Frequently Appeared Keywords, and (b) Network Map Showing The Keywords Co-Occurrence	16
Figure 2.5	Proposed Methods of Carbonation Curing in Cementitious Materials (Amended from Lim et al. (2019))	18
Figure 2.6	Classification of Mineral Carbonation Routes (Amended from Ahmed et al. (2024))	19
Figure 2.7	Direct Aqueous Carbonation Process Routes (Amended from (Jaschik et al., 2014))	22
Figure 2.8	Reported CO_2 Uptake for Selected Alkaline Feedstocks Under Gas–Solid Direct Carbonation (wt% of Feedstock).	25
Figure 2.9	Stages in Direct Aqueous Carbonation of Ca-Bearing Solids: Ca/Mg Mobilisation, Carbonate Speciation In Solution, and $Caco_3$ Or $Mgco_3$ Precipitation (Amended from Li and Wu (2022))	27
Figure 2.10	Indirect Mineral Carbonation Concept (Amended from Azdarpour et al. (2015))	28

Figure 2.11 Indirect Aqueous Carbonation Process Routes (Amended from Jaschik et al. (2014)) 31

Figure 2.12 SEM images of CRA from Steel Slag: (a) Uncarbonated and (b) Carbonated (Adopted from Mo et al. (2020)) 35

Figure 2.13 Reported 24-hour Water-Absorption Reductions for Carbonated RCA Relative to Untreated RCA 36

Figure 2.14 Carbonation Reaction System: (a) Flow-Through Reactor and (b) Enclosed Reactor (Adopted from Liu And Meng (2021)) 40

Figure 2.15 Early-Age Carbonation Mass Gain and CO_2 Uptake on Cement Mortar Sample: (a) OPC and (b) PLC (Adopted from Zhang et al. (2020)) 41

Figure 2.16 Early Age ACC Mechanism Schematic (Adopted from Bertos et al. (2004) with Minor Modification) 42

Figure 2.17 Early-Age Carbonation Compressive Strength in Mega Pascal (MPa) on Cement Mortar Sample: (a) OPC and (b) PLC (Adopted from Xian, Logan, et al. (2022)) 44

Figure 2.18 SEM Images of Carbonated Cement Suspensions with CO_2 Injection of (a) 2000 scc and (b) 4000 scc, Showing Progressive $CaCO_3$ Crystal Deposition and Pore Refinement (Adapted from Fu et al. (2024)) 45

Figure 2.19 Experimental setup for CO_2-Supersaturated Aqueous Solution Preparation (Adapted and Amended from Ferrara et al. (2024) with Minor Modifications) 48

Figure 2.20 CO_2 Uptake Versus Carbonation Time Under Aqueous Mineralisation (Adapted and Amended from Ferrara et al. (2024) 49

Figure 2.21 Relationship Between CO_2 Uptake And 28-Day Compressive Strength Change Relative to The Non-Carbonated Reference (Adapted from Davolio et al. (2025)) 51

Figure 2.22	Effect of Fly Ash (FA) Dosage and Curing Age on (a) Flexural Strength, and b) Compressive Strength, and the Reduction Rate for CO_2-Cured Alkali-Activated Binder Specimens (Sourced from Peng et al. (2022))	58
Figure 2.23	Example Of Pore-Size Class Redistribution with Extended Carbonation Duration, Illustrating Refinement of The Pore Structure (Adapted from Ye et al., 2025)	59
Figure 2.24	Backscattered Electron (BSE) Micrographs Comparing OPC Paste and PLC Paste, Highlighting The Spatial Distribution of Limestone Particles (Yellow Shade) within the Hydrated Matrix (Adapted from Tennis et al. (2024))	61
Figure 3.1	Experimental Framework and Data Streams	68
Figure 3.2	Grade 30 OPC Supply Obtained from Tasek Corporation Berhad	69
Figure 3.3	Schematic of Gas–Liquid Atomization Rig for H2CO3 Preparation	71
Figure 3.4	Bench-top assembly of the H_2CO_3 preparation rig according to Schematics	72
Figure 3.5	pH Measurement of CO_2-Water Using a Hach sensION-378	73
Figure 3.6	Casted Cement Pastes in 50mm Plastic Cube Moulds	75
Figure 3.7	Vicat Apparatus for Setting Time Evaluation	77
Figure 3.8	Hardened CO_2 Cured Cement Samples	78
Figure 3.9	(a) UTM for Compressive Testing, (b) Samples in Between UTM Plates	79
Figure 3.10	JEOL JSM-6460LA Modelled SEM Machine for Microstructure Analysis	81
Figure 3.11	Sample Fragments for Sputtered Coating and SEM Imaging	82

Figure 3.12 JEOL JFC-600 Auto Fine Coater for Conductive Sputter Coating Prior to SEM Imaging 82

Figure 3.13 (a) XRF Analyzer Machine for Chemical Composition Analysis and (b) The Mechanical Components 83

Figure 3.14 Rigaku Ultima IV Diffractometer XRD Pattern Characterization Machine 84

Figure 3.15 Perkin Elmer Pyris 1 TGA Instrument 85

Figure 4.1 Conceptual Screened Batching pH Windows and Expected Early-Age Chemical State 87

Figure 4.2 pH vs Time (Min) Analysis with Variation of CO_2 Gas Flow (10, 15, and 20 L/Min) and Flowrate of Aqueous CO_2 Solution During Mixing (5, 10, and 15 L/h) 88

Figure 4.3 Initial and Final Setting Time of H3CO3-Mixed OPC Paste Containing CaCO3 Replacement 91

Figure 4.4 Compressive Strength vs. Mixing-Water pH Band Under Liquid-Phase CO_2 Batching 94

Figure 4.5 Compressive Strength vs CaCO3 Content at 3, 7 and 28 Days with Addition of H_2CO_3 96

Figure 4.6 Compressive Strength vs $CaMg(CO_3)_2$ Content at 3, 7, 14 and 28 Days with Addition of H_2CO_3 97

Figure 4.7 Post-Immersion Mass Response of OPC Paste After 14-Day Water Exposure for Selected Aqueous CO_2 Mixing-Water pH Ranges 99

Figure 4.8 XRF Spectra of Selected Binders and Carbonate Precursor, Presented as Separate Panels with Labelled Major Elemental Peaks (Ca, Si, Al, Mg, Fe, S, K) 102

Figure 4.9 SEM Micrographs of Samples: (a) Cement + Water (Control), (b) $CaMg(CO_3)_2$ Powder, H_2CO_3 + $CaCO_3$ Mixed Samples; (c)

M6A, and H_2CO_3 + $CaMg(CO_3)_2$ Samples; (d) M10A, (e) M12C and (f) M15B at 7 Days 104

Figure 4.10 EDX Spectra of Selected Samples at 7 Days, Measured from the Selected Area of Each Specimen, Highlighting Relative Changes in Ca, Si, Al, Mg and C/O Related Signals 106

Figure 4.11 TG Curves of OPC Paste and OPC Mixed CaCO3 Pastes Prepared Under Different Mixing-Water pH Conditions 110

Figure 4.12 TG Mass-Loss Partition by Temperature Window for Selected Mixes (Control and Representative $CaCO_3$ Pastes) to Distinguish Dehydration-Dominated Loss (<600 °C) from Carbonate Decomposition (600 To 1000 °C) 114

Figure 4.13 Compressive Strength Versus Carbonate-Related TG Loss (600 to 1000°C) 115

LIST OF ABBREVIATIONS

Abbreviations

ACC	Accelerated Carbon Curing
BSE	Backscattered Electron
CCUS	Carbon Capture, Utilization and Storage
CRA	Carbonated Recycled Aggregate
DTG	Derivative Thermogravimetry
EDX / EDS	Energy-Dispersive X-ray
ITZ	Interfacial Transition Zone
NZE	Net Zero Emissions
OPC	Ordinary Portland Cement
PCC	Precipitated Calcium Carbonate
PLC	Portland Limestone Cement
RCA	Recycled Concrete Aggregate
ROI	Region of Interest
SEM	Scanning Electron Microscope
SLR	Systematic Literature Review
SOP	Standard Operating Procedure
TGA	Thermogravimetric Analysis
UTM	Universal Testing Machine
XRD	X-ray Diffraction
XRF	X-ray Fluorescence

LIST OF NOMENCLATURE

Nomenclatures

Ca	Calcium
CaCO3	Calcium Carbonate
CaO	Calcium Oxide
CO_2	Carbon Dioxide
CO_3^{2-} / CO_3	Carbonate Ion
$CaMg(CO_3)_2$	Dolomite
CH	Portlandite
C-S-H	Calcium-Silicate-Hydrate Gel
H_2O	Water
H_2CO_3	Carbonic Acid
Mg	Magnesium
MgO	Magnesium Oxide
OH^- / OH	Hydroxide
pH	Acidic or alkalinity of solvent
MPa	Megapascal
kN	Kilonewton
SD	Standard Deviation
µm	Micrometre
nm	Nanometre
mm	Millimetre
wt%	Weight Percent

CHAPTER 1
INTRODUCTION

1.1 Research Background

Ordinary Portland cement (OPC) is indispensable to modern infrastructure yet remains one of the most carbon-intensive manufactured materials because carbon dioxide (CO_2) is released both from fuel combustion in clinker production and from limestone calcination during the clinkering reaction (Andrew, 2018; IEA, 2024). Best-available global inventories attribute approximately 1.50 ± 0.12 gigatonnes of CO_2 in 2018 to cement process emissions alone, equal to roughly 4% of fossil-fuel CO_2. Sector tracking further indicates that overall emissions from cement today remain higher than in 2015, while the direct CO_2 intensity of cement production has been broadly flat in recent years and even increased slightly in 2022, a trajectory inconsistent with the rapid intensity declines required for a net-zero pathway (IEA, 2024). These trends crystallise a hard-to-abate challenge in cement research: proposed mitigation routes must be technically measurable, reproducible and capable of maintaining mechanical performance. Alongside clinker substitution and alternative fuels, carbon capture, utilisation and storage (CCUS) and CO2 utilisation in cementitious materials have emerged as complementary strategies. However, climate outcomes depend on CO2 source and purity, capture or delivery energy, binder replacement level and durability performance, which means aqueous CO2 integration should be treated as a material-level utilisation route rather than a complete life-cycle carbon-reduction solution (Huang et al., 2019; Ravikumar et al., 2021).

Two mechanistically distinct early-age pathways are relevant to this study. The first is accelerated carbonation curing (ACC), where fresh or demoulded cementitious products are exposed to controlled CO_2 concentration, relative humidity and curing duration. Well-controlled ACC can promote carbonate formation, improve selected early-age properties and refine pore structure, but it usually requires a carbonation chamber or controlled curing environment (Liang et al., 2024; Pacheco-Torgal et al., 2018; Xia et al., 2025). The second pathway introduces CO_2 through the mixing water as an H_2CO_3-rich solution, shifting the process from gas-solid transport to aqueous chemistry during batching. Since the present work focuses on this mixing-water route,

the key variables are the pH of the mixing liquid, CO_2 charging condition, exposure duration, water-to-binder ratio, precursor type and precursor replacement level.

In the aqueous route, the pH of the H_2CO_3 solution is controlled by the gas-liquid contact condition, CO_2 exposure duration and short-term stability of dissolved CO_2 before batching. Longer exposure or stronger CO_2 charging conditions can lower the solution pH until the system approaches a practical equilibrium range. Once the solution is mixed with OPC, the initial acidic condition interacts rapidly with alkaline cement phases, releasing calcium ions and encouraging carbonate-related precipitation during the early hydration period. Therefore, pH is used in this study as a practical batching control parameter to represent the condition of the CO_2-conditioned mixing water.

Within the early-age carbon dioxide strategies outlined above, calcium-rich mineral precursors strongly condition early hydration–carbonation because they supply nucleation surfaces, alter particle packing, and participate in limited carbonate chemistry that together govern setting kinetics and later-age strength. Working with Portland systems, J. Zhang et al. (2024), showed that ultra-fine $CaCO_3$ powders accelerate early hydration and sustain strength when dosage and fineness are balanced, whereas coarser or high-replacement $CaCO_3$ introduces dilution that depresses later performance. Independent investigations confirm the same mechanism split: appropriately fine $CaCO_3$ acts as a filler–nucleant that refines porosity and advances hydration, while excess replacement tips the balance toward clinker dilution and slower late-age strength development (Campagiorni et al., 2025; Kang et al., 2024; Shao et al., 2024). High-volume studies further demonstrate that microstructural evolution hinges on the fineness–dosage window, with carboaluminate formation contributing to early strength in blends where sulphate and aluminate availability are tuned (Kim et al., 2024; Phan et al., 2025). For $CaMg(CO_3)_2$, recent work reports fineness- and content-dependent benefits: waste or calcined $CaMg(CO_3)_2$ powders can densify the matrix and raise mechanical properties when added at moderate levels, but gains diminish or reverse at higher replacement ratios (Akhil et al., 2024). For this reason, $CaCO_3$ and $CaMg(CO_3)_2$ were selected in this study to compare a calcium-carbonate precursor and a calcium-magnesium carbonate precursor under the same aqueous CO_2 mixing route, allowing their effects on setting behaviour, compressive strength, water absorption and hydration-carbonation indicators to be evaluated within a common OPC paste system.

The introduction of carbon dioxide as H2CO3 in the mixing water changes the pore solution before setting and therefore redirects hydration from the very start.

Lippiatt et al. (2019), showed that supersaturated aqueous CO_2 used as mixing water can increase dissolved calcium, generate fine calcium-carbonate nuclei and improve early-age performance when conditions are controlled. Other studies similarly indicate that CO_2-mixed systems are governed by rapid aqueous reactions and carbonate nucleation, so practical control rests on pH, water-to-binder ratio, mixing sequence and binder composition rather than gas-phase transport alone (Ferrara et al., 2024). In this setting, $CaCO_3$ and $CaMg(CO_3)_2$ may provide nucleation surfaces and limited buffering, but over-replacement can still reduce the amount of reactive OPC and weaken matrix continuity (Hu et al., 2024; J. Zhang et al., 2024). This shows that aqueous CO_2 integration requires a controlled parameter window rather than a general assumption that more carbonate addition will always improve performance.

Evaluating the effectiveness of low-pH aqueous CO_2 mixing requires both engineering performance data and supporting reaction evidence. Setting time and compressive strength provide the main indicators of fresh and hardened paste performance, while water absorption gives a short-term indication of physical response related to pore connectivity. Chemical, thermal and microstructural analyses are then used to support interpretation of whether the measured behaviour is associated with hydration-carbonation reactions, carbonate-related phases, filler packing or matrix densification. These tests do not provide a complete durability or life-cycle assessment, but they allow the early behaviour of the modified OPC paste system to be interpreted consistently (Phung et al., 2019; C. Wang et al., 2024).

Despite the growing interest in early-age CO_2 routes, the mixing-water pathway remains less specified than chamber-based accelerated carbonation curing. Reviews point out that many studies on CO_2 added during mixing report incomplete or inconsistent parameters, including the pH of the mixing liquid, CO_2 dissolution route, water-to-binder ratio, precursor fineness and dosage, and curing regime (Ahmed et al., 2024; Davolio et al., 2025). Lippiatt et al. (2019) reported strength gains when supersaturated aqueous CO_2 was used as mixing water, yet the test matrix did not fully define the combined effect of pH and carbonate precursor dosage for $CaCO_3$ or $CaMg(CO_3)_2$ under ambient curing. Guidance for $CaCO_3$ during ordinary hydration is well developed, but many studies still assess $CaCO_3$ without low-pH carbonic-acid mixing water. As a result, the buffering, nucleation and dilution roles of $CaCO_3$ and $CaMg(CO_3)_2$ under aqueous CO_2 conditions remain insufficiently quantified at paste scale (Hu et al., 2024; Xu et al., 2024).

There remains a practical need for parameterised guidance on the mixing-water route, where low-pH H2CO3 is paired with calcium-rich carbonate precursors under ambient curing. Previous studies have reported promising outcomes for aqueous CO_2 mixing, but comparison remains difficult because the pH of the mixing liquid, dissolution method, water-to-binder ratio, precursor type, replacement level and curing condition are not always reported consistently (Lippiatt & Ling, 2020; Lippiatt et al., 2019; Lippiatt et al., 2020). Sector analyses further underline the importance of solutions that preserve mechanical performance while being implementable on existing plants, which is consistent with an aqueous-CO2 approach grounded in standardised tests and clear reporting (IEA, 2024). This thesis responds by mapping a defensible window under ambient curing that links low pH in the mixing liquid and moderate fine $CaCO_3$ or $CaMg(CO_3)_2$ to Vicat setting and ASTM C109 compressive strength, with phase or thermal evidence to support interpretation; the next section states the problem, research questions and hypothesis that structure this evaluation.

1.2 Problem Statement

1.2.1 General Problem

The cement sector remains a major source of carbon dioxide. Direct CO_2 intensity of cement has been broadly flat in recent years and even rose slightly in 2022, while a sustained decline is required this decade to align with net-zero pathways (IEA, 2024). Multiple decarbonisation levers exist, including clinker reduction, alternative fuels, carbon capture and CO_2 utilisation. However, near-term adoption depends on options that preserve mechanical performance, are reproducible in laboratory and plant practice, and remain compatible with conventional batching and ambient curing conditions (GCCA, 2021; Yu, 2025). Within this context, early-age CO_2 strategies delivered through the mixing water are attractive because they avoid new curing chambers and may promote carbonate nucleation during early hydration when parameters are controlled (Lippiatt et al., 2019). Table 1.1 shows the previous research on the implications of global CO_2 emissions.

Table 1.1
Previous Research on The Implications of Global CO_2 Emissions

Indicator	Status	Implication	Source
Share of global CO_2 attributable to cement, including process and energy components	Approximately 7 to 8% of global CO_2	Confirms cement is a material decarbonisation priority	Friedlingstein et al. (2024)
Direct CO_2 intensity of cement	Broadly flat in recent years; slight rise in 2022	Sector off-track. Hence, look for plant-ready levers	IEA (2024)
Required annual intensity decline to align with NZE by 2030	Approximately 4% per year	Benchmark for urgency and scale	IEA (2021)
Industry near-term commitment	GCCA roadmap: −25% CO_2 by 2030 vs baseline	Aligns study with sector targets	GCCA (2021)
Implementation constraint from plants	Predominantly ambient curing and conventional batching	Favour mixing-water CO_2 (H_2CO_3) over chamber ACC	Yu (2025)

The current state shows that cement remains a priority material for decarbonisation, but the present study does not directly quantify net CO2 uptake or full life-cycle carbon reduction. Instead, the study addresses a narrower material-level problem: whether CO_2-conditioned mixing water can be incorporated into OPC paste while maintaining acceptable setting behaviour, compressive strength and physical performance. The potential contribution to CO2 reduction is therefore indirect and must be interpreted through the use of CO2 as a reactive input, the partial replacement of OPC with carbonate-based precursors and the possibility of developing a batching-compatible route. Direct carbon-balance measurement and life-cycle assessment remain necessary before the approach can be claimed as a verified carbon-reduction technology.

1.2.2 Specific Problem

Evidence for using carbon dioxide in the mixing water as H_2CO_3 is promising yet fragmented. Lippiatt et al. (2019) showed that supersaturated aqueous CO_2 used as mixing water can create fine carbonate nuclei and improve early-age performance when conditions are controlled. However, the preparation of H_2CO_3 mixing water is sensitive to CO_2 charging condition, exposure time, gas-liquid contact and the stability of the solution before batching. Therefore, the first specific problem is the need to clarify how

the preparation condition affects the pH behaviour of H_2CO_3 solution used for OPC paste mixing.

Independent studies report both gains and setbacks when CO_2-conditioned water and calcium-rich precursors are used in cementitious systems. This indicates sensitivity to pH at mixing, water-to-binder ratio, and the presence, fineness and dosage of calcium-rich precursors in ordinary Portland cement systems (Wang et al., 2025; Xia et al., 2025). The second specific problem is that the influence of $CaCO_3$ and $CaMg(CO_3)_2$ under low-pH H_2CO_3 mixing conditions is not yet sufficiently defined, especially in relation to setting time, compressive strength and water absorption. These precursors may contribute through filler action, nucleation and carbonate-related reactions, but excessive replacement may also reduce the amount of reactive OPC and weaken paste continuity. The third specific problem is that strength and setting results alone cannot explain the reaction behaviour of the modified paste system. Reviews note inconsistent reporting of key levers, including pH, CO_2 dissolution route, precursor fineness and dosage, and curing regime, which limits comparison across studies and slows transfer to practice (Suescum-Morales et al., 2022). Therefore, chemical composition, thermal response and microstructural evidence are required to support the interpretation of whether the measured physico-mechanical behaviour is associated with hydration-carbonation reactions, carbonate precipitation, pore refinement or dilution.

There is therefore no reproducible operating window that links low pH in the mixing liquid and moderate, fine $CaCO_3$ or $CaMg(CO_3)_2$ under ambient curing to standard performance outputs (Vicat initial/final set; ASTM C109 compressive strength at 3, 7 and 28 days) with phase/thermal evidence to support interpretation. Reported successes and failures suggest such a window exists, but it is not defined across pH bands, precursor type and fineness, dosage ranges, and water-to-binder ratio within one coherent dataset (Lippiatt et al., 2019; Suescum-Morales et al., 2022; Wang et al., 2025).

1.3 Objectives of Study

This study aims to investigate the integration of carbonic acid (H_2CO_3) and calcium-based precursors, specifically $CaMg(CO_3)_2$ and $CaCO_3$, as alternative binder components in OPC-based cementitious materials. The research focuses on the following objectives:

a) To characterise the effect of CO_2 exposure condition and exposure time on the pH behaviour of H_2CO_3 solutions at a controlled water temperature of 25 °C.
b) To evaluate the influence of H_2CO_3 solutions with varying pH levels used as mixing liquids on the physico-mechanical properties of OPC-based binders incorporating $CaCO_3$ and $CaMg(CO_3)_2$, based on compressive strength, water absorption and setting time.
c) To assess the hydration-carbonation reaction indicators using thermal analysis (TGA), chemical composition (XRF), phase analysis (XRD), and microstructural examination (SEM-EDX) for binders produced with H_2CO_3 and calcium-based precursors.
d) To correlate the hydration-carbonation reaction indicators with the physico-mechanical performance of the modified cementitious binders, in order to establish the relationship between aqueous CO_2 integration, precursor replacement and material behaviour.

1.4 Significance of Study

This study delivers parameterised guidance for using aqueous CO_2 (H_2CO_3) as the mixing liquid in OPC systems with $CaCO_3$ and $CaMg(CO_3)_2$ under ambient curing. The work defines a reproducible operating window by crossing pH bands with precursor type, fineness and dosage, and it reports results using standard tests so that plants and laboratories can repeat them. The study also provides a minimum reporting set for this route which are pH at mixing, dissolution method, precursor characteristics, water-to-binder ratio, curing conditions and test ages. Together, these outputs reduce ambiguity seen in prior aqueous-CO_2 studies and support practical transfer.

The parameter window proposed in this study is experimental rather than predictive. It is derived from the tested pH bands, precursor types, replacement levels, water-to-binder ratio and ambient curing conditions used in the laboratory programme. Therefore, the window should be interpreted as a paste-level guide for mixture evaluation and future optimisation, not as a universal design model for all OPC-based cementitious systems.

1.4.1 Technical Contribution

The study links pH at mixing, precursor variables and water-to-binder control to Vicat initial or final set and ASTM C109 compressive strength at 3, 7 and 28 days. It complements performance data with phase evidence from TGA and XRD, and microstructure or chemistry from SEM–EDS, hence, changes in setting and strength are traceable to underlying reactions. The protocol documents pH measurement at batching and the CO_2 dissolution route, addressing the reporting gaps common in aqueous-CO_2 studies.

1.4.2 Materials Insight

Testing $CaCO_3$ and dolomite side-by-side at moderate, fine fractions clarifies when these additions act as filler–nucleants that support early hydration, and when dilution or over-buffering slows setting or depresses later strength. Phase identification of portlandite consumption and carbonate polymorphs connects microstructural evolution to macroscopic properties, strengthening interpretation of early aqueous carbonation during mixing.

1.4.3 Practical Relevance

The route operates with conventional batching and ambient curing, so it fits existing plant constraints without chambers. Results are framed as plant-relevant parameters that may be monitored in future process development. pH at mixing, dissolution method, precursor type/fineness/dosage, water-to-binder ratio, curing conditions and test ages. Durability interpretation follows recognised carbonation-testing guidance to keep claims credible. This thesis delivers an experimental parameter map across pH, precursor dosage and ambient curing conditions, together with a reporting checklist to support replication. It does not claim field service-life durability, whole-life carbon outcomes or optimisation of chamber-based curing; these are outside the present scope and identified for future work.

1.5 Scope of Works

This study focuses on the laboratory-scale evaluation of OPC incorporating aqueous H_2CO_3 solution and calcium-based carbonate precursors. The binder system is

limited to OPC paste, with $CaCO_3$ and $CaMg(CO_3)_2$, used as partial binder replacement materials. The work does not cover mortar or concrete containing fine and coarse aggregates.

The experimental scope covers the preparation of aqueous H_2CO_3 solution through CO_2 integration into water, followed by pH screening of the mixing liquid from acidic to near-neutral conditions. The main pH bands considered in the study include pH 3.5 to 4.0, 4.0 to 4.5 and 4.5 to 5.0, with near-neutral water used as the control reference where applicable. The precursor replacement programme focuses on $CaCO_3$ and $CaMg(CO_3)_2$ replacement levels within the tested range to evaluate how precursor type and dosage affect the behaviour of the modified OPC paste. The measured properties are limited to setting time, compressive strength, water absorption and selected reaction indicators. Setting behaviour is evaluated using the Vicat method, while compressive strength is determined using 50 mm cube specimens based on the testing procedure adopted in this study. Water absorption is included as a short-term physical indicator related to moisture uptake and pore connectivity. Chemical, thermal and microstructural evidence is obtained using XRF, TGA, XRD and SEM-EDX to support the interpretation of hydration-carbonation behaviour. The scope of this study does not include flexural strength, tensile strength, elastic modulus, shrinkage, creep, chloride penetration, sulphate resistance, carbonation depth, direct CO_2 uptake measurement or full life-cycle assessment. These aspects are outside the present experimental programme and are recommended for future work. Therefore, the findings should be interpreted as a paste-level experimental parameter map for aqueous CO_2 integration rather than as a final design recommendation for structural concrete.

1.6 Limitations of Study

The work is limited to one OPC paste system and two calcium-rich precursors, namely $CaCO_3$ and $CaMg(CO_3)_2$. Hence, the findings apply to the paste mixes tested and should not be generalised to all binders, mortars or concretes without further validation. The aqueous CO_2 route was controlled through pH bands at 25 °C, with pH recorded at batching and after mixing. However, total inorganic carbon was not measured and continuous in-line pH logging was not used, which means small pH drifts during mixing may occur. A single dissolution method was adopted to reach the target

pH; therefore, alternative preparation routes may behave differently at the point of batching.

The mix design was explored in discrete steps for pH and precursor dosage, with the water-to-binder ratio held constant within each series. Therefore, the operating window is mapped within the tested ranges rather than optimised across the full design space. All specimens were cured under ambient laboratory conditions without controlled CO_2 or humidity exposure. Hence, the results do not represent chamber curing, external weathering or field-scale production. Mechanical performance focuses on Vicat setting, compressive strength of 50 mm paste cubes and water absorption. Flexural strength, tensile properties, modulus, shrinkage, creep and comprehensive durability indicators were not measured. Reaction interpretation was based on TGA, XRD, XRF and SEM-EDX, with known constraints such as TGA peak overlap, limited XRD sensitivity to amorphous C-S-H, XRF matrix effects and SEM field-of-view limitations. Access to specialised equipment for direct CO_2 uptake, total inorganic carbon measurement, continuous pH monitoring and advanced pore-structure analysis was also limited. Therefore, environmental benefits are not quantified in this study and should be verified through future carbon-balance, durability and scale-up investigations.

1.7 Thesis Layout

Chapter 1 introduces the topic, states the problem and objectives, explains the study's significance, and outlines the thesis. Chapter 2 reviews the literature on aqueous CO_2 used at mixing, on limestone and dolomite as calcium-rich precursors, and on the standard tests and characterisation methods relevant to this work. Chapter 3 describes the materials, mix designs and preparation of H_2CO_3 mixing liquids, the experimental procedures for setting and strength, and the TGA, XRD and SEM–EDS protocols, together with the acceptance criteria and analysis approach. Chapter 4 presents and discusses the results for setting, compressive strength and phase/microstructural evidence, and assembles the parameter map across pH, precursor dosage and fineness under ambient curing. Chapter 5 concludes the study, states the practical operating window and reporting checklist, and recommends directions for future work. The References list all cited sources. The Appendices provide detailed mix proportions, raw data tables and supplementary figures.

CHAPTER 2
LITERATURE REVIEW

2.1 Introduction

Ordinary Portland cement (OPC) is the principal hydraulic binder in pastes and concretes. Under EN 197-1, Portland cement consists mainly of Portland clinker with calcium sulphate and minor constituents and is designed to set and harden by hydration under water (Standardization, 2011). Hydration of alite and belite forms calcium-silicate-hydrate (C–S–H) and portlandite (CH), which control setting and strength when mixture design and curing are managed appropriately (Mehta & Monteiro, 2014; Neville, 1995). In the context of this study, these hydration products are important because aqueous CO_2 introduced through the mixing water may influence early calcium availability, carbonate precipitation and the balance between hydration and carbonation during paste formation.

Sustainability pressure on OPC has been established in Chapter 1 and is briefly retained here only to frame the relevance of CO_2-based cement research. As shown in Figure 2.1, the cement sector remains under pressure to reduce direct CO_2 intensity, which supports continued investigation of material-level CO_2 utilisation routes (Friedlingstein et al., 2024; IEA, 2024). However, the focus of this chapter is not the broader emissions pathway, but the mechanisms by which CO_2 can interact with cementitious binders. In particular, this review emphasises CO_2 integration through aqueous mixing water, where dissolved CO_2 forms H_2CO_3 and may influence hydration, carbonate nucleation, setting behaviour, strength development and pore refinement.

Accordingly, the literature review proceeds from CO_2 utilisation routes in cementitious systems to the specific mechanism of aqueous CO_2 incorporation during mixing. The roles of $CaCO_3$ and $CaMg(CO_3)_2$ are then reviewed as calcium-based carbonate precursors, followed by studies relating carbonation behaviour to setting time, compressive strength, water absorption, chemical composition, thermal response and microstructural evidence. This structure keeps the review aligned with the experimental scope of the thesis.

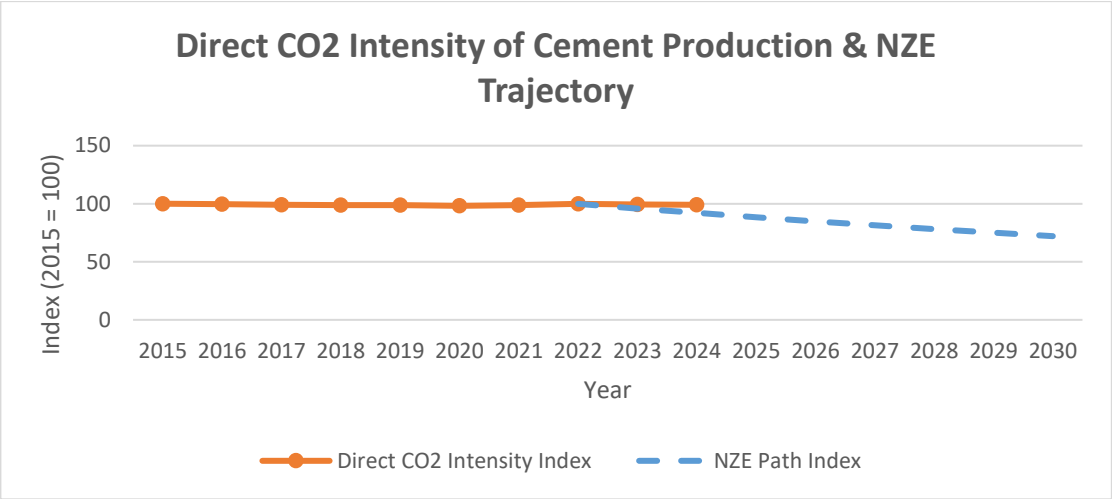


Figure 2.1 Direct CO Intensity of Cement Production and The NZE Pathway to 2030 IEA (2024).

2.2 Trend Analysis on CO_2 Sequestered Cement

A systematic literature review (SLR) was used to synthesise prior work in building engineering and cementitious materials. Following the guidance of Tranfield et al. (2003) and Page et al. (2021), the review process was organised into five stages which are (1) identifying the research problem and topic boundary, (2) selecting suitable databases, (3) screening documents relevant to the topic, (4) analysing and appraising the selected documents, and (5) synthesising the findings according to research themes. Scopus was used as the main bibliographic database, while Google Scholar was used to support forward and backward citation tracking. This approach was adopted to provide both a broad overview of publication trends and a focused basis for identifying studies most relevant to aqueous CO_2 integration in cementitious systems.

2.2.1 Search String Utilized

Searches were executed in Scopus as the core database, with Google Scholar used only for forward and backward citation chasing. The window was 2000–2025, run on 25th of December 2022. In Scopus the query was built from three concept blocks in TITLE-ABS-KEY to keep the search precise and reproducible: a material block *(cement, concrete, mortar)*, a CO_2 block *("carbon dioxide", CO_2, carbonic acid, H_2CO_3)*, and a process or route block *(carbonation, sequestration, hydration, "mixing water", "aqueous CO_2")*. Limits for language, document type and subject area were

applied after the broad run. The review was limited to English-language articles and reviews within *(Engineering, Materials Science and Energy)* to reduce irrelevant records while retaining studies related to cementitious materials. The bibliometric analysis was used to identify publication trends, dominant research themes and keyword relationships, while the detailed discussion in the following sections was organised thematically around studies most relevant to aqueous CO_2 mixing water, carbonate precursor replacement and cementitious performance.

Records from Scopus and Google Scholar were exported, de-duplicated, screened by title and abstract, and then appraised in full text against predefined inclusion and exclusion criteria. Studies were included when they addressed CO_2 or H_2CO_3 incorporation in cementitious systems and reported at least one relevant outcome, such as setting behaviour, compressive strength, water absorption, CO_2 uptake, phase composition or microstructural evidence. Studies were excluded when they focused on unrelated non-cement materials, purely theoretical work without experimental data, patents, theses, non-English texts or carbonation routes outside the scope of this review. The workflow is summarised in Figure 2.2.

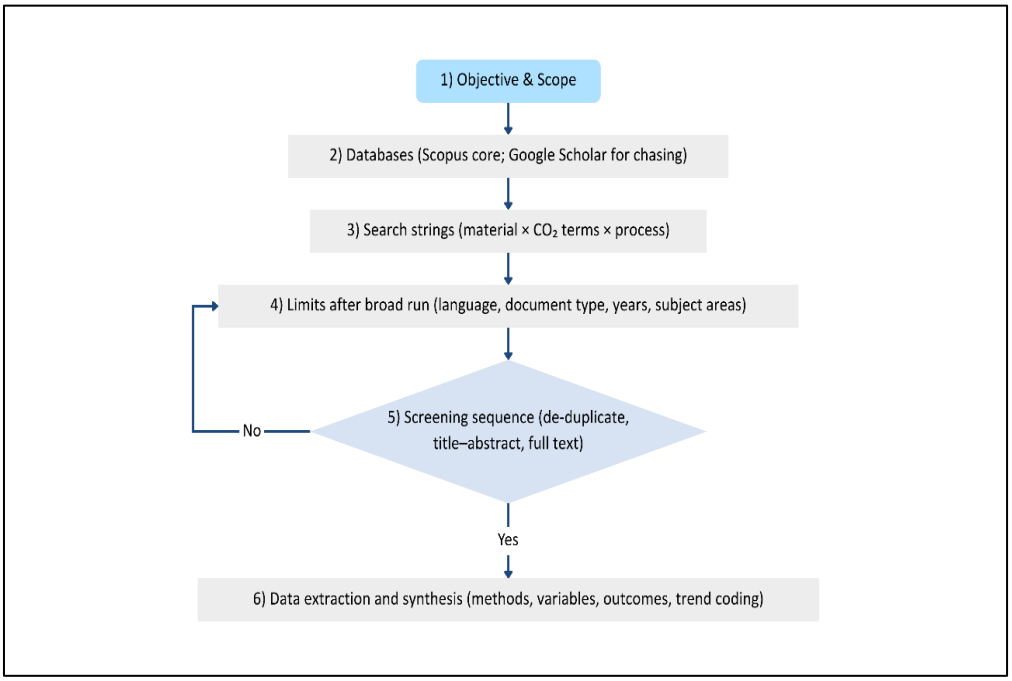


Figure 2.2 Workflow for The Systematic literature review (SLR)

2.2.2 Bibliometric Analysis

In total, 2050 English-language research publications spanning from the year 1981 to 2023 were obtained. Annual and cumulative numbers of research articles on CO_2-sequestered concrete indexed in Scopus from 1981 until 2023 can be observed in Figure 2.3(a), which were derived from the acquired publications in Scopus. Research on CO_2 sequestration in cementitious materials has shown a clear increase in publication output, especially in recent years, indicating growing interest in carbonation mechanisms, CO_2 utilisation and low-carbon construction materials. Figure 2.3 (b) illustrates the top ten countries with the highest number of publications, where China has the largest number of publications, followed by the United States, with totals of 590 and 318, respectively.

The data indexed from Scopus were then analysed using VOSviewer, as depicted in Figure 2.3 (c), to show the co-authorship network between countries and the relative research contribution of the major publishing countries. The publication trend in Figure 2.3 (a) suggests that CO_2-related cement research has shifted from a niche topic to a rapidly expanding research area, particularly after the growing emphasis on carbon capture, utilisation and storage in construction materials. The dominance of China and the United States in Figure 2.3 (b) may be related to their large cement and concrete industries, high infrastructure demand and active research programmes in low-carbon construction and carbon utilisation technologies.

The co-authorship network in Figure 2.3 (c) further indicates that the topic is increasingly collaborative, with research activity distributed across several major regions rather than confined to a single country. However, the broad increase in publication output does not necessarily mean that all sub-topics are equally developed. In relation to this thesis, the bibliometric trend confirms the relevance of CO_2-sequestered cement research, while also highlighting the need to examine more specific routes such as aqueous CO_2 mixing water in OPC paste.

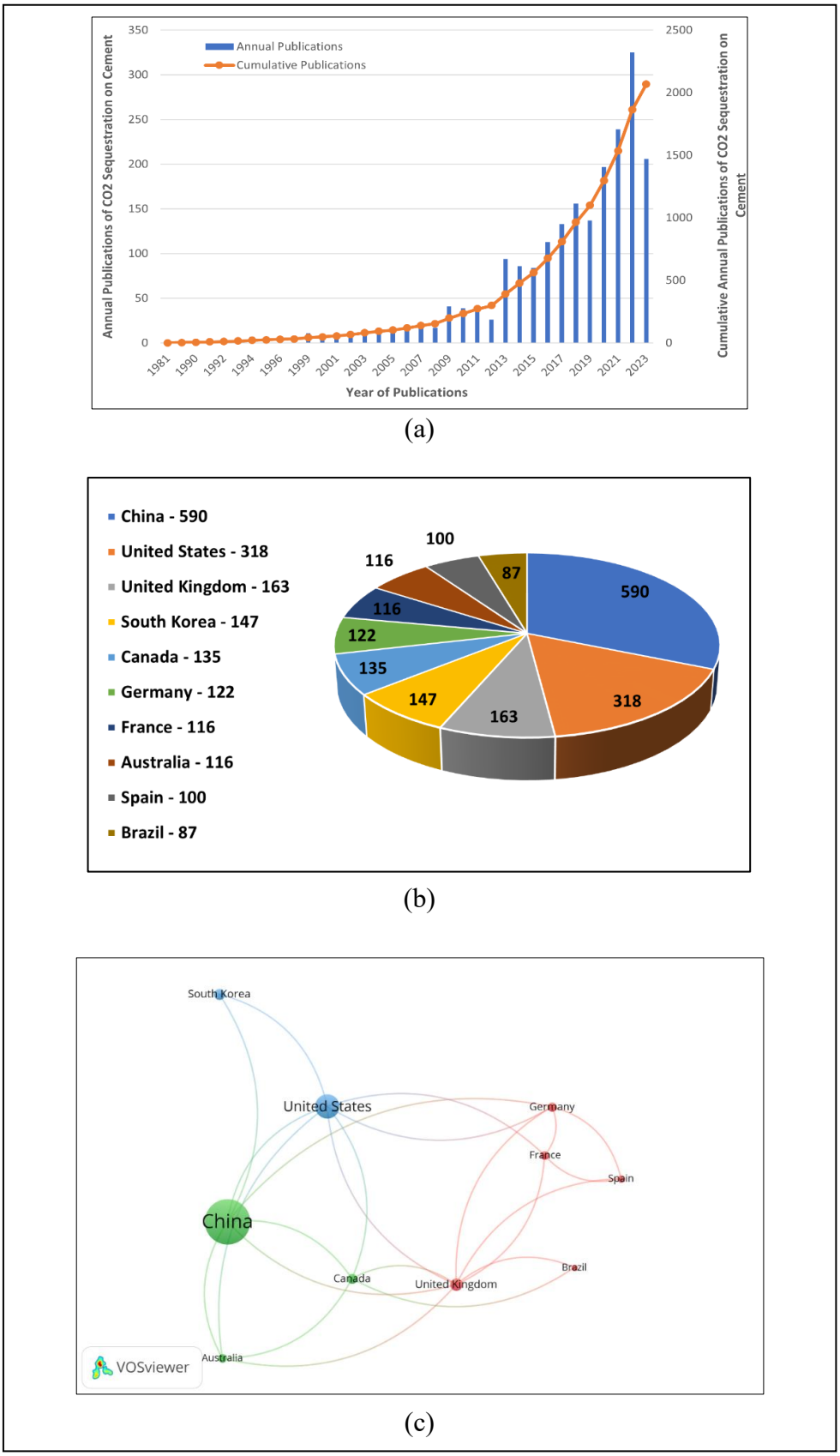
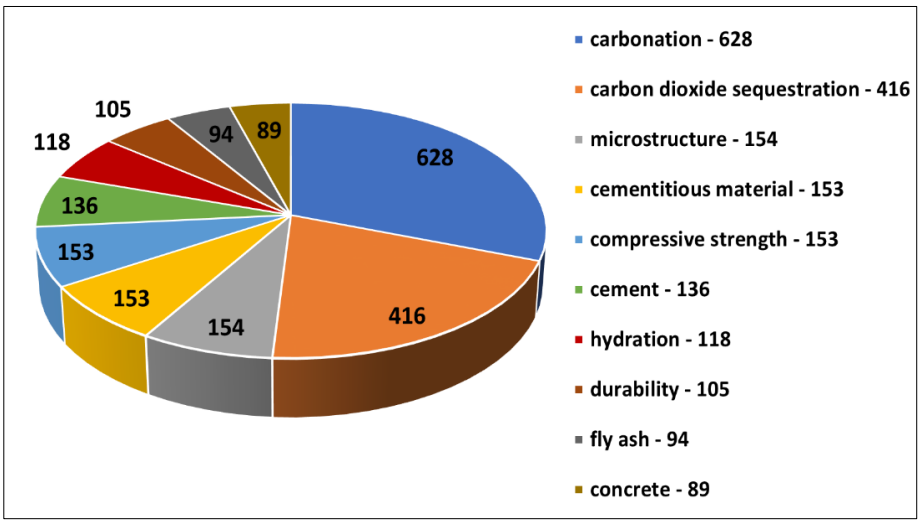
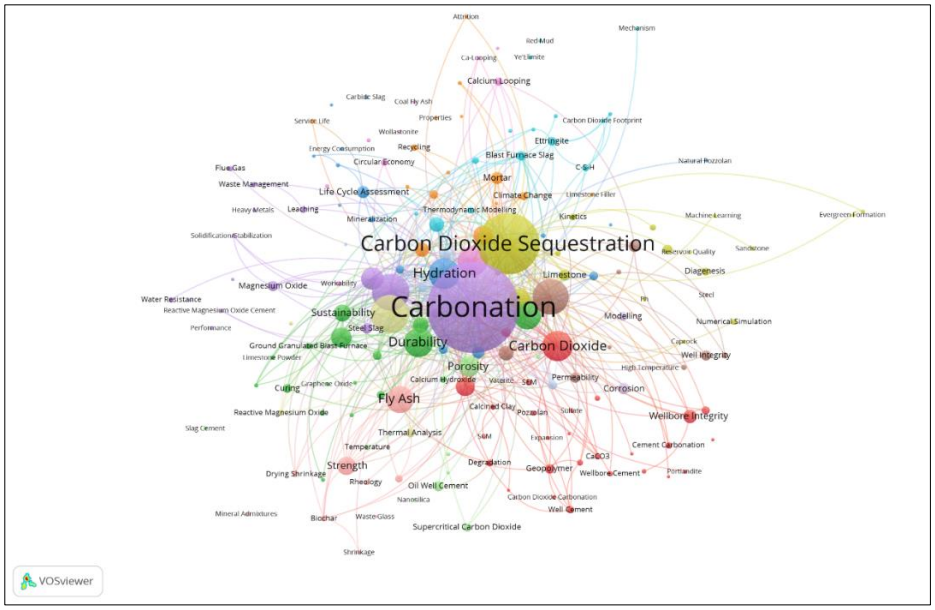


Figure 2.3 Overview of Publications on CO_2-Cement (Scopus, 1981–2023): (a) The Annual Trend, (b) Countries with The Largest Number of Publications, and (c) Network Map Showing The Co-Authorship Between Countries



(a)



(b)

Figure 2.4 Overview of Keywords in Publication Related to Topic of Interest: (a) Pie Chart Depicting Frequently Appeared Keywords, and (b) Network Map Showing The Keywords Co-Occurrence

Repetitively appeared keywords in relevant publications were then analysed and illustrated as pie chart in their respective frequency of terms as observed in **Error! R eference source not found.**2.4(a). Five (5) terms incorporating of "carbonation", "carbon dioxide sequestration", "microstructure", "cementitious material", and "compressive strength" are the most frequently encountered terms derived from the

analysed publications. Relevant keywords were outlined using VOS Viewer according to its co-occurrence, revealing twelve (12) distinct clusters represented by different colours which is depicted in **Error! Reference source not found.**2.4(b). The cluster m ost relevant to the present thesis is the group connecting carbonation, hydration, microstructure and compressive strength, because this study evaluates how aqueous CO_2 mixing and carbonate precursor replacement affect OPC paste behaviour. However, terms directly related to "mixing water", "carbonic acid", "pH" and "dolomite" are less dominant than general carbonation-related terms. This supports the research gap of the thesis, where the aqueous CO_2 mixing route and $CaMg(CO_3)_2$ precursor effect require clearer experimental evaluation. Counts and maps reflect Scopus indexing and an English-language filter; author-keyword practices vary by journal, and co-occurrence maps are descriptive rather than direct measures of research quality or impact. These factors are considered when interpreting topic prominence and collaboration intensity.

2.3 CO_2 Utilisation Methods & Mechanism in Cementitious Systems

In cement manufacture, carbon dioxide arises mainly from limestone calcination during clinkering, fuel combustion for kiln heat, and indirect emissions from electricity and logistics (Andrew, 2018; Cheng et al., 2023). These source terms explain why CO_2 utilisation has become relevant to cementitious materials. However, the present thesis does not investigate industrial carbon capture technologies or plant-scale CO_2 recovery systems. Instead, this chapter reviews CO_2 utilisation mechanisms only to the extent that they support the experimental focus of the study, namely aqueous CO_2 integration in OPC paste with $CaCO_3$ and $CaMg(CO_3)_2$ precursors.

As summarised in Figure 2.5, CO_2 can be engaged at three points: aqueous carbonation at mixing (CO_2 dissolved as H_2CO_3 in the mixing water), accelerated carbonation curing (ACC) in a CO_2 chamber shortly after casting or demoulding, and natural service-life carbonation of hardened concrete. The first two are active early-age routes considered in this review; service-life carbonation is treated later as a durability phenomenon rather than a utilisation process. Among the routes shown in Figure 2.5, the aqueous mixing-water route is the most relevant to this thesis because CO_2 is introduced before setting as dissolved CO_2 or H_2CO_3 rather than after casting through chamber curing.

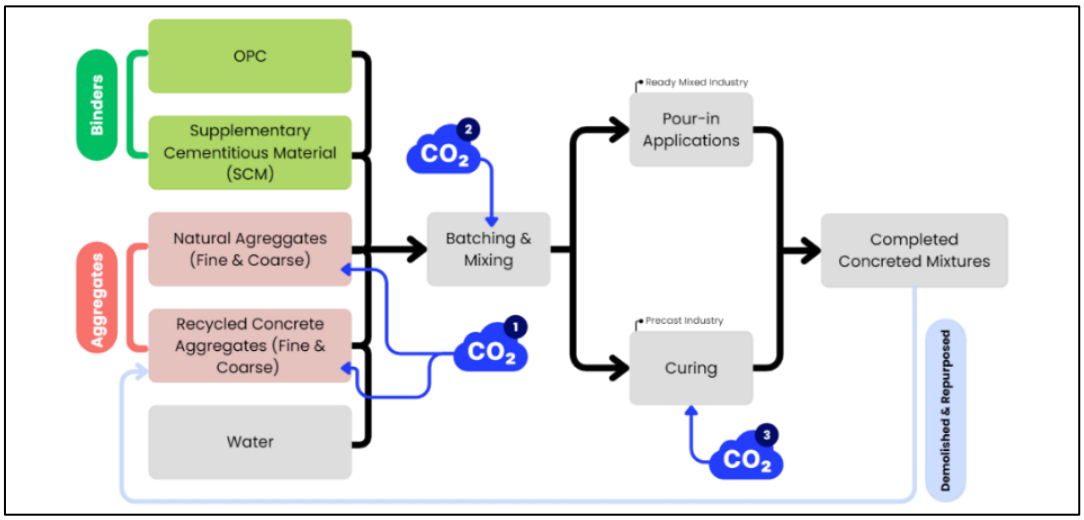


Figure 2.5 Proposed Methods of Carbonation Curing in Cementitious Materials (Amended from Lim et al. (2019))

Approaches to utilise CO_2 at early age fall into two families with different rate-controlling steps. ACC exposes fresh or demoulded elements to a controlled CO_2 atmosphere; performance depends on gas-solid transport, moisture state and curing schedule, and can deliver strength gains and CO_2 mineralisation when the process window is controlled. However, excessive or poorly controlled carbonation may over-densify the surface layer or hinder subsequent hydration. In contrast, aqueous carbonation at mixing dissolves CO_2 into the mixing water as H_2CO_3, shifting the controlling factors to solution chemistry, particularly pH, alkalinity, ionic speciation and liquid-phase nucleation. Previous studies show that, within a defined pH and water-to-binder window and with appropriate precursor dosage, pastes mixed with CO_2-conditioned water can promote early carbonate formation and improve early strength. Outside this window, excessive acidity or dilution may retard setting or reduce strength development (Bernal et al., 2024; Lippiatt et al., 2019).

2.3.1 Mineral Carbonation

Mineral carbonation in cementitious systems is commonly classified into direct and indirect pathways, each expressed as gas–solid contact or as aqueous processing, aiming to convert reactive calcium or magnesium sources to stable carbonate phases while influencing hydration and microstructure. It has emerged as a focal point of

research within the broader Carbon Capture, Utilization, and Storage (CCUS) framework, driven by its potential to mitigate climate change and enhance concrete properties. Although mineral carbonation includes a wide range of natural minerals and industrial residues, these materials are reviewed here only as background to explain the general conversion of Ca- and Mg-bearing phases into stable carbonates. The experimental programme of this thesis is narrower and focuses on OPC paste incorporating aqueous H_2CO_3 mixing water with $CaCO_3$ and $CaMg(CO_3)_2$ precursors. Therefore, discussion of olivine, serpentine, steel slag, fly ash and recycled aggregates is treated as supporting context rather than as the main basis of the present experimental work.

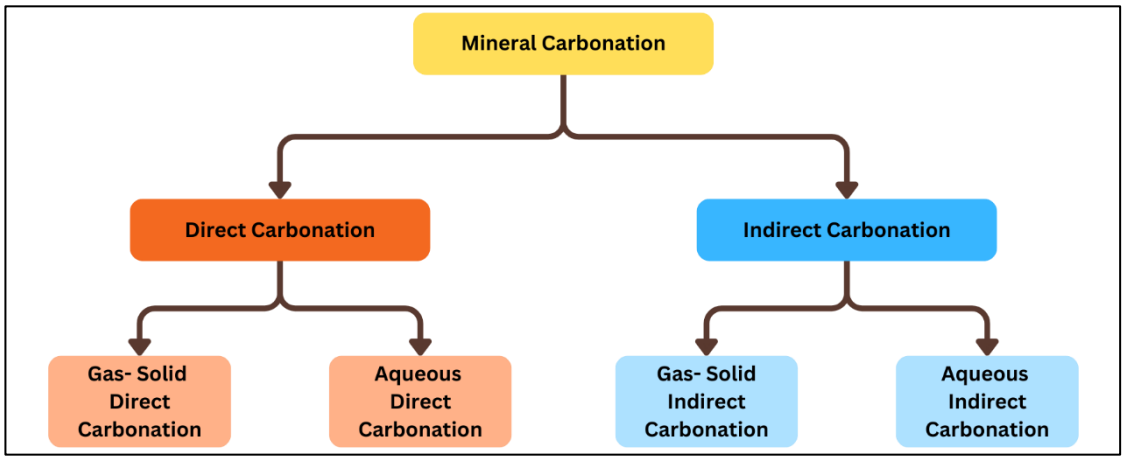


Figure 2.6 Classification of Mineral Carbonation Routes (Amended from Ahmed et al. (2024))

A comprehensive analysis, as depicted in Error! Reference source not found. (a) a nd (b), reveals a remarkable total of 628 publications dedicated to this subject. This surge in research interest underscores the critical role mineral carbonation can play in sustainable construction practices. Various techniques associated with mineral carbonation in concrete, such as carbonation curing, mineral carbonation, and early-age carbonation, have been explored and refined. Mineral carbonation can be classified into direct and indirect carbonation routes, each with gas-solid and aqueous subcategories, as depicted in Figure 2.5. These techniques are continuously being optimized to maximize the benefits of CO_2 carbonation in concrete while addressing associated challenges and ensuring long-term performance (Liu & Meng, 2021). Mineral carbonation however involves the reaction of CO_2 with Ca and magnesium silicates ($MgSiO_3$) to form stable carbonates, which are then integrated into the concrete matrix. This process not only sequesters CO_2 but also enhances the mechanical properties and

durability of the concrete. Although the sequestration rate of CO_2 within the concrete is limited, the resultant strength improvement presents an opportunity to reduce the cement content in concrete production. This reduction in cement content not only lowers the carbon footprint of concrete but also demonstrates the feasibility of achieving comparable performance with less cement (Winnefeld et al., 2022a).

Extensive research as in comprising both experimental and theoretical studies had been conducted in exploring mineral carbonation and examining its potential as a method for sequestering CO_2 in concrete (Huang et al., 2019; Kusin et al., 2020a; Molahid et al., 2021). The process of mineral carbonation involves acceleration of weathering process with silicate aggregates containing Ca, Iron (Fe) and Magnesium (Mg) substantial minerals consisting of olivine, serpentine, brucite, wollastonite, or basalt, through exposing it to CO_2, leading to the formation of stable $CaCO_3$ or Magnesium Carbonate ($MgCO_3$) (Kusin et al., 2023; Owais et al., 2019; F. Wang et al., 2021).

$$Mg_2SiO_4 + 2CO_2 + 2H_2O \rightarrow 2MgCO_3 + H_4SiO_4 \quad (2.1)$$

$$Mg_3Si2O_5(OH)_4 + 3CO_2 + 2H_2O \rightarrow 3MgCO_3 + 2H_4SiO_4 \quad (2.2)$$

$$Fe_2SiO_4 + 2CO_2 + 2H_2O \rightarrow 2FeCO_3 + H_4SiO_4 \quad (2.3)$$

$$CaSiO_3 + CO_2 + 2H_2O \rightarrow CaCO_3 + H_4SiO_4 \quad (2.4)$$

Comprehensive experimental and theoretical work as in Table 2.1, documents mineral carbonation for CO_2 sequestration in cementitious systems and alkaline wastes. Accelerated weathering of Ca- and Mg-bearing silicates or industrial residues in the presence of CO_2 and H_2O forms stable carbonates that can be retained in the binder or recycled fines, as described in Equations 2.1, 2.2, 2.3, and 2.4. Accelerated-carbonation curing studies commonly report approximately 10–20% of CO_2 uptake by cement mass within hours, with attendant early-age densification and strength gains (Ferrara et al., 2024; Li et al., 2019). Plant-scale demonstrations further confirm feasibility under industrial conditions (Wang et al., 2022). Beyond cement, feedstock-focused studies show that mine wastes and steelmaking slags supply reactive Ca or Mg for mineral carbonation, with process windows mapped for indirect aqueous and gas–solid routes (Kusin et al., 2020b; Molahid et al., 2021; Owais et al., 2019). Broader syntheses

explain the thermodynamic preference for Ca or Mg systems, and visualise that route selection between direct vs indirect and gas–solid vs aqueous, determines the controlling mechanisms, kinetics and attainable utilisation (National Academies of Sciences et al., 2019).

As implemented in concrete practice, mineral carbonation is used to (i) upgrade recycled aggregates or fines prior to batching, (ii) introduce CO_2 during mixing via carbonic-acid water to create fine $CaCO_3$ nuclei, or (iii) apply chamber-based accelerated carbonation curing shortly after casting. Across these variants, the immediate material benefits are linked to filler-nucleant effects and microstructural densification, upon verification by standard tests, allows cement reduction at equal performance, thus lowering life-cycle emissions (Winnefeld et al., 2022b).

2.3.1.1 Direct Mineral Carbonation

Direct mineral carbonation involves the conversion of Ca or Mg-bearing solids into stable carbonates by contacting them with CO_2, providing durable storage and, for construction feeds, useful microstructural effects. Two variants are used in practice which are gas–solid carbonation, whereby CO_2 contacts with dry or moist solids, and direct aqueous carbonation, where CO_2 first dissolves in water and reacts in slurry. These routes are well established in the CO2-utilisation literature and specifically reviewed for cementitious streams such as recycled-concrete fines, steel slags and cement by-pass dust (Sanna et al., 2014; Winnefeld et al., 2022b).

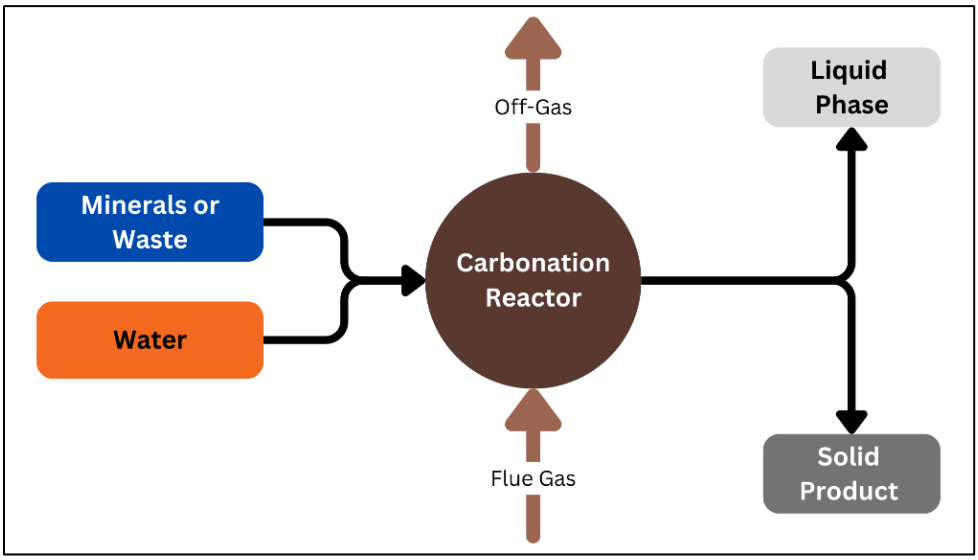


Figure 2.7 Direct Aqueous Carbonation Process Routes (Amended from (Jaschik et al., 2014))

Table 2.1
Variation of Cementitous Materials Integrated Into CO_2 Fused Concrete and Findings

Materials											CO_2 Form Conversions			Findings	Remarks	Ref
Aggregates		Lime-stone Cement	OPC	Sand	Water	Fly Ash	Super-plasticizer	Slag	CO_2	Others	Gas to Solid	Gas to Liquid	Liquid to Solid			
Course	Fine															
✓	✓		✓				✓		✓		✓			• Decrease drying shrinkage by 25% to 45% • Reduce pore volume	Significantly improve early age compressive strength	(Xiao et al., 2022)
									✓		✓	✓		• Reduce H_2O absorption by 16.4% • Lower permeability rate by 42.4%	Enhance strength gained (up to 6 times)	(Meng et al., 2022)
✓	✓	✓		✓	✓		✓		✓		✓			H_2O absorption ability remains	Higher compressive strength	(Russo & Lollini, 2022)
✓			✓						✓	Carbonated & non-carbonated reinforced concrete aggregate	✓		✓	• Higher compressive strength than recycled aggregate by 24.1% and 32.9% • Decrease H_2O absorption by 15.2% to 20.6% • Reduce drying shrinkage by 16.6% to 25.1% • Reduce porosity	Comparable with neutral aggregate	(Lu et al., 2021)
✓	✓		✓		✓	✓		✓	✓				✓	No change in workability	Reduce binder (7% to 8%) reducing compressive strength	(Monkman & MacDonald, 2017)
✓	✓		✓	✓	✓		✓		✓		✓			• Greater surface resistivity • Lower porosity		(Xian & Shao, 2021)
✓	✓		✓						✓	Carbonated masonry aggregates		✓		Increase dry bulk density	Improve mechanical properties	(Suescum-Morales et al., 2022)
✓	✓		✓	✓	✓		✓		✓	Recycled concrete aggregates	✓			• Enhance flexural strength • Reduce the usage of natural aggregate by up to 60%		(Xuan et al., 2016)
✓	✓		✓	✓			✓		✓	Crushed pavement concrete aggregates	✓			Higher compressive strength than recycled		(Luo et al., 2018)

											aggregate by 2.3% to 14.5%	
✓	✓			✓				✓	Carbonated sand & gravel, & CEM II/A Cement	✓	Improve the compressive strength	(Torrenti et al., 2022)
			✓	✓				✓	Carbonated & non-carbonated reinforced concrete aggregates	✓	• Higher compressive strength by 17% on 28th day • Higher compressive strength by 12% on 90th day	(Li et al., 2017)
			✓	✓				✓	Limestone and Quartz Powder	✓	Higher electrical resistivity	(Lin & Wang, 2021)
✓	✓		✓	✓				✓	Carbonated & non-carbonated recycled aggregate	✓	Reduce brittleness	(Lu et al., 2022)
								✓	Cement paste	✓	Flowability	(Wu et al., 2022)
✓	✓			✓	✓		✓	✓		✓	Enhance compressive strength & surface electrical resistivity	(Xian, Zhang, et al., 2022)
✓	✓							✓	Aggregates obtained from crushed mortar	✓	• Reduce H_2O absorption • Lower pH and increased freezing-thawing resistance	(Liang et al., 2020)
✓	✓		✓				✓	✓		✓	Reduce permeability while improving its durability	(Zhang & Shao, 2016)
			✓	✓			✓	✓	Crushed Limestone	✓	Increase compressive strength	(Ahmad et al., 2017)
✓				✓	✓			✓	Ordinary Silicate Cement & Recycled Coarse Aggregate	✓	Enhanced compressive & tensile strength	(Feng et al., 2023)

At a high level, gas–solid routes are limited by CO_2 transport and growth of a passivating carbonate rim, whereas aqueous routes are governed by solution chemistry and nucleation. Figure 2.7 sketches a typical direct-aqueous process block: a Ca/Mg-bearing mineral or alkaline waste is slurried with water, CO_2 is contacted in a carbonation reactor, off-gas is vented or recycled, and the outputs are a solid carbonate product and a treated liquid phase. This schematic aligns with industrially used aqueous-carbonation flowsheets and sets up the deeper mechanism-and-parameter discussion that follows in the gas–solid and aqueous sub-subsections.

2.3.1.2 Gas-Solid Direct Carbonation

Gas–solid carbonation reacts gaseous CO_2 directly with alkaline solids rich in Ca or Mg such as, olivine or serpentine, basic oxygen furnace and stainless-steel slags, cement paste in recycled concrete aggregates. Reaction progress is typically controlled by CO_2 transport through a growing carbonate rim and by the availability of reactive Ca or Mg at the surface. Hence, temperature, CO_2 partial pressure, moisture, particle size and pretreatment dominate kinetics (Baras et al., 2023; Quaghebeur et al., 2015; Romanov et al., 2015). Under optimised conditions, gas–solid routes can mineralise a fraction of the theoretical capacity while producing mechanically and environmentally improved products; slag stabilisation via f-CaO→$CaCO_3$ for example (Wang et al., 2022; X. Wang et al., 2021).

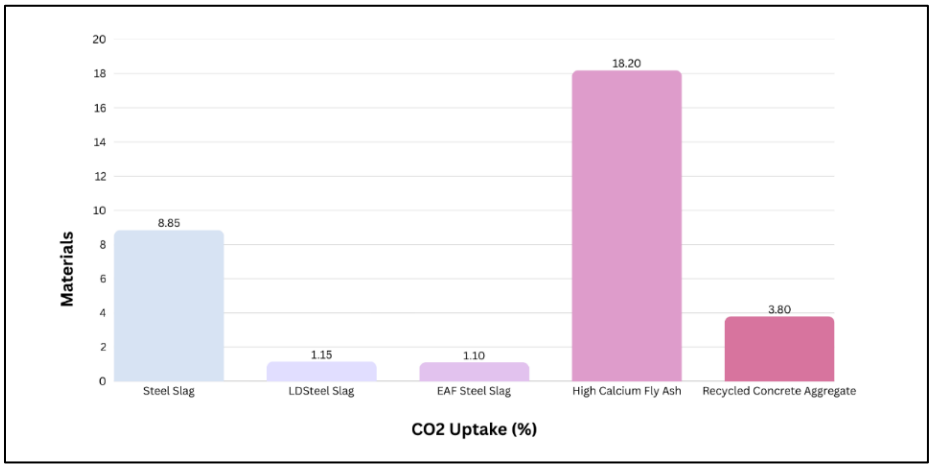


Figure 2.8 Reported CO_2 Uptake for Selected Alkaline Feedstocks Under Gas–Solid Direct Carbonation (wt% of Feedstock).

As reported across multiple studies, steel slags typically carbonise in the CO_2 range of 4 to 16 wt% under elevated CO_2 and temperature, with the exact value

depending on slag type and particle size (X. Wang et al., 2021; Zhao et al., 2025). High-calcium fly ash can reach approximately 18 wt% when free CaO is available, as shown by Mazzella et al. (2016). For recycled concrete aggregates (RCA), pilot and demo lines reported at 0.5–4 wt% uptake (≈5–40 kg CO_2 t^{-1} aggregate), with ~3–4 wt% representative for non-aggressive conditioning (Merino-Lechuga et al., 2023; Torrenti et al., 2022). Figure 2.8 illustrates these representative CO_2 uptakes (wt% of feedstock) for steel slags, high-calcium fly ash and recycled concrete aggregates under gas–solid direct carbonation. Values correspond to specific laboratory or pilot conditions (CO_2 concentration, temperature, exposure time, particle size), and comparisons are only valid on the same basis and with stated conditions (Romanov et al., 2015). Its relevance to this thesis is limited to the general carbonation principle because the experimental programme focuses on OPC paste with $CaCO_3$ and $CaMg(CO_3)_2$, rather than steel slag, fly ash or recycled aggregate feedstocks.

2.3.1.3 Aqueous Direct Carbonation

In the aqueous route, CO_2 first dissolves so reactions proceed in solution rather than across a gas–solid interface. The driving force is governed by carbonate speciation and pH: dissolved CO_2 distributes among H_2CO_3, HCO_3^-, and CO_3^{2-}, while Ca^{2+} or Mg^{2+} mobilised from the solid subsequently precipitates as carbonates; the formal sequence is summarised in Eqs. (2.5), (2.6), and (2.7). Figure 2.9, which was amended from Li and Wu (2022), summarises three stages relevant to cement and alkaline residues which are, mobilisation of Ca or Mg from the solid, carbonate speciation in solution, and precipitation and growth of $CaCO_3$ or $MgCO_3$ at the reaction front. This mechanistic feature illustrates how pH, liquid-to-solid ratio and residence time, control uptake and product phases (Winnefeld et al., 2022b).

$$(Ca/Mg)SiO_2 + 2H^+ \rightarrow (Ca^{2+}/Mg^{2+}) + SiO_2 + H_2O \quad (2.5)$$

$$HCO_3^- \rightarrow H^+ + CO_3^{2-} \quad (2.6)$$

$$(Ca^{2+}/ Mg^{2+}) + CO_3^{2-} \rightarrow (Ca/Mg)CO_3 \quad (2.7)$$

Using CO_2-equilibrated mixing H_2O increases early nucleation through nanometric $CaCO_3$ and can shorten setting when pH is controlled. It was discovered

that the mechanical benefits under supersaturated aqueous CO_2 used as mixing water, provided the water-to-binder ratio and acidity were kept within a workable window (Lippiatt et al., 2019; Lippiatt et al., 2020). Time-resolved measurements on OPC pastes have quantified about 19 % of cement mass within roughly 40 min under aqueous mineralisation, with concurrent portlandite consumption and carbonate formation (Ferrara et al., 2024). Direct aqueous carbonation of concrete fines at atmospheric pressure has also shown practical uptake and a recoverable carbonate product, confirming suitability for construction residues (Ho et al., 2020). Outcomes depend strongly on the pH window. Insufficient buffering or excessive acidity can retard setting or create premature surface coatings, so reports should state the uptake basis together with pH, liquid-to-solid ratio and exposure time (Owais et al., 2019)

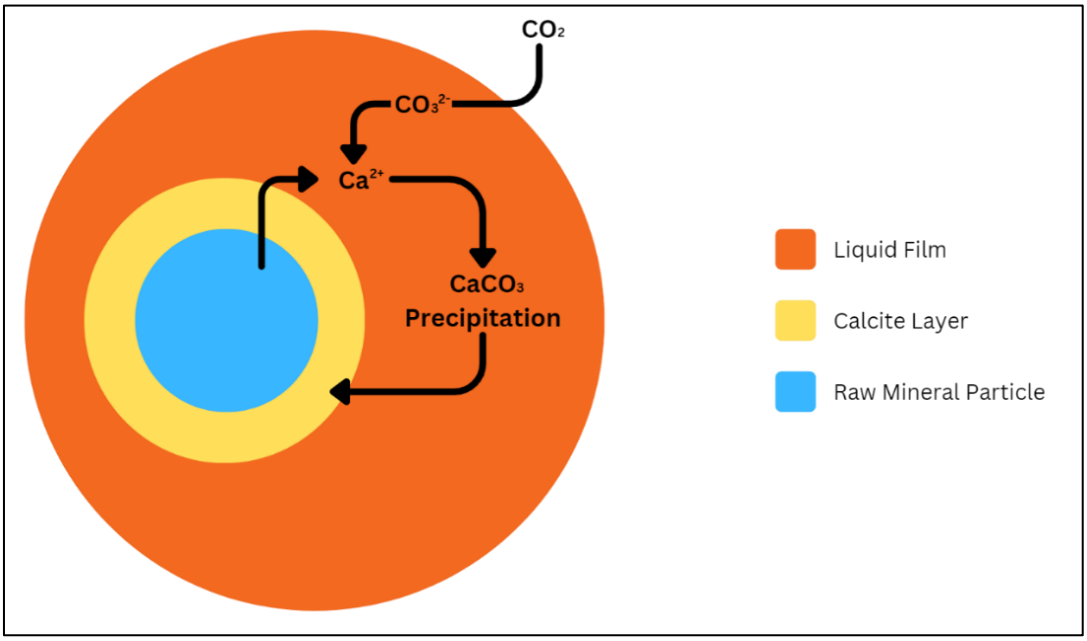


Figure 2.9 Stages in Direct Aqueous Carbonation of Ca-Bearing Solids: Ca/Mg Mobilisation, Carbonate Speciation In Solution, and Caco₃ Or Mgco₃ Precipitation (Amended from Li and Wu (2022))

Research outcomes vary mainly with the aqueous-phase operating window, especially pH of the liquid, liquid-to-solid ratio, residence time, because these parameters control Ca or Mg mobilisation (Eqs. 2.5) and carbonate availability (Eqs. 2.6). Reviews of carbonation in cement systems emphasise that results should state whether uptake is by cement mass or by total feedstock mass and disclose the controlling conditions (Winnefeld et al., 2022). In mixing-water implementations, controlled pH and water-to-binder ratio are decisive for achieving nucleation benefits

without setting retardation; when acidity is excessive, premature carbonate coatings can form and slow hydration (Ferrara et al., 2024; Ho et al., 2020).

2.3.1.4 Indirect Mineral Carbonation

Indirect mineral carbonation separates dissolution and carbonation into two (2) steps which involves Ca or Mg leached from an alkaline solid into solution, before Ca-rich liquor is carbonated and the lixiviant is regenerated for reuse. This decoupling gives stronger control over selectivity and product quality such as precipitated calcium carbonate (PCC) than one-step routes, at the cost of solvent circulation and energy overheads (Sanna et al., 2014; S. Wang et al., 2024). Indirect schemes hence, are widely studied for steel or iron slags and recycled concrete fines, where Ca can be mobilised efficiently and converted to PCC while upgrading the residue for use in cementitious systems (Huijgen et al., 2005; X. Zhang et al., 2024). Figure 2.10 summarises the generic indirect mineral carbonation flowsheet, which involves the process of leaching, solid–liquid separation, liquor carbonation, and then solvent regeneration respectively.

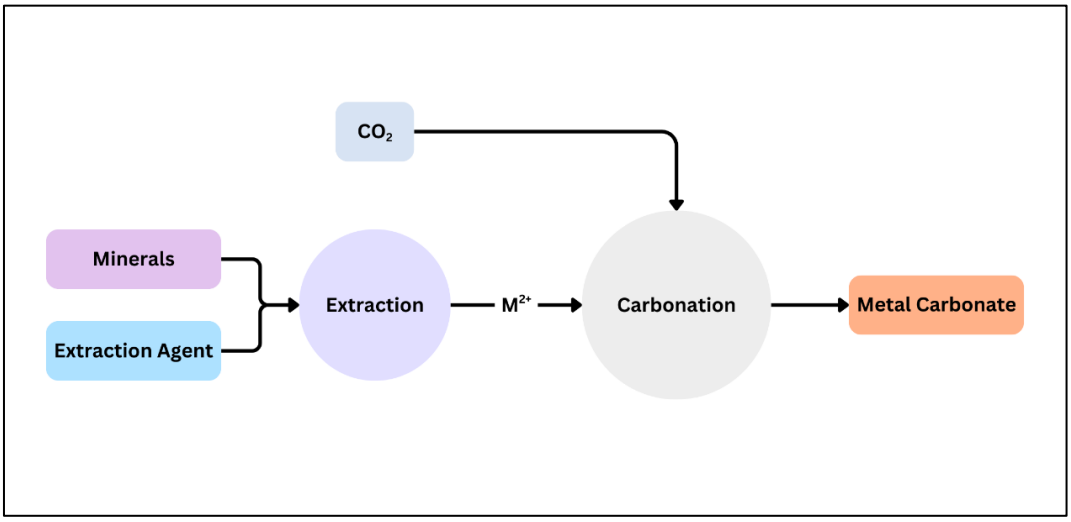


Figure 2.10 Indirect Mineral Carbonation Concept (Amended from Azdarpour et al. (2015))

Evidence from recent studies shows why this two-step control matters. Using ammonium-salt lixiviants for example like, ammonium nitrate (NH_4NO_3), ammonium chloride (NH_4Cl), and acetate, ($C_2H_3O_2^-$). Gasós et al. (2024) discovers that higher Ca extraction from recycled-concrete aggregate in a packed-bed reactor than in stirred vessels under comparable concentrations and residence times, highlighting the role of

hydrodynamics and solid–liquid ratio. For steel converter slag, the acetic-acid loop dissolves Ca selectively and can deliver PCC with more than 99% purity and approximately 86% conversion of dissolved Ca, while regenerating the weak acid during precipitation (L. Liu et al., 2024; Ruiying et al., 2025). Across indirect schemes, advantages are selectivity and PCC quality; constraints are lixiviant losses/corrosion, alkali use for carbonation/pH swing, and closed-loop regeneration (Sun et al., 2025; S. Wang et al., 2024). Reported percentages are basis-dependent (% of Ca extracted from solid vs % of dissolved Ca converted to PCC), so comparisons are only meaningful when reagent strength, temperature, pH swing, and solid–liquid ratio, are stated alongside the metric (Gasós et al., 2025).

After the leaching step in indirect mineral carbonation, the carbonation stage can proceed in two practical ways. In a gas-solid route, the Ca-rich intermediate is first recovered as a solid; often $Ca(OH)_2$ or a hydrated phase and then contacted with gaseous CO_2 to form $CaCO_3$. In an aqueous route, the Ca-bearing liquor is directly carbonated by CO_2 sparging or a pH-swing to precipitate $CaCO_3$ from solution. Both variants are documented for steel slags and recycled-concrete fines, and both can yield high-purity PCC when conditions are controlled, although their operating constraints differ. Although, gas–solid indirect mineral carbonation is typically preferred when a dry, easily handled intermediate (e.g., $Ca(OH)_2$) is available and simple gas–solid contact minimises wastewater, whereas aqueous indirect carbonation is preferred when tight pH control, continuous precipitation, and particle-size tuning are priorities—accepting added alkali use and solvent-loop management, respectively (Gao et al., 2025).

2.3.1.5 Gas-Solid Indirect Carbonation

In the gas–solid variant of indirect mineral carbonation, the Ca-bearing liquor obtained after leaching is first converted to a dry intermediate; commonly $Ca(OH)_2$, which is then contacted with gaseous CO_2 so that $CaCO_3$ forms at the particle surface. Recent slag-focused reviews treat this pathway as complementary to aqueous precipitation because it enables low-effluent operation and tight control of product morphology/brightness when producing PCC fillers (Biava et al., 2024; DiGiovanni et al., 2024; X. Zhang et al., 2024). Arias et al. (2022) show that carbonation rates of fine $Ca(OH)_2$ are governed by CO_2 transport through a growing carbonate rim and by moisture or temperature which allows higher CO_2 partial pressure, adequate humidity

and smaller particle sizes accelerate conversion, whereas premature surface densification slows it.

Recent engineering studies illustrate practical levers. For blast-furnace slag systems, pressure-swing carbonation increases overall conversion without additional chemicals by alternating pressure states during gas–solid contact (Ho et al., 2020). When the intermediate originates from selective weak-acid leaching of converter slag, gas–solid carbonation of $Ca(OH)_2$ yields high-purity PCC; the classic acetic-loop work reported more than 99% purity with high liquor-to-product conversion (Eloneva et al., 2008), and newer process-intensification studies use ultrasound to boost upstream Ca release and to tune PCC habit (L. Liu et al., 2024; Ouyang et al., 2025; Yang et al., 2024). Although gas–solid indirect mineral carbonation is typically preferred when a dry, easily handled intermediate is available and straightforward gas–solid contact minimises wastewater, aqueous indirect carbonation is preferred when tight pH control, continuous precipitation and particle-size tuning are priorities, accepting added alkali use and solvent-loop management, respectively (DiGiovanni et al., 2024; X. Zhang et al., 2024).

2.3.1.6 Aqueous Indirect Carbonation

Indirect aqueous carbonation retains the Ca-bearing leachate in solution and precipitate $CaCO_3$ through CO_2 sparging or a controlled pH-swing, with the lixiviant regenerated to enable cyclic operation. The attraction is tight control over pH/alkalinity and crystal habit, yielding high-purity PCC with tuneable particle size; the trade-offs are alkali demand, solvent-loop management, and effluent (DiGiovanni et al., 2024; X. Zhang et al., 2024). Figure 2.10 which was amended from Jaschik et al. (2014), summarises this flowsheet: leaching transfers Ca to the liquor, solid-to-liquid separation removes inert residue, the clarified liquor is carbonated with CO_2 to form PCC, and the mother liquor is conditioned and returned to the leach step. This configuration is now common for steel or iron slags and recycled-concrete fines.

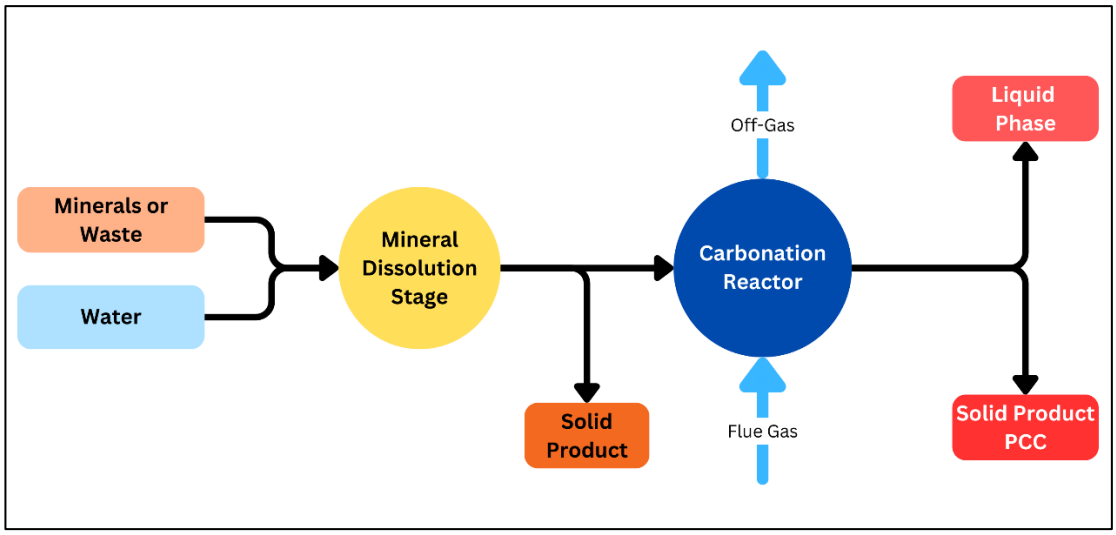


Figure 2.11 Indirect Aqueous Carbonation Process Routes (Amended from Jaschik et al. (2014))

Gasós et al. (2024) demonstrate the crucial of hydrodynamics and contactor design by switching from stirred tanks to a packed-bed increased Ca extraction from recycled concrete aggregates at comparable reagent strength and residence time, which simplified ammonium-nitrate recovery. This eventually improve the downstream liquor-carbonation step. Across lixiviants, ammonium-salt systems such as NH4NO3, NH4Cl or acetate can deliver about 50 to 80% calcium extraction from steelmaking slags at near-2 M and practical solid-to-liquid ratios, enabling a single-salt pH swing with partial recycle (Kohitlhetse et al., 2024). For converter-slag leachates, weak-acid acetic loops remain competitive, where earlier research produces more than 99% of PCC purity with high conversion of dissolved Ca to product, while recent ultrasonic-assisted leaching enhances upstream Ca release while tuning PCC whisker morphology, which is crucial when particle engineering is a objective (L. Liu et al., 2024).

Early industrial activity is now visible. A 100 kg CO_2 h-1 demonstration operated a continuous ammonium-nitrate loop to carbonate calcium-rich liquors into PCC using pure and simulated flue gas, with stable multi-cycle performance provided reagent utilisation and effluents were actively managed (Gasós et al., 2024). Synthesis papers converge on a practical reading: aqueous indirect carbonation is generally preferred when continuous precipitation, product purity and particle-size tuning are priorities, accepting the cost and complexity of the solvent loop; gas–solid paths are chosen when a dry intermediate is preferred and wastewater volumes must be minimised (Biava et al., 2024; S. Wang et al., 2024). Because reported percentages are basis-dependent, for example percent calcium extracted from solid, percent of dissolved

calcium converted to PCC, or kilograms of CO_2 stored per tonne of residue, comparisons are only meaningful when reagent strength, temperature, solid-to-liquid ratio, pH set-points and the measurement basis are stated alongside the metric (DiGiovanni et al., 2024; Gasós et al., 2024)

2.3.1.7 Quantification of CO_2 Uptake & Carbonation Efficiency

Reliable comparison across studies requires clear bases, consistent instrumentation, and transparent calculations. As Bernal et al. (2024) emphasise, metrics and test conditions vary widely across labs and standards, which can obscure like-for-like assessment of the capacity of CO_2 storage. RILEM TC 281-CCC's recent reviews and databases provide the context and pitfalls for interpreting carbonation data in blended and conventional systems. For direct mineral carbonation routes in cementitious mixes (ACC or mixing-water H_2CO_3), the primary figure is the net CO_2 stored per unit binder, often derived from TGA mass losses assigned to portlandite dehydroxylation and carbonate decarbonation, supported by XRD/Rietveld and, where available, carbon analysers or off-gas balances (Namiki et al., 2025; Oh et al., 2024). Recent work shows that well-documented aqueous routes can achieve rapid mineralisation and early strength when pH and dosage windows are respected, yet reported uptake still spans orders of magnitude because studies use different bases and ramps; representative papers show both the promise and the variability (Ferrara et al., 2024; Fu et al., 2024). Indirect mineral carbonation of alkaline residues meanwhile, performance is routinely disaggregated into extraction efficiency (fraction of calcium released to the leach liquor), precipitation efficiency (fraction of dissolved calcium converted to solid carbonate) and an overall specific storage expressed as kilograms of CO_2 per tonne of feedstock. This separation prevents over-interpretation when one step is rate-limiting and is now common in slag and recycled-concrete studies as well as recent engineering demonstrations of continuous loops (Bonfante et al., 2024; Gasós et al., 2024).

Thermogravimetry remains crucial in quantifying carbonate and portlandite by pairing TGA or DTG with XRD reduces mis-assignment when polymorphs overlap. Carbon analysers based on combustion–infrared detection provide a total inorganic carbon cross-check. Off-gas balances or non-dispersive infrared sensors are used during chamber curing, and acidimetric back-titration can validate carbonate content.

Comparative studies evaluate agreement and uncertainty among these methods and give practical advice on specimen conditioning, temperature ramps and calibration to avoid bias (Bui et al., 2023; Kalkreuth et al., 2024; Li et al., 2023; Namiki et al., 2025; Takahashi & Maruyama, 2024). In the present experimental programme, direct CO_2 uptake was not quantified using gas balance, total inorganic carbon analysis or continuous CO_2 monitoring. Instead, the study used pH behaviour, XRD, TGA and SEM-EDX as supporting indicators of hydration-carbonation response. TGA was selected because carbonate-related decomposition can be observed at higher temperature ranges, while XRD and SEM-EDX provide complementary evidence of crystalline phases, elemental distribution and microstructural changes. Therefore, CO_2 uptake discussion in this chapter is used to explain possible mechanisms and literature context, while the experimental interpretation is limited to comparative reaction indicators rather than direct carbon-balance measurement.

2.3.2 Applications of Carbonated Solids

Carbonated solids produced via CO_2–mineral reactions are now used in two practical ways in cement-based systems which are (i) as aggregate substitutes, typically by carbonating RCA or other alkaline granular wastes to densify the adhered paste and plug pores, and (ii) as OPC additives or fillers, by precipitating high-purity $CaCO_3$ (PCC) or stabilising recycled concrete fines for partial cement replacement. Both routes can improve early mechanical performance and durability when the process window is controlled, while delivering measurable CO_2 uptake. Reviews and recent demonstrations agree that property gains depend on feedstock chemistry, particle grading, CO_2 delivery, moisture state, and curing or programme specifics rather than a universal method (Bernal et al., 2024; X. Liu et al., 2024; Vollpracht et al., 2024). Table 2.2 summarises representative applications, claimed effects, and common restriction.

Table 2.2
Applications of Carbonated Solids in Cementitious Systems

Application	Feedstock & Route	Illustrative window	Measured outcomes	Sources
Pre-carbonated recycled aggregates	Recycled concrete aggregates	Controlled CO_2, moisture and exposure time	Water absorption reduced by 10 to 30% Compressive strength maintained	(Izoret et al., 2023; Shuvo et al., 2024; Torrenti et al., 2022; Zhang et al., 2025)

Application	Feedstock & Route	Illustrative window	Measured outcomes	Sources
	Chamber or wet carbonation before batching		or increased at 3–28 days Denser Interfacial Transition Zone (ITZ) by SEM or XRD.	
Carbonated recycled fines as SCM or filler	Recycled paste/mortar fines Direct gas–solid or aqueous carbonation	Mild temperature Defined CO_2 dose or pH window	Earlier hydration and lower transport at modest replacement Dilution risk at high dosages.	(Torrenti et al., 2022; S. Wang et al., 2024)
PCC from indirect mineralisation (filler)	Ca-rich residues (for example, slags or ashes) Leach carbonate regenerate loop	pH-swing precipitation with CO_2 sparging Solvent recycles	High-purity PCC with tuneable particle size Mechanical parity or gains as filler.	(DiGiovanni et al., 2024; Gasos et al., 2024)

Evidence at scale now exists where for aggregates, research showed that accelerated carbonation of recycled concrete aggregates can improve aggregate quality and be used in ready-mix production; two industrial demonstrators validated the concept in plant settings (Izoret et al., 2023; Torrenti et al., 2022). Wet-carbonation trials on returned or recycled aggregates report sizeable drops in water absorption within hours and associated improvements in concrete made with the treated aggregates; for example, Shuvo et al. (2024) report a clear reduction after two hours of treatment. A recent synthesis concludes that concretes with carbonated recycled aggregates generally outperform those with untreated recycled aggregates on durability indicators, although natural-aggregate concretes still set the upper bound unless mixture design and curing are carefully controlled (Zhang et al., 2025). For additives and fillers, indirect mineralisation pilots have produced high-purity precipitated $CaCO_3$ at continuous throughputs of approximately one hundred kilograms of CO_2 per hour with solvent-loop stability over multiple cycles, indicating practical readiness for filler use in cementitious composites (Gasos et al., 2024). Method comparisons consistently warn that headline percentages are not comparable unless the basis and operating window are stated alongside the metric (DiGiovanni et al., 2024).

2.3.2.1 Aggregate Substitutes

Pre-carbonation of RCA is used to densify the adhered paste, cut open porosity and stabilise the interfacial transition zone (ITZ) before batching. Industrial

demonstrators and follow-on plant trials show that controlled exposure to carbon dioxide upgrades RCA quality and can be implemented at scale with conventional handling (Izoret et al., 2023; Torrenti et al., 2022). Systematically, carbonate precipitation forms a tighter, carbonate-rich skin on the residual paste and bridges microcracks. Figure 2.12 illustrates this surface densification clearly, which underpins the observed drops in water absorption and the stronger ITZ in downstream concretes which was adopted from Mo et al. (2020).

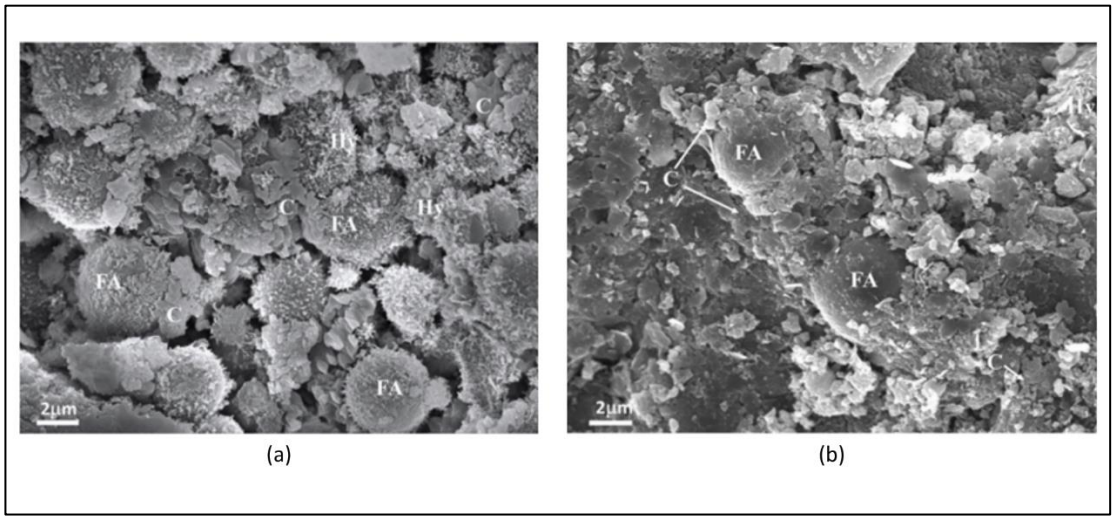


Figure 2.12 SEM images of CRA from Steel Slag: (a) Uncarbonated and (b) Carbonated (Adopted from Mo et al. (2020))

Quantitatively, the magnitude is now well documented. According to Bergmans et al. (2024), most pre-carbonation protocols deliver approximately 20 to 30% reductions in RCA water absorption at fixed grading and test basis. Short wet-carbonation steps can already move the needle as Shuvo et al. (2024) reported a 12.2% reduction after 10 minutes on returned-concrete aggregates, while extended wet-carbonation windows achieved larger effects, with (Shuvo et al., 2025) discovers 25.8% of reduction and associated strength gains in the concretes made with treated aggregate. Beyond absorption, durability indicators also trend positively when design variables are controlled. Zhang et al. (2025) reviews chloride and gas-transport results showing that concretes with carbonated RCA approach or exceed mixes with untreated RCA, and a synthesis by Alibeigibeni et al. (2025), highlights the reduced chloride penetration depths in carbonated-RCA concretes. For fine recycled aggregates, a recent comparative study reports the largest absorption decreases under wet carbonation, particularly for fines (Zhong et al., 2025). As summarised in Figure 2.13, wet

carbonation typically lowers 24-hour water absorption of RCA by about 20–30%, with study-specific outcomes spanning roughly 12% to 38% depending on grading and treatment duration (Bergmans et al., 2024; Hadjari et al., 2025; Shuvo et al., 2024, 2025; Zhong et al., 2025).

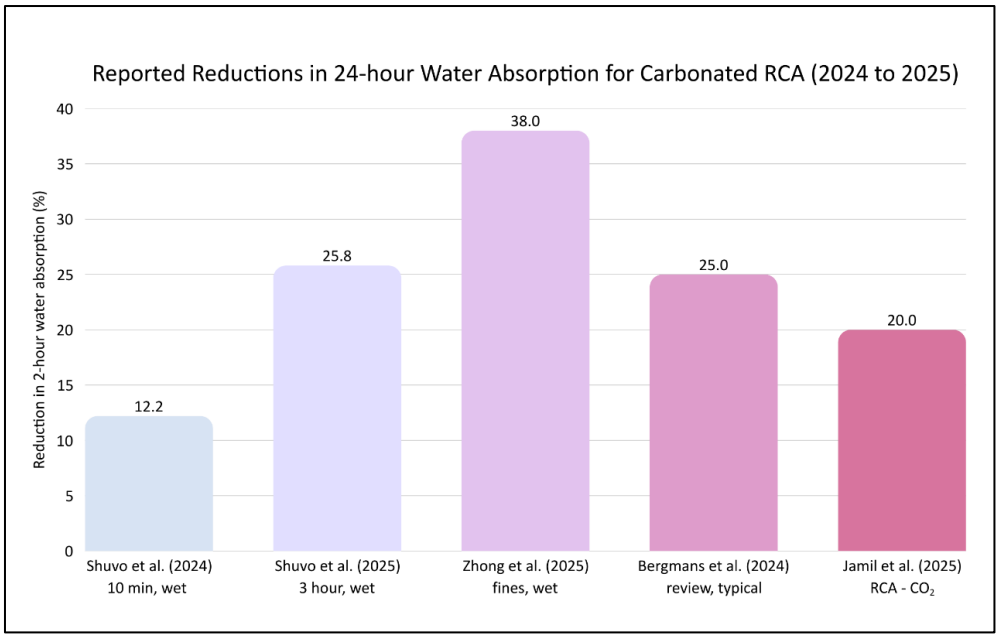


Figure 2.13 Reported 24-hour Water-Absorption Reductions for Carbonated RCA Relative to Untreated RCA

Although carbonated recycled aggregates and aggregate substitutes are relevant to broader CO_2 utilisation in concrete, their role in this thesis is only contextual. The present experimental programme uses OPC paste without fine or coarse aggregates; therefore, the main transferable concept from these studies is that carbonate formation and pore refinement can influence water absorption, density and mechanical performance.

2.3.2.2 OPC Additives and Fillers

Calcium-carbonate family additives used with OPC operate primarily through three coupled mechanisms: a physical filler effect that improves particle packing, an early-age nucleation effect that accelerates hydration, and a chemical effect that steers aluminate–sulphate reactions toward carboaluminate formation rather than monosulphate. De Weerdt et al. (2011) showed that fine limestone promotes monocarbonate formation in ternary cements and contributes to strength by refining the

hydrate assemblage. Reports discovers that limestone contents increased up to about 15% in Type IL or Portland Limestone Cement (PLC) cements are now common practice, with performance governed by fineness relative to clinker and by the full particle size distribution rather than by a single Blaine value (Tennis et al., 2011). Current standards frame the allowable ranges whereby EN 197-1 defines CEM II/A-L and CEM II/B-L at roughly 6 to 20% and 21 to 35% limestone, respectively. EN 197-5 extends the family to multi-component cements, provided conformity testing verifies strength and durability (EN, 2011, 2021).

Table 2.3
Compact Ranges & Efect of $CaCO_3$ Family Additives in OPC

Additive	Typical dosage	Main mechanism & outcome	Sources
$CaCO_3$	• 5 to 20% in PLC • Higher in CEM II/B-L and CEM II/C-M with verified performance	• Filler + nucleation promotes carboaluminate formation • Earlier strength and refined pores when fineness matches clinker • High, coarse replacement risks dilution and faster carbonation	(Benjeddou et al., 2021; De Weerdt et al., 2011; Tennis et al., 2011)
PCC	2 to 10%	• Tailored morphology and sub-5 µm size give strong nucleation, workability tuning, early strength. • Requires sulphate balance and admixture compatibility.	(DiGiovanni et al., 2024; Li & Cao, 2024; Photong & Pragot, 2022)
$CaMg(CO_3)_2$	5 to 15% (system-dependent)	• Similar filler–nucleation benefits • Mg content can affect rheology and late-age behaviour. • Moderate dosages densify matrix, high dosages dilute.	(Divekar & Sawant, 2023; Kumar & Prabagharb, 2023)

PCC differs from ground $CaCO_3$ because morphology and size can be tailored at synthesis, which allows tuning of workability and early strength. Photong and Pragot (2022) reported that monohydrocalcite additions modify microstructure and can improve mechanical response when dosed judiciously. Industry-focused work on PCC from carbon-mineralisation loops shows that producing scalenohedral or rhombohedral PCC with sub-5 µm median size tends to raise early strengths and reduce permeability at low dosages, provided sulphate balance is maintained (DiGiovanni et al., 2024). Nano-$CaCO_3$ and micro-$CaCO_3$ likewise notes that performance hinges on coupling particle size with admixture demand and on reporting both specific surface and size distribution so that results are comparable across studies (Qiu et al., 2024).

$CaMg(CO_3)_2$ functions as a mixed carbonate filler where Mg-bearing phases may affect rheology and late-age behaviour. Recent studies indicate that moderate

dolomite dosages can densify the matrix and sustain or improve strength, while excessive replacement introduces dilution penalties; outcomes depend on fineness, the aluminate–sulphate balance, and curing (Akhil et al., 2024; Chen et al., 2022). For systems where carbon dioxide is introduced via carbonic acid in the mixing water, finely divided $CaCO_3$ or $CaMg(CO_3)_2$ can also buffer acidity and provide abundant nucleation sites for early C-S-H and carbonate precipitation, while the same fineness–dosage window applies. When positioning $CaCO_3$-family additives as OPC fillers, it is essential to report at minimum the percentage by mass of binder, the full particle size distribution or a D50 plus Blaine, the water-to-binder ratio, sulphate content, and any use of carbonated mixing water, because these parameters co-determine whether the net effect is acceleration and pore refinement or dilution and later-age loss of strength (De Weerdt et al., 2011; Tennis et al., 2011). Table 2.3 condenses typical dosage and fineness ranges that have produced positive outcomes in peer-reviewed studies, alongside the reporting items needed for reproducibility.

2.3.3 Accelerated Carbonation Curing (ACC)

ACC is a chamber-based, early-age process in which fresh or demoulded cementitious products are exposed to a specified CO atmosphere under controlled relative humidity, temperature, and time so that a portion of the CO_2 mineralises as calcium carbonate while hydration continues. Contemporary reviews and committee recommendations position ACC as a distinct curing route with gas-phase transport control and typical operating ranges spanning low to pure CO_2, moderate humidity, ambient to moderately elevated temperature, and pressures up to a few bar depending on equipment and product format. When scheduled appropriately for the binder and moisture state, ACC can shorten curing cycles while delivering comparable or superior early performance relative to conventional moist or steam curing (Li et al., 2022; Pu et al., 2023; Yao et al., 2023).

Evidence from independent experiments converges on rapid early responses: measurable CO_2 uptake, densification of the near-surface zone, and significant early strength gains. He et al. (2023) reported about a 47% increase in early compressive strength for pastes subjected to chamber carbonation, with microstructural analyses linking the gains to finely divided $CaCO_3$ precipitation and pore refinement. Broader performance syntheses indicate that these benefits persist when chamber schedules are

matched to mixture chemistry and moisture history, although durability indicators still require verification because chamber curing alters pH and moisture trajectories versus standard regimes (Guleria et al., 2024; Vollpracht et al., 2024).

Two variables are repeatedly highlighted as decisive which are (i) moisture state at the start of CO_2 exposure and (ii) the pre-hydration interval before chamber entry. Zhang et al. (2018) showed that delaying chamber exposure from 0 to 71 hours reduced net CO_2 uptake while mass gain trends reflected evaporation driven by reaction heat, emphasizing that the level of carbonation significantly influences the storage capacity. Current recommendations ask researchers to report, at minimum, CO_2 concentration or partial pressure, relative humidity, temperature, exposure time, pre-conditioning and pre-hydration details, mix design, and sample geometry, because these govern comparability and scale-up (Bernal et al., 2024; Merah, 2024; Yao et al., 2023). In practical terms, ACC may shorten the curing cycle because early carbonation can rapidly form calcium carbonate and densify the near-surface matrix, allowing certain precast products to reach handling or demoulding strength earlier than conventional curing. However, this benefit depends strongly on CO_2 concentration, moisture condition, exposure duration and binder composition. If the process is not controlled, surface densification may restrict later hydration or create non-uniform carbonation. Therefore, ACC is useful as a comparative CO_2 utilisation route, but it is not the main focus of this thesis. The present work emphasises aqueous CO_2 incorporation during mixing because this route can be evaluated through batching pH, precursor replacement and ambient curing without requiring a carbonation chamber.

2.3.3.1 Process Configurations and Operating Windows

Process windows in accelerated carbonation curing are defined by the pre-hydration age before exposure, gas composition and pressure, relative humidity and temperature in the chamber, and the total exposure schedule. In ACC, rate control sits with gas–solid transport and the surface moisture state; too dry limits CO_2 dissolution, too wet blocks pores. Reviews and test-method papers consistently show that performance depends on keeping moisture in an optimal band, managing CO_2 dosage and timing the exposure relative to early hydration, rather than simply maximising any single variable (Bernal et al., 2024; Merah, 2024; Zhang et al., 2017).

Zhang et al. (2018) demonstrated that pre-hydration age is decisive: very early exposure can densify the surface layer and hinder continuing hydration, whereas short pre-hydration periods which hours up to roughly one day, often balance uptake with strength. Typical CO_2 contents span 10 to 100% in laboratory rigs, but viable curing has also been shown with flue gas around 15 to 20% CO_2 at ambient pressure when exposure time is extended and cycling is used. Liu et al. (2022) reported larger 12-hour strength and uptake with flue gas compared with pure CO_2 in their set-up. Relative humidity is commonly maintained in a mid-range to keep surfaces wet yet air voids open. Merah (2024) recommend controlling moisture rather than targeting a single RH value because mix design and pre-hydration age shift the optimum. Temperature is usually near room temperature to moderate heat release and avoid drying, although 30 to 60 °C can accelerate reactions if moisture is controlled (Li et al., 2024; Liyew et al., 2024). Exposure time is typically minutes to a few hours for pastes and small elements, scaling longer for denser or larger products (Zhang et al., 2017). Gas purity is a design choice whereby pure CO_2 simplifies mass balance, while flue gas reduces energy for purification and compression at the cost of slower early rates (Liu et al., 2022). Figure 2.14 illustrates the flow-through in continuous gas feed and vent, and enclosed in sealed-chamber configurations that underpin these operating windows.

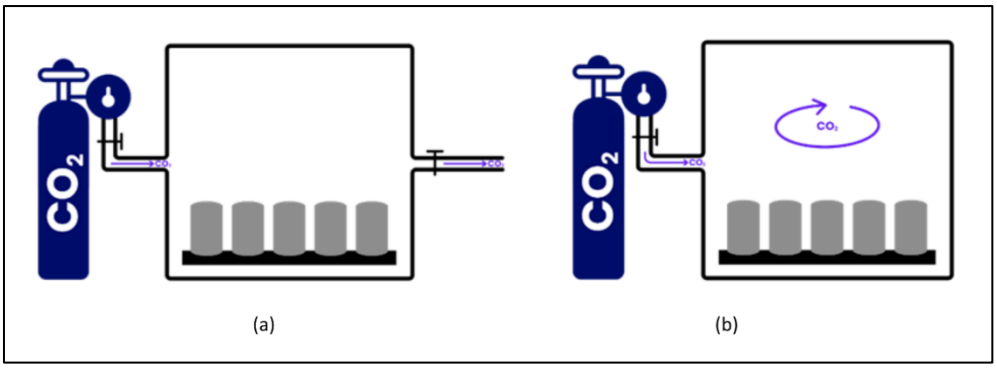


Figure 2.14 Carbonation Reaction System: (a) Flow-Through Reactor and (b) Enclosed Reactor (Adopted from Liu And Meng (2021))

Scheduling can be one continuous exposure or stepped or pulsed. Recent engineering studies show that pulsed or pressure-swing schedules improve conversion without additional reagents by intermittently refreshing the CO_2 gradient and relieving product-layer diffusion limits. Ho and Iizuka (2025) report higher overall conversion with pressure cycling in slag systems. For plant-oriented precast work, a common baseline is short pre-hydration followed by exposure at controlled moisture and CO_2,

then conventional curing, with set-points tuned to the product and mix (Padmalal et al., 2024). Where cost or simplicity dominates, ambient-pressure flue-gas ACC has been validated for paste and concrete with comparable 28-day strength to pure-gas curing under matched windows (Liu et al., 2022). Figure 2.15 shows that CO_2 uptake falls steadily as pre-carbonation hydration increases from 0 to 71 h, while mass gain peaks near one day and then declines. PLC starts with higher uptake at 0 h but converges with OPC by 71 h (Zhang et al., 2020).

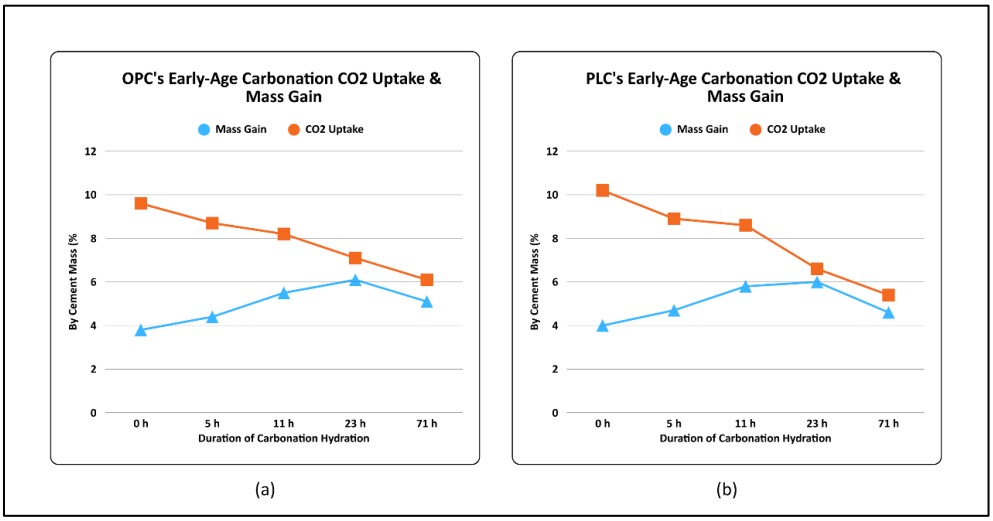


Figure 2.15 Early-Age Carbonation Mass Gain and CO_2 Uptake on Cement Mortar Sample: (a) OPC and (b) PLC (Adopted from Zhang et al. (2020))

2.3.3.2 Early-Age Reaction Mechanisms Under ACC

At early age, ACC proceeds by gaseous CO_2 entering the capillary network, dissolving into the pore solution and speciating as carbonic acid, bicarbonate and carbonate; in parallel, calcium-bearing phases (notably portlandite and the outer hydration layers of C_3S/C_2S) supply Ca^{2+} to solution. Where Ca^{2+} meets CO_3^{2-}, fine calcium-carbonate nuclei form and grow while ordinary hydration continues. A widely used mechanistic summary shows the sequence of gas ingress, dissolution or speciation, Ca mobilisation and $CaCO_3$ nucleation with possible near-surface densification when exposure is aggressive which is illustrate in Figure 2.16 which amended from Bertos et al. (2004). Tracer experiments at low CO_2 concentration corroborate this chain, capturing the early dissolution of portlandite and rapid precipitation of calcite in the

first hours of curing (Chen et al., 2024). The net portlandite reaction is often expressed as:

$$CaOH + CO_2 \rightarrow CaCO_3 + H_2O \quad (2.5)$$

Kinetically, three (3) influential factors are moisture state, CO_2 supply and pre-hydration age. Relative humidity in the mid-range keeps surfaces wet while leaving air pathways open; reviews recommend controlling internal moisture rather than a single fixed value, with effective bands commonly reported between roughly 50% and 75% depending on mix and age (Merah, 2024). CO_2 concentration and exposure schedule matter because product layers can passivate the surface; stepped or pulsed schedules maintain a concentration gradient and limit dense skins.

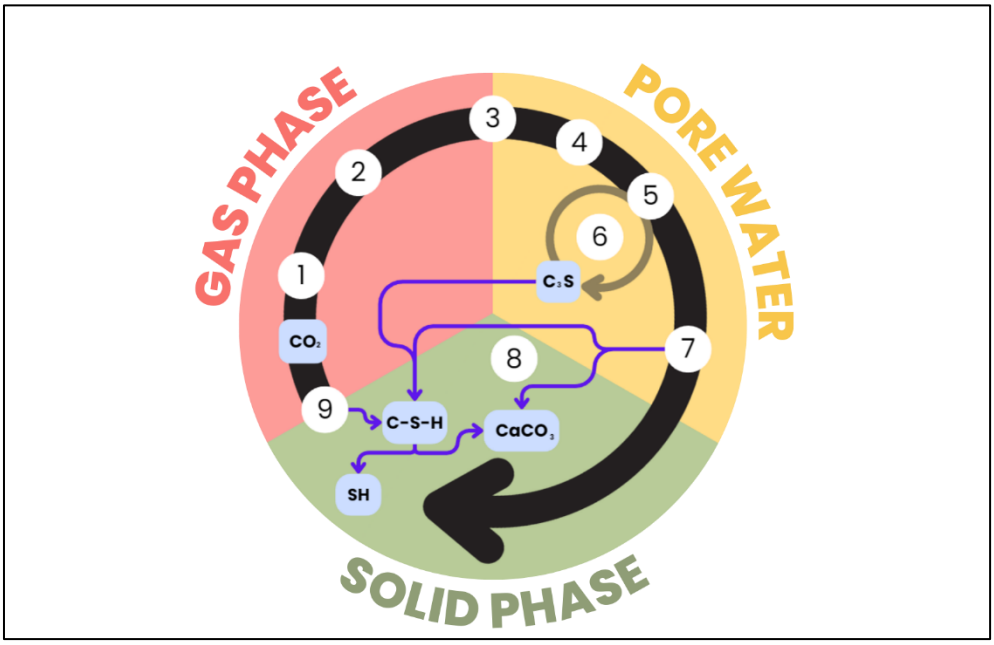


Figure 2.16 Early Age ACC Mechanism Schematic (Adopted from Bertos et al. (2004) with Minor Modification)

Very early exposure can over-densify the surface and hinders continuing hydration, whereas short pre-hydrates often balance uptake with strength, as reported by (Zhang et al., 2020) and confirmed in later optimisation studies for pastes and mortars (Chen & Gao, 2019; Padmalal et al., 2024). Temperature is usually near room temperature to moderate heat release and avoid drying, although modest heating can accelerate reactions if moisture is maintained (Li et al., 2024).

Systematic interpretations re quired to be anchored in measurements that separate true CO_2 uptake from mass changes caused by water movement. TGA able to quantify portlandite consumption and carbonate formation when the mass-loss intervals are assigned with care, and XRD confirms carbonate polymorphs and residual CH. Figure 2.15 shows that TGA-based uptake decreases as pre-hydration increases from 0 to 71 h, while mass gain peaks around one day and then declines, consistent with heat-related water loss at very early age and milder carbonation later (Zhang et al., 2020). Recent standardisation work recommends reporting CO_2 concentration, relative humidity, temperature, pre-hydration time and the analytical basis alongside any mechanistic claims because these variables shift the reaction pathway and the risk of over-carbonation (Bernal et al., 2024).

2.3.3.3 Effects on Hardened & Fresh Properties Under ACC

Early-age exposure to CO_2 modifies fresh behaviour by shifting the balance between hydration and near-surface carbonation. Mixtures typically show shorter setting and reduced bleeding when internal moisture is kept high enough for ion transport while air pathways remain open; if exposure is too aggressive at very early ages, a dense carbonate skin can form that impedes continuing hydration. Practice-focused reviews recommend managing moisture and gas delivery rather than targeting one relative-humidity value, due to the optimum window shifts with mix design and pre-hydration age (Liyew et al., 2024; Lu et al., 2021; Merah, 2024). Very early exposure has been observed to over-densify the skin, whereas short pre-hydrates of hours to about a day often balance uptake with workable fresh behaviour (Zhang et al., 2018).

On hardened performance, ACC commonly delivers pronounced early-age strength gains when carbon-dioxide content, exposure time, temperature and moisture are tuned. As shown in Figure 2.17, early-age compressive strength of OPC and PLC increases rapidly under early-age carbonation, with the magnitude controlled by binder chemistry and the curing schedule. The dataset depicts that across 0 to 71 hour of pre-hydration interval, the carbonated mortars reached 13 to 17 MPa, and 11 to 20 MPa, for OPC and PLC respectively, while the non-carbonated were approximately lesser than 9 to 13 MPa. This concludes that the strength gap is largest at very short pre-hydrates and narrows as conventional hydration proceeds (Xian, Logan, et al., 2022). Laboratory

studies report improvements across 4 to 24 hours exposures and a range of carbon-dioxide concentrations when moisture is controlled (Kim et al., 2023), and ambient-pressure curing with flue gas at about 15 to 20% CO_2 is viable when exposure is extended or cycled, although early rates are slower than with pure gas (Liu et al., 2022). Conversely, if pre-hydration is too short or moisture falls, surface densification can suppress later hydration and depress longer-age strength, underscoring the importance of scheduling and moisture control (Qin et al., 2018).

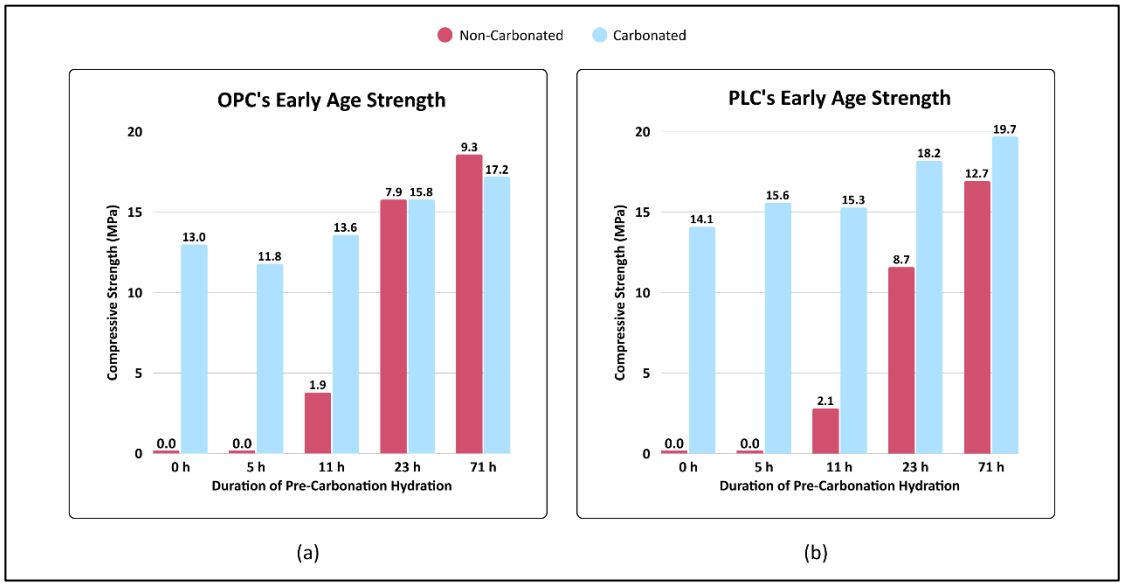


Figure 2.17 Early-Age Carbonation Compressive Strength in Mega Pascal (MPa) on Cement Mortar Sample: (a) OPC and (b) PLC (Adopted from Xian, Logan, et al. (2022))

2.3.3.4 Microstructure and Durability Considerations

The incorporation of CO_2 in the aqueous phase during mixing modifies the microstructural development of OPC pastes by simultaneously influencing hydration and carbonation pathways. Dissolved CO_2, present predominantly as H_2CO_3, reacts with calcium hydroxide ($Ca(OH)_2$) released during early hydration, yielding finely dispersed $CaCO_3$ that precipitates within pores and at the ITZ. Dissolved CO_2, present predominantly as H_2CO_3, reacts with $Ca(OH)_2$ released during early hydration, yielding finely dispersed $CaCO_3$ that precipitates within pores and at the ITZ. This reaction not only refines pore connectivity but also enhances the packing density of the C–S–H gel (Fu et al., 2024). Figure 2.18 of SEM images revealed carbonate deposition progressively filling voids and reducing porosity. CO_2 injections were quantified in terms of standard cubic centimetres (scc), corresponding to the volume of gas

introduced under standard conditions. At 2000 scc, needle-like $CaCO_3$ precipitates were evident on particle surfaces, initiating pore refinement, while at 4000 scc the crystal deposition became denser and more interlocked, indicating intensified carbonation and greater microstructural consolidation. These features are consistent with the early precipitation of amorphous calcium carbonate (ACC), which subsequently stabilises into crystalline polymorphs, thereby reinforcing the microstructure and improving durability potential. Rostami et al. (2012) further confirmed, via SEM and Nuclear Magnetic Resonance (NMR) analyses, that C–S–H phases became intermixed with carbonate products, forming a secondary amorphous calcium–silicate–hydrocarbonate binding phase. Such alterations lead to a more cohesive microstructure at early ages, characterised by reduced microcrack initiation points and improved ITZ densification. The precipitation pathway can be simplified by the following fundamental reaction:

$$Ca(OH)_2 + H_2CO_3 \rightarrow CaCO_3 + 2H_2O \quad (2.6)$$

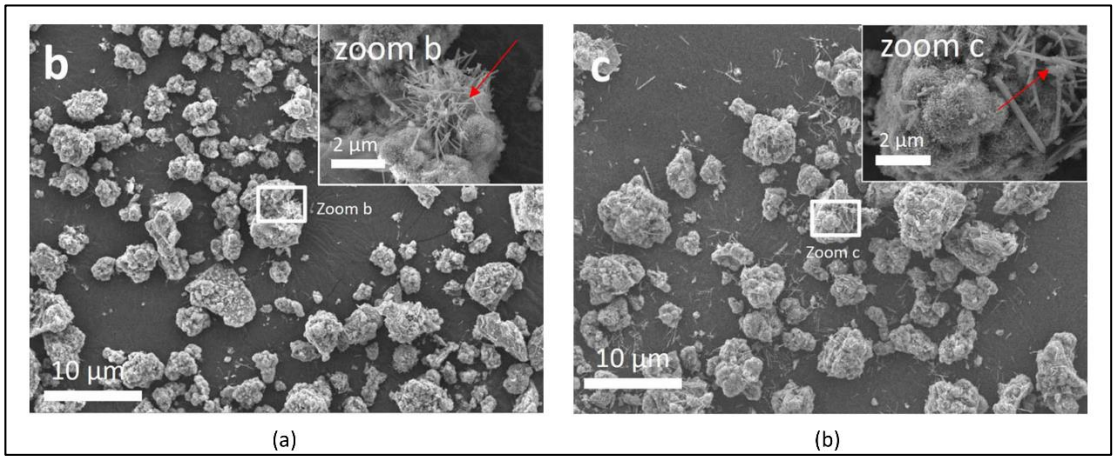


Figure 2.18 SEM Images of Carbonated Cement Suspensions with CO_2 Injection of (a) 2000 scc and (b) 4000 scc, Showing Progressive $CaCO_3$ Crystal Deposition and Pore Refinement (Adapted from Fu et al. (2024))

$$C_3A+CaCO_3+12H \rightarrow C_3A\cdot CaCO_3\cdot 11H \quad (2.7)$$

Over prolonged curing, polymorph stability becomes a critical factor for durability. Studies by Silva et al. (2022) revealed the sequential transformation of amorphous calcium carbonate (ACC) and metastable vaterite into calcite, accompanied by changes in the Ca or Si ratio of the C–S–H gel as shown Figure 2.19. The presence of calcite not only provides long-term thermodynamic stability but also promotes

secondary reactions with aluminate phases. Lu et al. (2021) reported that $CaCO_3$ interacted with C_3A to form mono-carboaluminate hydrates, further refining the pore structure and stabilising the hydration assemblage, as expressed in Equation 2.7. These transformations collectively reduce permeability and improve dimensional stability. Empirical durability tests corroborate these microstructural benefits. (Song et al., 2021) observed significant reductions in chloride diffusivity in carbonated pastes, while Monkman et al. (2022) demonstrated that concretes incorporating CO_2-treated wash waters retained or improved resistance to chloride ingress, freeze–thaw cycling, and drying shrinkage compared with conventional mixes. Interestingly, Xian, Logan, et al. (2022) documented an initial shrinkage followed by mild expansion and secondary shrinkage under early-age carbonation, suggesting that dimensional responses are transient but ultimately contribute to better resistance against long-term carbonation ingress.

2.3.4 CO_2 as Supersaturated Aqueous Solutions

Delivering CO_2 as a supersaturated aqueous phase, where CO_2 dissolved under pressure to form H_2CO_3, enables uniform contact between dissolved inorganic carbon species and cementitious ions during mixing, rather than relying on gas–solid transport at early ages. Under supersaturation, the dissolved CO_2 partitions as H_2CO_3, HCO_3^-, and CO_3^{2-} according to acid–base equilibrium, which depends on pH and temperature. This is due to the aqueous concentration governed at first order by Henry's law as shown in Equation 2.8, with temperature-dependent k_H values well established by (Sander, 2023). In alkaline pore solutions, the rapid reaction of H_2CO_3/HCO_3^- with portlandite forms finely divided $CaCO_3$ that acts as nucleation sites for C–S–H, promoting early densification and more homogeneous carbonate distribution than chamber carbonation as shown in Equation 2.9, 2.10, and 2.11 (Kwasny et al., 2014; Millero et al., 2002; Suescum-Morales et al., 2022). Emerging CO_2-nanobubble waters further enhance gas hold-up and interfacial area, reporting additional strength gains and suppressed carbonation shrinkage compared with conventional water, supporting the process-intensification angle of the aqueous route (Choi et al., 2024).

$$C_{aq}A = k_H pCO_2 \tag{2.8}$$

$$CO_{2(aq)} + H_2O \rightleftharpoons H_2CO_3 \quad (2.9)$$

$$H_2CO_3 \rightleftharpoons H^+ + HCO_3^- \quad (2.10)$$

$$Ca(OH)_2 + H_2CO_3 \rightarrow CaCO_3 + 2H_2O \quad (2.11)$$

Studies shows that replacing conventional mixing water with supersaturated CO_2 water enhances early hydration and compressive strength, provided CO_2 doses are carefully controlled. Kwasny et al. (2014) demonstrated that mixing mortars with carbonated water improved strength and porosity compared with controls, while Suescum-Morales et al. (2022) reported up to a 181% increase in CO_2 uptake and measurable gains in strength for mortars with recycled aggregates when carbonated water was used. Nanobubble CO_2 water was discovered to achieving higher strength gains and carbonation efficiency due to improved gas retention and interfacial area (Choi et al., 2024). Monkman et al. (2022) extended the concept to industry by showing that CO_2-beneficiated wash water mineralises suspended fines into $CaCO_3$ without durability penalties, even improving chloride resistance and dimensional stability. A closely related line of work by Lippiatt and co-authors deliberately combined hydration and carbonation by using super-saturated aqueous CO_2 solutions as mixing water. Their results demonstrated that the simultaneous supply of H_2CO_3, HCO_3^-, or CO_3^{2-} to fresh cement pastes promotes early nucleation of $CaCO_3$, refining pores and densifying the matrix. Importantly, they highlighted the need to balance solution acidity with dissolved inorganic carbon availability: while adequate CO_2 enhances nucleation and early densification, excessive acidity risks delaying hydration (Lippiatt & Ling, 2020; Lippiatt et al., 2019).

According to Figure 2.19, Ferrara et al. (2024) illustrated a typical schematic for aqueous CO_2 sequestration, where cement powder is suspended in H_2O and subjected to controlled CO_2 injection. The process involves gas dissolution into the liquid phase followed by mineralisation reactions with Ca-bearing phases, ultimately leading to the precipitation of $CaCO_3$. This schematic is broadly representative of direct aqueous carbonation methods, as the fundamental mechanism such as CO_2 dissolution, speciation, and reaction with $Ca(OH)_2$, is common across similar studies. However, this approach is adapted by preparing supersaturated CO_2 water in advance and using it directly as mixing water for mortar production. This modification enables carbonation and hydration to occur simultaneously during mixing, while also allowing investigation

of the additional role of dolomite and limestone in stabilising carbonate phases and enhancing durability performance.

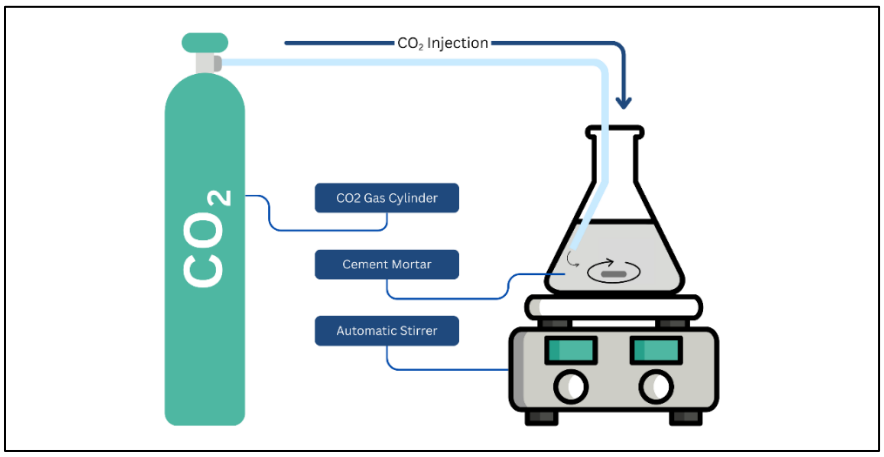


Figure 2.19 Experimental setup for CO_2-Supersaturated Aqueous Solution Preparation (Adapted and Amended from Ferrara et al. (2024) with Minor Modifications)

2.3.4.1 Mechanistic Framework

Supersaturated CO_2 water shifts the earliest reactions into a liquid-phase regime whereby dissolved inorganic carbon species present at mixing $CO_2(aq)$, H_2CO_3, HCO_3^- and CO_3^{2-}, are fixed by Henry's relation and the carbonic equilibria shown in Equations 2.9 and 2.10. When this preloaded solution contacts fresh paste, H_2CO_3, or HCO_3^- neutralise against portlandite, precipitating finely divided $CaCO_3$ as in Equation 2.11. The crystallites act as preferential nucleation sites for C–S–H, reducing the induction period and compacting the interfacial transition zone provided the solution pH is moderate and the water is used immediately after pre-saturation (Millero et al., 2002; Sander, 2023; Suescum-Morales et al., 2022).

As shown in Figure 2.20, CO_2 uptake rises rapidly during the first ten to twenty minutes and then transitions to a gradual approach to an asymptote at about forty minutes Ferrara et al. (2024). The steep rise reflects liquid-phase availability and interfacial neutralisation captured by Equation 2.8 whereby the slower tail corresponds to a shift to silicate-dissolution control once portlandite is consumed, consistent with Equation 2.11. This justifies a finite pre-saturation and prompt use of the CO_2-charged water: most of the kinetic gain is realised on the rising limb, while pursuing additional uptake near the asymptote adds little and increases the risk of over-acid conditions that

can form inhibiting films and depress strength (Suescum-Morales et al., 2022). Over-dosing or excessively low pH can retard clinker dissolution and reduce strength; the operating window used here therefore targets moderate pH, sensible pre-saturation, and immediate mixing, aligning the mechanism with the kinetic envelope (He et al., 2017).

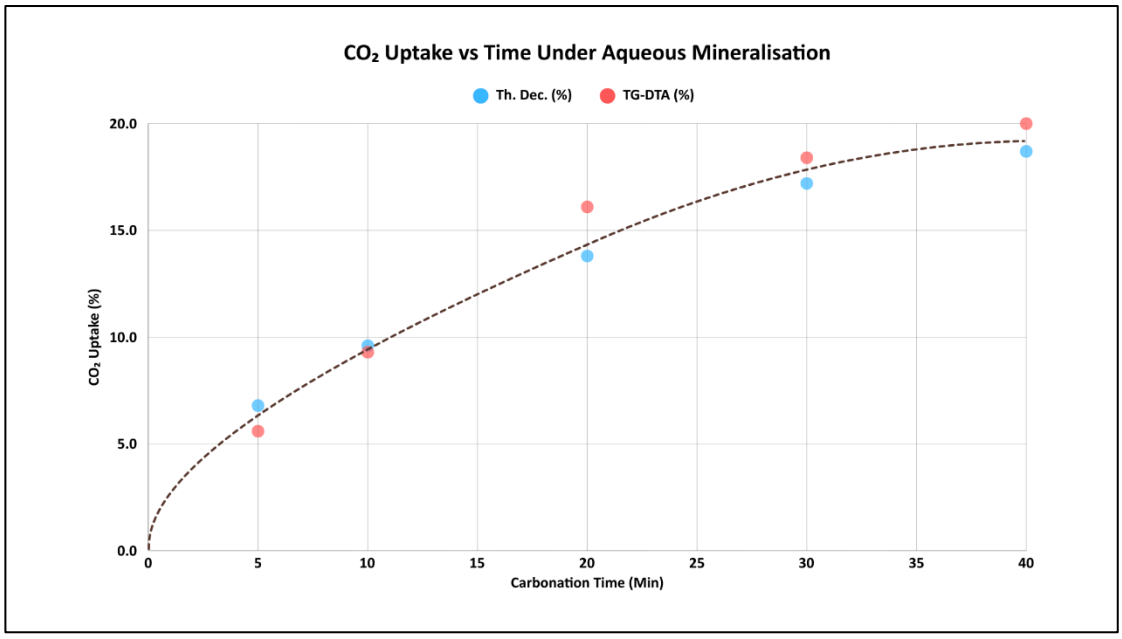


Figure 2.20 CO_2 Uptake Versus Carbonation Time Under Aqueous Mineralisation (Adapted and Amended from Ferrara et al. (2024)

pH bands and CO_2–water residence times to three (3) outcomes discussed in the liquid-phase neutralisation rate which are $CaCO_3$ nucleation density, and risk of hydration interference, using a 0 to 3 evidence rubric as mapped in Table 2.4. Value of 0, 1, 2, and 3 denotes negligible or inconsistent evidence, moderate, strong and recurring, and excessive or adverse outcomes consistently noted respectively. The scoring is anchored to the kinetic envelope in Figure 2.20 and to boundaries documented across studies. For example, the band pH 3.0 to 3.4 is frequently associated with rapid neutralisation and appreciable nucleation but also with elevated risk of hydration interference due to early carbonate films (He et al., 2017). By contrast, pH 3.5 to 5.0 is repeatedly reported as balancing neutralisation and nucleation with only mild interference, where most uptake benefit is realised (Ferrara et al., 2024; Kwasny et al., 2014).

Table 2.4
Reported Operating Ranges for Supersaturated CO_2 Mixing Water (0 to 3 Evidence Rubric)

Setting	Neutralisation Rate	Nucleation Density	Hydration Interference Risk	Source
pH 3.0 to 3.4	3	2	3	He et al. (2017)
pH 3.5 to 5.0	2	2	1	Kwasny et al. (2014)
pH 5.1 to 6.0	1	1	0	Suescum-Morales et al. (2022)
Residence 1 to 3 min	1	1	0	Ferrara et al. (2024)
Residence 5 to 10 min	2	2	1	Ferrara et al. (2024)
Residence more than 15 min	2	1	1	Ferrara et al. (2024)

Across studies, lower pH consistently accelerates liquid-phase neutralisation and increases early $CaCO_3$ precipitation, but excessive acidity elevates hydration interference through surface films; mid pH bands balance seeding with limited disruption, while higher pH reduces seeding efficacy yet is safest for hydration. Residence time primarily governs how closely dissolved CO_2 approaches its Henry-law capacity and, the rising portion of the uptake curve is captured before diminishing returns set in.

2.3.4.2 Fresh & Hardened Properties

Introduction of CO_2 into a water-bearing cementitious system is governed by dissolved inorganic carbon speciation and rapid equilibration within a highly alkaline pore solution. Under these conditions, dissolved CO_2 is quickly converted into bicarbonate or carbonate species and can promote early precipitation of Ca-carbonate phases once sufficient Ca^{2+} becomes available, rather than remaining predominantly in dissolved form. This aligns with carbonation frameworks that describe mineral carbonation in cementitious matrices as a dissolution–precipitation process that is sensitive to pore-solution alkalinity, ionic strength, and Ca availability (Ahmed et al., 2024; Silva et al., 2023; Davolio et al., 2025). Quantitative descriptor frequently used to indicate the extent of reaction is CO_2 uptake, defined as the fraction of CO_2 retained

or fixed within the reacting system. Across carbonation-mixing datasets, reported uptake values are commonly within the low-percent range by binder mass, yet the corresponding mechanical response exhibits substantial variability. This indicates that uptake alone is insufficient for performance prediction unless interpreted alongside complementary descriptors such as reaction extent, spatial distribution of carbonate products, and the degree to which hydration continuity is preserved (Davolio et al., 2025; Ravikumar et al., 2021; Shaqraa et al., 2024).

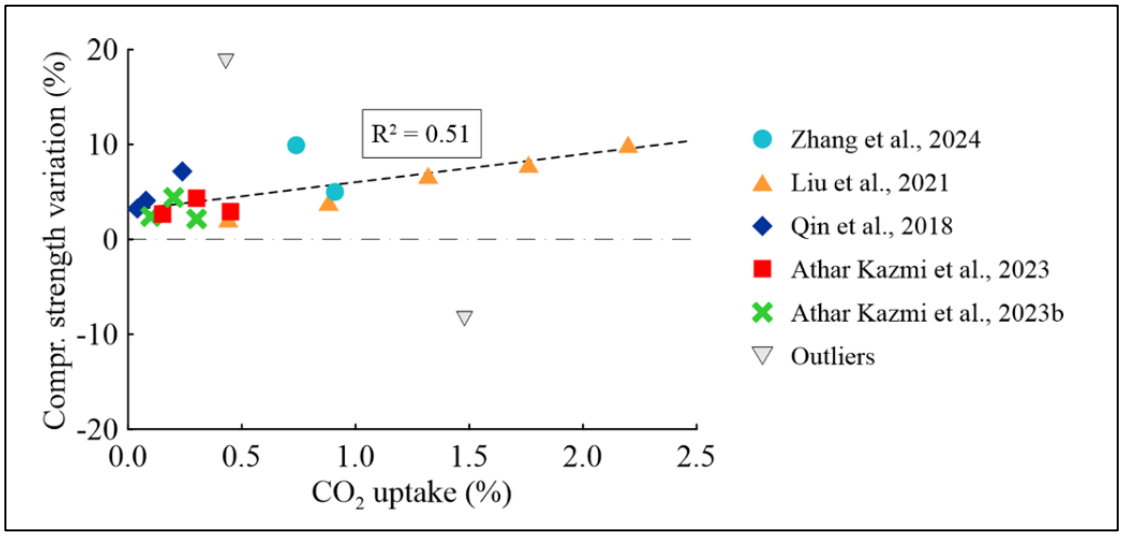


Figure 2.21 Relationship Between CO_2 Uptake And 28-Day Compressive Strength Change Relative to The Non-Carbonated Reference (Adapted from Davolio et al. (2025))

Figure 2.21 visualises this relationship by plotting CO_2 uptake (%) against the 28-day compressive strength variation (%) relative to the non-carbonated reference. The trend is moderately positive ($R^2 = 0.51$), but the scatter is substantial as most points at low uptake cluster around small positive gains, while higher uptake extends to larger gains and also includes negative deviations (Davolio et al., 2025). From a reaction standpoint, this spread is coherent with two competing effects which are (i) limited carbonate precipitation can enhance particle packing and provide nucleation sites that promote a denser early microstructure, while (ii) excessive or poorly distributed carbonation products can form localised carbonate networks or coatings that interfere with continued hydration and disrupt the continuity of load-bearing C–S–H formation (Wang et al., 2023; Kim et al., 2024; Silva et al., 2023)

Figure 2.21 should be read as evidence that aqueous CO_2 supersaturation is necessary but not singularly predictive: the mechanical outcome depends on where

carbonate forms (matrix vs. interfaces), how quickly it forms relative to hydration progress, and how strongly it perturbs the evolving pore solution and solid assemblage. Recent reviews continue to flag this as a reporting gap as studies often provide injected CO_2 dosage but not always the verified uptake and phase allocation needed for consistent cross-comparison (Ahmed et al., 2024; Davolio et al., 2025; Silva et al., 2023).

2.3.5 Carbonation Curing

Carbonation curing refers to the early-age exposure of cementitious materials to elevated CO_2 such that CO_2 transport, dissolution into pore water, and subsequent precipitation of carbonate products occur concurrently with ongoing hydration. In contrast to CO_2 supplied as dissolved inorganic carbon at mixing, carbonation curing performance is strongly governed by external boundary conditions, because CO_2 must enter the pore network through gas transport before reacting in the aqueous phase. Reviews consistently show that CO_2 concentration or partial pressure, relative humidity, temperature, and exposure duration control whether carbonation proceeds as a near-surface densification process or penetrates sufficiently to influence bulk hydrate development (Ravikumar et al., 2021; Xu et al., 2022; Davolio et al., 2025).

Temperature and moisture state are repeatedly reported as decisive variables because they regulate both reaction kinetics and the availability of a continuous aqueous medium for ionic transport. Lu et al. (2022) demonstrated that curing temperature within 5 to 50 °C significantly changes carbonation rate and the resulting microstructure of CO_2-cured cement paste, with kinetics consistent with product-layer diffusion control and an activation energy on the order of ~10 kJ/mol. In parallel, broader carbonation studies highlight that humidity has a non-linear effect: insufficient pore water limits carbonate formation by restricting CO_2 dissolution and ionic mobility, whereas excessive saturation reduces effective gas diffusivity and delays CO_2 ingress, producing different carbonation front characteristics and product distributions (Xu et al., 2022; Merah, 2024). These coupled controls explain why nominally similar CO_2 dosages can yield different strength or durability trends when chamber conditions are not aligned. Mechanical response under carbonation curing is therefore not expected to scale monotonically with CO_2 supply. Dataset-level synthesis indicates that compressive strength can increase, remain comparable, or decrease depending on whether carbonate

precipitation complements hydration such as pore refinement and particle packing, or instead disrupts hydrate continuity and pore-solution chemistry at critical early stages (Ravikumar et al., 2021; Davolio et al., 2025). Experimental studies also report that early-age gains are more consistently observed than later-age advantages, and that later-age convergence is common when subsequent hydration under conventional moisture conditions proceeds and offsets early microstructural differences (Wang, 2022; Lu et al., 2022). This reinforces that carbonation curing should be evaluated using paired descriptors CO_2 uptake or mass gain together with strength development and microstructural evidence, rather than using any single metric in isolation.

Accordingly, a parameter-based comparison is necessary to interpret carbonation curing literature in a way that supports cross-study synthesis and aligns curing regimes with targeted performance outcomes. The key reporting items and test-condition ranges commonly used in recent studies are consolidated in Table 2.5, to support consistent discussion of how curing variables map to CO_2 uptake, phase evolution, and compressive strength response.

Table 2.5
Compiled Research on the CO_2 Concrete Testing Parameters

Parameter	Experimental Testing	CO2 Detection Method	CO2 Phase	Findings	Ref
Variety of Concrete Sample Mixture Volume Ratio of solid binder to aggregates	Compressive Strength Test pH value Testing SEM Test XRD Test MIP Test FT-IR Test TG-DTG Test CO2 adsorption Test Carbonation Degree Test	Fixed CO2 at a pressure of 0.7 Bar (NA)	Carbonation Curing (Gas)	High pH value (alkali) resulted to high compressive strength Combination of Silica Sand with CO2 produce high compressive strength	(Soares & Castro-Gomes, 2022)
Variation of CaCO3 content Type of H2O used (Distilled & Tap Water)	pH value Testing Compressive Strength Test XRD Test ITC Test TGA Test VICAT Test	Fixed CO2 at a pressure of 8 Bar (NA)	Super-saturated aqueous (Gas to Liquid)	CaCO3 powder in H2O reduces setting time and increases strength. CaCO3 in H2CO3 increase calcium in solution and hydration rate. Carbonation without CaCO3 reduces compressive strength Carbonation solution increases rate of reaction.	(Lippiatt et al., 2019)
Variation of cement mix proportions	ITC Test Mortar Flow Test Compressive Strength Test XRD Test TGA Test MIP Test	Fixed CO2 at a pressure of 8 Bar (NA)	Super-saturated aqueous (Gas to Liquid)	pH value of 4.2 causes rapid dissolution pH can be expected to increase overtime due to CO2 degassing. Reduced further hydration due to equilibrium pH lower than if pure H2O used Low pH value increases solubility phases and dissolution rate.	(Lippiatt & Ling, 2020)
Variation of Applied Temperature Duration of Curing Time	Compressive Strength Test Thickening Time Test Durability Test Shear Bond Test	Fixed CO2 of H2CO3 (NA)	Aqueous H2CO3 Solution (Liquid)	Geopolymer can resists H2CO3 corrosion effect Portland cement is fragile due to H2CO3 infiltration	(Salehi et al., 2016)
Variation of cement additives Variety of applied relative humidity Duration of Curing Time	Compressive Strength Test Tensile Strength Test Flexural Strength Test Density Test Pulse Velocity Test Carbonation Test Porosity Test	Fixed CO2 percentage at 0.03% in carbonation chamber (NA)	Carbonation Curing (Gas)	Carbonation process requires 180 days to fully complete Addition of cement additives increases durability to carbonation	(Molina et al., 2015)

Variation of CO2 pressure Variety of conditions applied Degree of Temperature Duration of reaction time	IC Test ICP-OES Test Acidimetric Titration Test SEM Test XRD Test TG-DTA Test	Fixed CO2 at room temperature & at a pressure range of 1, 11, 31 & 50 Bar (NA)	Room Temperature CO2 (Gas)	Carbonation rate depends on pressure & temperature Carbonation reaction degree reaches 18% at pressure of 11 Bar	(Hernández-Rodríguez et al., 2021)
Duration of Curing Time Variation of curing method (air or water infused)	Mortar Flow Test Compressive Strength Test TGA-DTA Test	Atmospheric CO2 (NA)	Air-Conditioned Room CO2 (Gas)	Curing Time Duration effect compressive strength Cement hydration slowed delayed from pozzolanic addition due to greater carbonation depth and low portlandite content.	(Boualleg et al., 2017)
Duration of hydration time (0, 5, 11, 23 & 71 h) Duration of carbonation process	SEM Test Compressive Strength Test TGA-DTA Test	Atmospheric CO2 (NA)	Pure Injected CO2 (Gas)	Carbonation rate depends on pressure & temperature Carbonation reaction degree reaches 18% at pressure of 11 Bar	(Zhang et al., 2018)
Type of aggregates (Natural or Recycled Masonry) Variety of liquid mixture (H2O or H2CO3) Method & Duration of Curing (Air or Water)	XRD Test XRF Test pH Test TGA-DTA Test	Atmospheric CO2 & Commercial Carbonated Water (NA)	Room Temperature CO2 (Gas)	Low pH value affect hydration of cement Usage of RMA increased CO2 sequestration but decrease its strength H2CO3 as mixing solvent increase porosity Air curing is better than Water curing	(Suescum-Morales et al., 2022)
Variety of CO2 concentrations (3% & 20%) Duration of carbonation curing Variation of curing condition	Phenolphthalein Spray Test Compression Strength Test XRD Test MIP Test TGA Test FTIR Test	Fixed CO2 at room temperature & at a concentration of 3 & 20% in carbonation chamber (NA)	Carbonation Curing (Gas)	CO2 carbonation depth and concentration increase parallelly CO2 concentration improved calcium carbonate crystalline. Amorphous silica gels formed through increase in CO2 concentration Cement paste cured at higher CO2 concentration has higher compressive strength	(Lu et al., 2021)
Variation of calcium silicate phases Variation of CO2 Concentration & Temperature	SEM Test XRD Test TGA-FTIR Test	CO2 applied using Pressure Regulator (NA)	Carbonation Curing (Gas)	Carbonation reaction depends on dissolution rate of calcium silicate phases	(Ashraf & Olek, 2016)

Variation of Curing Gas (Flue CO2 gas or pure CO2 gas) Duration of curing	Compressive Strength Test XRD Test Phenolphthalein Spray Test	Fixed CO2 at a pressure at 1 or 7 Bar (NA)	Carbonation Curing (Gas)	Flue gas is slower than pure CO2 gas in terms of carbonation rate Flue gas carbonation strengthens both the pores and the beneath cement particles Specimens cured with flue gas is stronger compared to pure CO2 Increasing gas pressure has little influence on carbonation curing capacity	(Liu et al., 2022)
Variation of HCP's carbonation phase (carbonated, calcined & re-carbonated) Variation of treatment applied on HCP mixture	XRD Test TGA-DTG Test FTIR Test	Fixed CO2 at a pressure at 2.5MPa in incubator (NA)	Carbonation Curing (Gas)	HCP incubated at 2.5MPa of CO2 capable sequestering CO2 Water is necessary for the re-carbonation process of HCP after calcination	(Kong et al., 2022)
Variation of applied CO2 concentration Duration of curing time (1, 3 & 7 days) Types of degrees (carbonation & hydration)	Compressive Strength Test SEM Test XRD Test TGA-DTA Test NMR Test	Fixed CO2 at relative humidity & at a concentration of 1%, 3%, 10% & 20% (NA)	Carbonation Curing (Gas)	Increased CO2 concentration resulted to increase in compressive strength of cement paste Samples cured with 20 % CO2 is higher than for air-carbonated samples in terms of carbonation degrees Increase of CO2 concentration accelerates the carbonation and hydration reaction	(Li & Ling, 2020)

Table 2.5 presents summarized overview of the research conducted on the testing parameters for carbonated concrete which provides insights on aqueous carbonated cementitious materials analysis. Based on the table, it is clearly observed that most researcher determined the carbonated concrete sample's composition and thermal stability, including the decomposition of hydrated cement phases and any changes induced by carbonation through thermogravimetric analysis (DTA-TG) (Hernández-Rodríguez et al., 2021; Lippiatt et al., 2019; Soares & Castro-Gomes, 2022). Incorporating SEM for microstructure testing provides valuable information on carbonation impacts towards concrete's internal structure, further enhancing the understanding of its chemical reactivity, performance and durability. Concrete samples were prepared, and cross-sectional slices are observed under the SEM, which provides high-resolution images, allowing researchers to analyze changes in the cement paste, aggregate distribution, and any microcracks or porosity induced by carbonation (Ashraf & Olek, 2016; Hernández-Rodríguez et al., 2021; Soares & Castro-Gomes, 2022; Zhang et al., 2018). Since the proposed carbonation is in aqueous solution, pH test is required to measure the pH scale of carbonated soluble (H_2CO_3) before and after mixing with cement additives (Lippiatt et al., 2019). Research by Lippiat et al. mainly implements a consistent 8 Bar of CO_2 pressure of liquid CO_2 to incorporate with calcium rich materials (Lippiatt & Ling, 2020; Lippiatt et al., 2019), which provides a pH value of 3.58 to 3.74 (Ryu et al., 2017).

2.4 CO_2 Carbonated Cured Concrete

2.4.1 Compressive Strength of Carbonated Cured Concrete Specimen

Compressive strength is usually treated as the main indicator for whether CO_2 utilisation routes in cement systems are practically adoptable because it integrates the net effects of (i) carbonate precipitation, (ii) hydration continuity, and (iii) microstructural refinement at paste scale and at interfaces. Across recent studies, strength gains are most consistently reported when CO_2 exposure is timed and metered to promote rapid Ca-carbonate formation while still preserving a continuous load-bearing hydrate skeleton. The spread in reported outcomes from clear early-age gains to later-age neutral or negative shifts, therefore not contradictory as it mainly reflects how far carbonation progresses relative to available Ca sources, moisture state, and

subsequent hydration capacity under the selected curing regime (Peng et al., 2022; Tang et al., 2023; Gao et al., 2024).

Mo et al. (2020) discovers that concrete specimens infused with carbonated recycled aggregates (CRA) demonstrated a significant increase in compressive strength in accordance with the curing period. At an early age of 3 days, compressive strength of concrete specimens containing CRA exhibits an increase in value exceeding 30.0 MPa. Maintaining the curing period of the concrete specimens to 90 days resulting the amplification of compressive strength value to a reading in the range of 56.0, 51.5 and 46.4 MPa. Additionally, Tang et al (Tang et al., 2023) stated that fully CRA infused concrete specimens displayed an increase of compressive strength upon aggregate carbonation up to 22.66% and 28.57%.

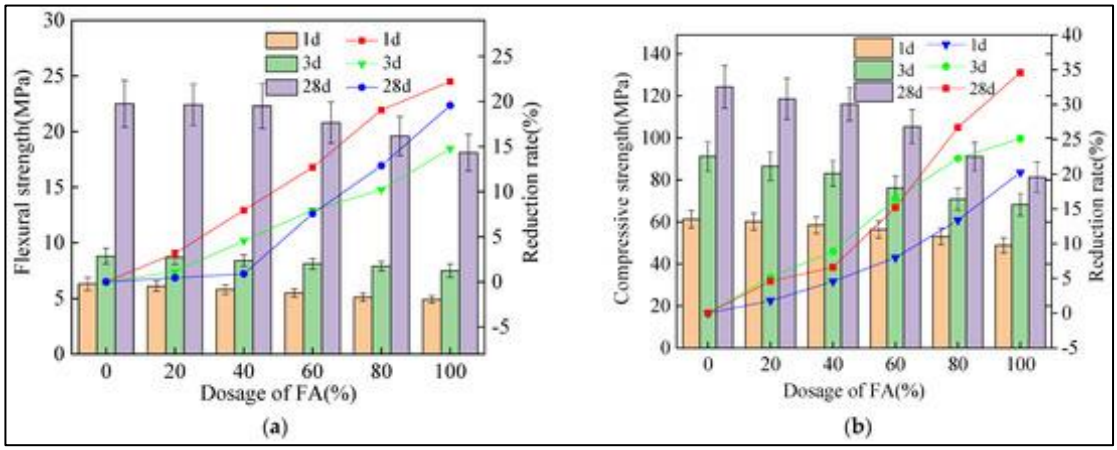


Figure 2.22 Effect of Fly Ash (FA) Dosage and Curing Age on (a) Flexural Strength, and b) Compressive Strength, and the Reduction Rate for CO_2-Cured Alkali-Activated Binder Specimens (Sourced from Peng et al. (2022))

In Figure 2.22 (a) and (b), flexural and compressive strength decreases systematically as FA dosage increases, while strength still rises with curing age across all mixes. The 28-day bars indicate a broad drop from roughly the 120 to 130 MPa range at low FA to around the ~70 MPa range at 100% FA, and the reduction-rate curves increase with FA dosage while decreasing with curing age. Within the same dataset, CO_2 curing is reported to increase compressive strength by 15.4% to 23.1% relative to standard curing, with the improvement weakening as FA content rises which is consistent with the interpretation that higher Ca availability supports greater carbonate formation and more effective pore refinement (Peng et al., 2022). This type of trend is frequently reported in CO_2 curing literature: strength benefits track the ability to generate pore-filling carbonates without suppressing the formation and connectivity of

load-bearing hydrates. The recycled-aggregate carbonation literature reinforces the same compressive-strength logic at a different scale. When recycled aggregate is carbonated before mixing, improvements in aggregate quality and ITZ compactness are commonly associated with measurable compressive strength increases in the resulting concrete; Tang et al. (2023) report compressive strength improvements on the order of approximately 16 to 23% for aggregate carbonation and approximately 22 to 29% for concrete carbonation under comparable conditions.

2.4.2 Densification of Carbonated Cured Concrete Specimen

Dissolved CO_2 reacts in a water-bearing cementitious system causes the most visually obvious microstructural consequence in not only the formation of $CaCO_3$, but also redistributing solids pore volume. Carbonation products preferentially precipitate where ion transport and nucleation are most favourable such as capillary pores, inter-particle contacts, and locally Ca-rich zones, which progressively reduces pore connectivity and shifts the pore population toward finer classes. This pore refinement pathway is repeatedly reported as the dominant explanation for densification during early-age carbonation exposure, especially when carbonation and hydration proceed together rather than as isolated stages (Liang et al., 2024; Hu et al., 2022; Wei et al., 2023).

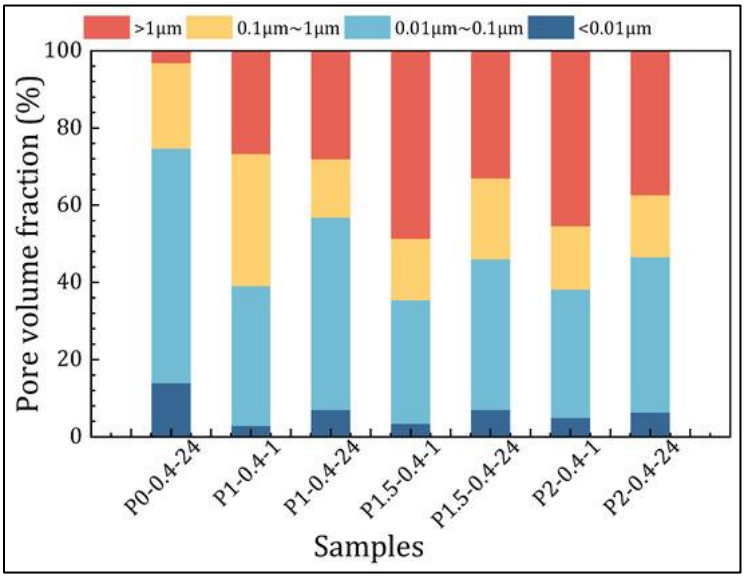


Figure 2.23 Example Of Pore-Size Class Redistribution with Extended Carbonation Duration, Illustrating Refinement of The Pore Structure (Adapted from Ye et al., 2025)

A clear pore-class example is depicted in Figure 2.23, where prolonged carbonation shifts the porosity volume fraction distribution toward smaller pore sizes. In the representative case reported by Ye et al. (2025), the fraction of pores < 0.01 μm increases slightly (13.50% → 14.05%) as carbonation duration increases, while the share of pores in the 0.1 to 1 μm band collapses (50.34% → 3.94%). This is consistent with a pore-filling mechanism where precipitation and continued hydration progressively consume the larger capillary space first, leaving a higher proportion of fine pores by volume fraction. The pore network becomes less percolated because the mid-range capillary band often most influential for transport shrinks substantially (Ye et al., 2025; Liang et al., 2024; Ba et al., 2023). At the paste scale, this densification behaviour is typically interpreted as a coupled dissolution–precipitation sequence whereby Ca-bearing phases dissolve or ionize, carbonate species accumulate locally, and $CaCO_3$ polymorphs precipitate into available pore space.

2.5 Mechanical Alteration of Calcium Precursor Integration

Calcium-based precursors such as $CaCO_3$ and $CaMg(CO_3)_2$ powders, alter cement paste performance through a coupled set of effects that are better treated as an integration problem rather than a simple replacement problem. In most modern interpretations, the dominant levers are (i) particle packing and surface-area availability, (ii) nucleation assistance for hydrates (physical–kinetic), and (iii) limited chemical participation through carbonate–aluminate interactions when aluminate availability and solution conditions permit (Li & Cao, 2024; Tennis et al., 2024; Kang et al., 2024).

In a CO_2-enabled mixing route; CO_2-bearing water or carbonated mixing liquid, the same precursors should not be described purely as inert fillers, because the aqueous carbonate environment can intensify early precipitation and change where solids form within the developing paste. Literature on carbonated-water mixing highlights that the mechanical outcome depends on whether carbonate formation proceeds as a fine, distributed precipitation that refines pores while hydration continues, or as localised deposits that do not restore load-bearing continuity when clinker contribution is reduced (Suescum-Morales et al., 2022; Fu et al., 2024). Hence, fineness and dispersion control become central whereby finer carbonate precursors increase available nucleation area and can accelerate early structuring, but the same surface-area advantage increases sensitivity to boundary conditions such as moisture availability, exposure window, and

alkalinity evolution, that decide whether densification translates into strength. $CaCO_3$ is often finer than clinker in practical PLC systems and therefore disproportionately contributes to early kinetics. Recent reviews separate limestone's effects into dilution and nucleation effect, plus carbonate-related chemical effects such as carbo-aluminate formation in aluminate-bearing systems, which can shift hydrate assemblage and early stiffness (Li & Cao, 2024; Kim et al., 2024). Design guidance compiled for PLC also emphasises that the particle size distribution (PSD) and grinding characteristics commonly produce a bimodal PSD that improves packing and offers abundant nucleation sites, explaining why similar limestone contents can produce different outcomes across cements if the limestone fineness differs (Tennis et al., 2024; Kang et al., 2024).

Figure 2.24 visualises integration of $CaCO_3$ in microstructural terms through a distributed particle population embedded within the hydrated matrix, hence, its influence on mechanics is mediated by (i) the effectiveness of its contribution to particle packing and (ii) interaction with hydrate growth in its vicinity.

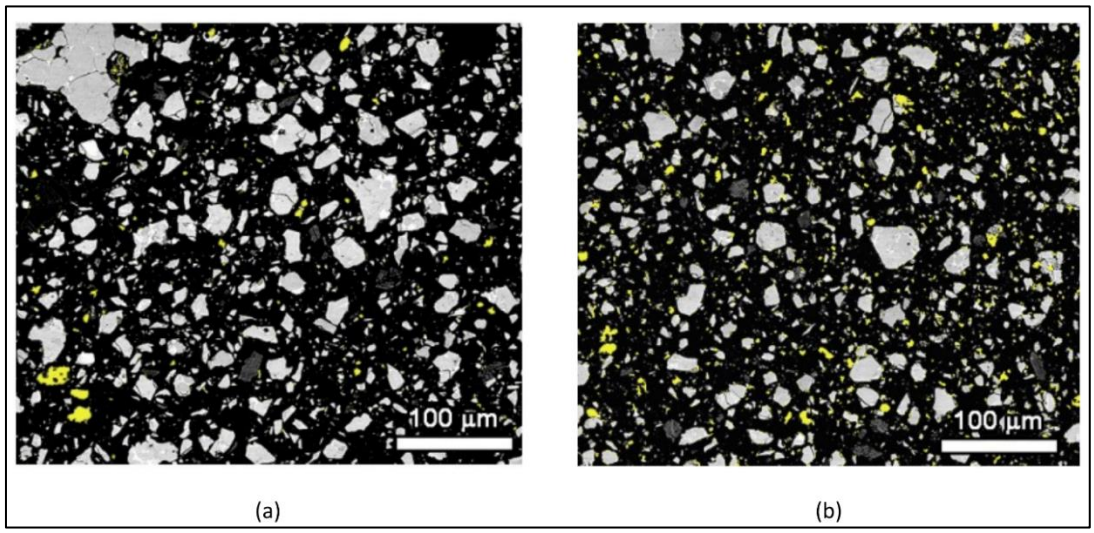


Figure 2.24 Backscattered Electron (BSE) Micrographs Comparing OPC Paste and PLC Paste, Highlighting The Spatial Distribution of Limestone Particles (Yellow Shade) within the Hydrated Matrix (Adapted from Tennis et al. (2024))

This population is fine and well-dispersed; the paste is more likely to develop a tighter early network. When the carbonate fraction becomes too high or when hydration continuity is disrupted (e.g., insufficient later-age hydration recovery after a strong early carbonate event), the resulting microstructure can become carbonate-rich but mechanically less effective due to reduced continuous C–(A)–S–H connectivity (Kim

et al., 2024; Fu et al., 2024). $CaMg(CO_3)_2$ changes similar framework as precursor introduces Mg and can exhibit a different reactivity profile versus pure $CaCO_3$, especially as curing temperature increases. Comparative paste-scale work on Portland–dolomite systems reports that $CaMg(CO_3)_2$ can show higher chemical reactivity than limestone at elevated temperature, and studies typically use XRD/TGA/SEM/MIP jointly to distinguish whether observed strength or densification is predominantly physical (filler/nucleation) or includes measurable chemical transformation (Xu et al., 2021; Hu et al., 2023).

Table 2.6
Chemical Composition of Dolomite and Limestone (wt/%)

Components	Dolomite ($CaMg(CO_3)_2$) **(Gusain et al., 2023)**	Limestone ($CaCO_3$) **(Nath & Dutta, 2010)**
CaO	30.40	45.00
MgO	20.50	1.20
SiO_2	1.50	14.0
Al_2O_3	0.50	5.00
Fe_2O_3	0.30	3.50
$CaCO_3$	56.60	90.00

It is observed that $CaMg(CO_3)_2$ contains key components as a cement additive with 30.40%, 20.5%, and 56.6% of CaO, MgO and $CaCO_3$ respectively as depicted in Table 2.6. The reactivity of H_2O with MgO content in $CaMg(CO_3)_2$, provides an accelerated carbonation (Gardeh et al., 2022). Utilizing 15% of $CaMg(CO_3)_2$ in conventional concrete provides maximum flexural and compressive strength (Gusain et al., 2023). Combining dolomite's properties with CO_2 carbonation would amplifies the strength of concrete rapidly due to its characteristics as a crystallization nuclei which in turn developed a skeleton of $CaCO_3$ nanometer (Yang et al., 2015).

2.6 Carbonated Concrete Parameter Analysis

Carbonation outcomes in cement paste are not governed by CO_2 availability alone, but by the concurrency of (i) CO_2 ingress and dissolution, (ii) moisture-mediated ionic transport, and (iii) the availability of reactive Ca-bearing phases while hydration continues to develop a continuous binding network. For this reason, high-quality reviews and technical reports consistently treat accelerated carbonation as a multi-parameter boundary-value problem, where CO_2 concentration/partial pressure, relative

humidity, temperature, exposure duration, and pre-conditioning collectively determine reaction extent, product distribution (including polymorph selection), and the extent of pore blocking or pore refinement. Within accelerated protocols, CO_2 concentration (or partial pressure) primarily sets the chemical driving force, but its effect is conditional on moisture state and transport accessibility. RILEM TC 281-CCC notes that concentrations used in accelerated testing commonly exceed atmospheric levels by orders of magnitude, and that very high CO_2 can promote non-representative artefacts such as pore blocking due to water production and rapid precipitation, implying that concentration must be interpreted together with RH and specimen condition rather than treated as a single intensity variable. In contrast, approaches that shift carbonation into an aqueous ionic mode such as CO_2 injection into a cement suspension, demonstrating that altering the reaction mode can raise sequestration efficiency while maintaining strength, reinforcing that delivery format is a first-order parameter rather than an implementation detail.

Relative humidity and internal moisture content are repeatedly identified as the most sensitive controls because they simultaneously regulate gas transport pathways and the existence of a continuous aqueous phase required for carbonate chemistry. Method-focused reviews emphasise that RH governs the transition between transport-limited fronts, distributed precipitation, and moisture-limited regimes, producing markedly different carbonation depths and phase assemblages even at comparable CO_2 concentrations. Experimental work on pre-conditioning further shows that the same binder system can exhibit different carbonation curing efficiencies and strengths depending on the moisture content at exposure.

Temperature and exposure duration cannot be treated as linear levers. Temperature accelerates carbonation kinetics and microstructural evolution, but also perturbs moisture distribution; thus, temperature effects are inseparable from RH control and exposure time. For instance, controlled studies on CO_2-cured paste show that temperature strongly modifies reaction rate and microstructure development across practical ranges, while excessive severity risks shifting the system toward less favourable assemblages or heterogeneous product distributions. Duration exhibits diminishing returns because longer exposure increases reaction extent but also increases susceptibility to precipitation localisation and pore blocking, particularly under high CO_2 when water generation and rapid near-surface precipitation restrict deeper ingress. To avoid ambiguity in cross-study comparison, parameter reporting must be paired with

a clear quantification basis for carbonation degree and CO_2 uptake. Thermogravimetric analysis is widely used because decarbonation provides a direct CO_2-release signal; however, recent experimental work shows that carbonation intensity can shift decarbonation peak temperatures and alter peak shape, making it essential to report the adopted integration window and assumptions rather than presenting uptake as a context-free scalar.

2.7 Concluding Remarks

This chapter reviewed the main literature related to CO2 utilisation in cementitious systems, with emphasis on carbonation mechanisms, aqueous CO2 incorporation, calcium-based carbonate precursors and the physico-mechanical behaviour of cement-based binders. The review shows that CO2 utilisation in cementitious materials has been widely studied through accelerated carbonation curing, mineral carbonation and carbonated recycled materials. These approaches demonstrate that CO2 can react with calcium-bearing phases to form carbonate products and may contribute to strength development, pore refinement and improved material performance when the reaction conditions are properly controlled.

However, much of the existing literature focuses on chamber-based carbonation curing, industrial residues, recycled aggregates or hardened concrete systems. Comparatively fewer studies evaluate the direct use of CO2-conditioned water or carbonic acid (H_2CO_3) as mixing water in fresh OPC paste. This route is important because CO2 is introduced at the batching stage, where pH, alkalinity, ionic speciation, water-to-binder ratio and early nucleation processes can influence both hydration and carbonation. Therefore, the behaviour of aqueous CO2 integration cannot be assumed to be the same as gas-solid carbonation curing. The review also indicates that calcium carbonate ($CaCO_3$) has been widely investigated as a filler and nucleation material in cementitious systems, but its performance depends strongly on replacement level, particle characteristics and curing condition. In contrast, the role of dolomite, CaMg(CO3)2, under aqueous CO2 mixing conditions is less clearly established. The combined influence of low-pH H2CO3 mixing water, CaCO3 or CaMg(CO3)2 replacement and ambient curing on setting behaviour, compressive strength, water absorption and reaction indicators remains insufficiently defined.

Based on these gaps, this study focuses on the aqueous CO2 mixing route in OPC paste by evaluating the effect of H2CO3 solution pH and calcium-based precursor replacement on physico-mechanical performance and hydration-carbonation indicators. The research gap addressed in this thesis is the lack of a clear experimental parameter window linking mixing-water pH, precursor type, precursor dosage and ambient curing to setting time, compressive strength, water absorption, phase development, thermal response and microstructural evidence. This provides the basis for the methodology developed in Chapter 3.

CHAPTER 3
RESEARCH METHODOLOGY

3.1 Introduction

Utilising supersaturated aqueous H_2CO_3 as the mixing liquid together with finely divided $CaMg(CO_3)_2$ and $CaCO_3$ was examined in this study to evaluate the effect of aqueous CO_2 integration on OPC-based cementitious binders. This chapter describes the experimental methodology used to prepare the H_2CO_3 solution, produce the modified OPC paste, cast the specimens, apply the curing condition and conduct the required testing.

The experimental programme focused on OPC paste systems, where H_2CO_3 solution was used as the mixing water and $CaMg(CO_3)_2$ and $CaCO_3$ were used as partial binder replacement materials. The main independent variables were the pH of the H_2CO_3 mixing water, the type of carbonate precursor and the replacement percentage of the precursor. The pH of the mixing water was varied from acidic to near-neutral conditions, while the precursor type was varied between $CaMg(CO_3)_2$ and $CaCO_3$. The replacement percentage was varied to evaluate the influence of precursor dosage on the behaviour of the modified OPC paste. The dependent variables measured in this study included setting time, compressive strength, water absorption, microstructure and phase composition. Setting time, compressive strength and water absorption were used to evaluate early stiffening, mechanical performance and moisture uptake behaviour, while XRD, TGA and SEM-EDX were used to support the interpretation of phase composition, thermal response and microstructural development. The summary of experimental variables and test responses is presented in Table 3.1.

Table 3.1
Experimental Design Summary

Factor	Variable	Level / condition	Control / fixed value	Response measured
A	Mixing-water pH	3.5 to 4.0, 4.0 to 4.5, 4.5 to 5.0, 5.0 to 5.5, 5.5 to 6.0	6.0–7.0	pH behaviour, setting time, strength
B	Precursor type	CaCO3, CaMg(CO3)2	OPC only	Strength, absorption, microstructure
C	Replacement level	5, 10, 15, 20, 25%	0%	Setting time, strength, absorption

Factor	Variable	Level / condition	Control / fixed value	Response measured
D	Water-to-binder ratio	0.40	0.40	Constant
E	Curing age	3, 7, 28 days	Ambient curing	Compressive strength
F	Characterisation	XRD, TGA, SEM-EDX	Selected mixes	Phase, thermal and microstructural indicators

3.2 Research Framework

The summary of the workflow is illustrated in Figure 3.1; from CO_2-water generation and verification, through batching and casting, to curing, testing, and the objectives to be achieve for this research study. The research framework was divided into four main phases, namely material preparation, mechanical and physical testing, microstructural and chemical analysis, and data interpretation.

Phase 1 involved material preparation. In this phase, OPC, $CaMg(CO_3)_2$ and $CaCO_3$ were prepared as the main cementitious binder and precursor materials. The supersaturated aqueous CO_2 solution was also prepared by controlling the CO_2 flow rate and exposure time until the selected H_2CO_3 pH range was achieved. The selected H_2CO_3 solution was then used as the mixing water for preparing modified OPC paste with $CaMg(CO_3)_2$ and $CaCO_3$ replacement.

Phase 2 involved mechanical and physical testing. The prepared paste was cast into 50 mm × 50 mm × 50 mm cube moulds and cured under ambient laboratory condition. Setting time was tested to evaluate early stiffening behaviour, while compressive strength was measured at selected curing ages to determine the mechanical performance of the binder. Water absorption were also measured to evaluate the physical behaviour of the hardened paste.

Phase 3 involved microstructural, chemical and thermal analysis. Selected hardened paste specimens were prepared for SEM-EDX, XRF, XRD and TGA/DTA analysis. SEM-EDX was used to observe the microstructural features and elemental distribution, XRF was used to determine chemical composition, XRD was used to identify phase composition, and TGA/DTA was used to support the interpretation of thermal response and carbonate-related reaction behaviour.

Phase 4 involved data interpretation. The results obtained from setting time, compressive strength, water absorption and material characterisation were compiled and compared. The data were then correlated to evaluate the effect of H_2CO_3 mixing-

water pH, carbonate precursor type and replacement percentage on the physico-mechanical behaviour and hydration-carbonation indicators of the modified OPC paste.

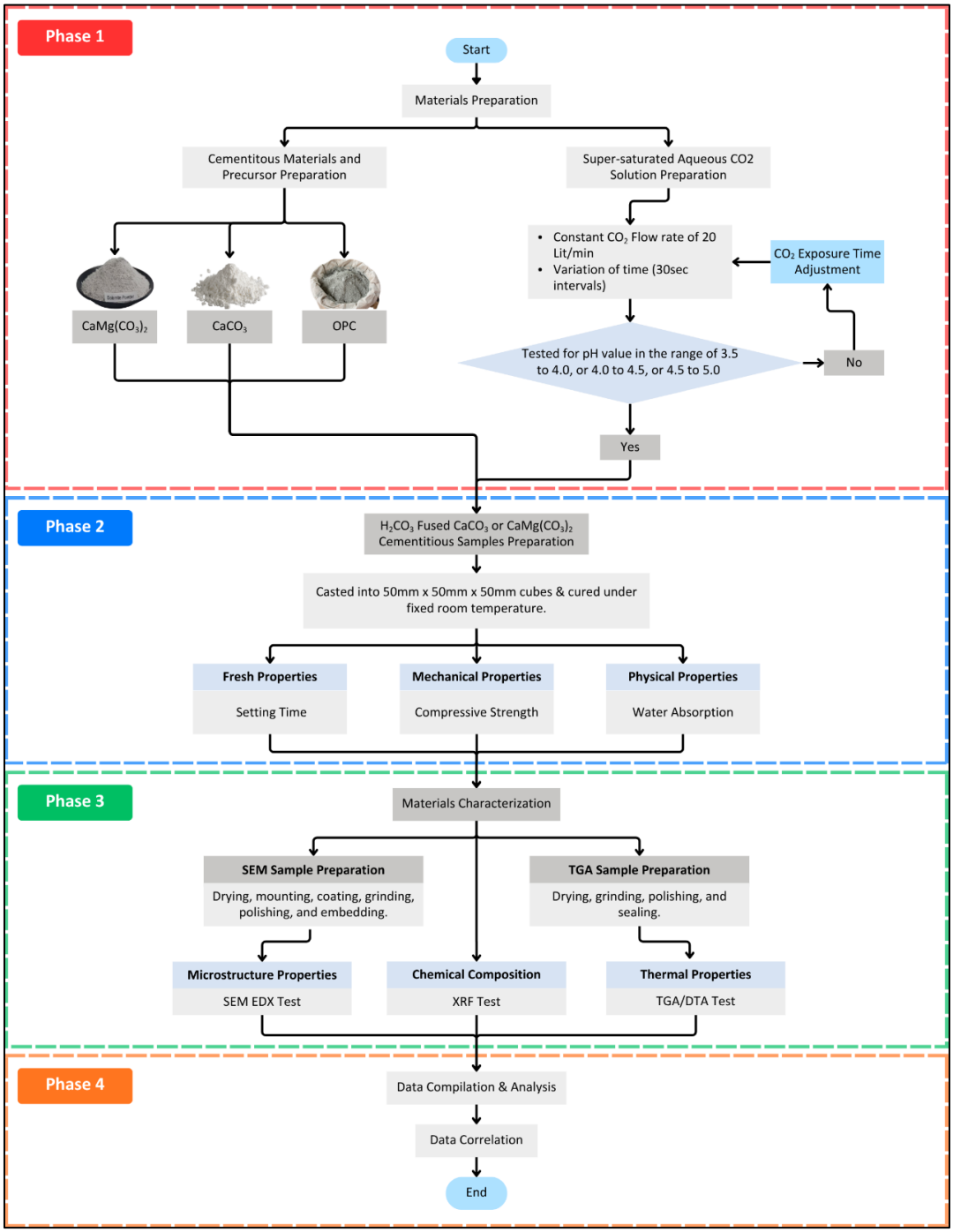


Figure 3.1 Experimental Framework and Data Streams

3.3 Raw Materials

The raw materials used in this study consisted of OPC, calcium carbonate ($CaCO_3$), dolomite, $CaMg(CO_3)_2$, tap water and carbon dioxide gas. The materials were

selected based on the scope of the study, which focused on OPC paste modified with aqueous H_2CO_3 mixing water and calcium-based carbonate precursors.

3.3.1 OPC

Cement pastes were produced with commercial Grade 30 OPC sourced from a local supplier, Tasek Corporation Berhad. The material was used as received to reflect typical practice in Malaysian construction supply chains. All mixtures in this chapter employed the same binder to ensure that observed differences arise from the mixing liquid and carbonate additions rather than cement variability. The OPC was treated as the reference binder in this study, while its chemical composition was considered through the available supplier information and XRF-based material characterisation. No additional modification was made to the OPC before mixing.

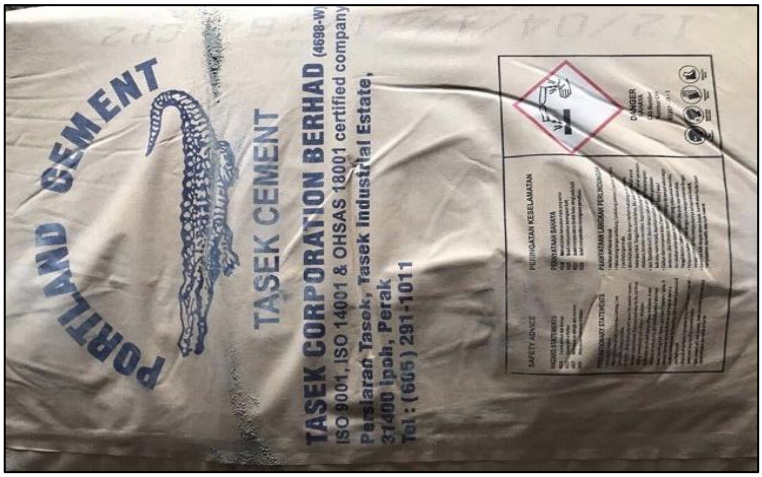


Figure 3.2 Grade 30 OPC Supply Obtained from Tasek Corporation Berhad

3.3.2 $CaMg(CO_3)_2$ & $CaCO_3$ Powder

$CaMg(CO_3)_2$ and $CaCO_3$ powders were obtained through the same local supplier network, Britestone Sdn. Bhd., Simpang Pulai, Perak, Malaysia, to ensure comparable packaging and logistics. Both materials arrived as dry powders in sealed bags and were used as received with laboratory conditioning only. In this study, $CaCO_3$ was used as a calcium-based carbonate precursor, while $CaMg(CO_3)_2$ was used as a calcium-magnesium-based carbonate precursor. Their function was to partially replace OPC by binder mass and to provide carbonate-bearing particles that may influence packing, nucleation and hydration-carbonation behaviour.

Table 3.2
Chemical Composition and Particle-Related Information of Raw Materials

Material	SiO_2 (%)	Al_2O_3 (%)	Fe_2O_3 (%)	CaO (%)	MgO (%)	Other major component	Particle-related information	Basis
OPC	21.28	5.60	3.36	64.64	2.06	SO_3: 2.10%	Specific gravity: 3.15; Blaine fineness: 340 m^2/kg	Reported Type I OPC data from Tasek Cement Corporation Berhad
$CaCO_3$ powder	1.29	0.21	0.08	54.3	0.02	$CaCO_3$: 97.4%; free moisture: <0.5%	100% passing 200 mesh; 95.9% passing 325 mesh	Representative commercial calcium carbonate powder data
$CaMg(CO_3)_2$ powder	0.3	0.2 to 0.5	0.1	30 to 35	15 to 18	$CaCO_3$: 65%; $MgCO_3$: 35%	90% passing 100 mesh	Supplier specification for Britestone Dolomite M-100 powder

The $CaMg(CO_3)_2$ powder composition was based on the XRF result obtained in this study. For the $CaCO_3$ powder, no batch-specific certificate of analysis was available; therefore, its chemical composition was represented using the nominal $CaCO_3$ formula and theoretical oxide equivalent. This approach was used only to define the expected calcium carbonate composition and does not represent independently measured impurity content of the supplied $CaCO_3$ powder. Full particle size distribution of the carbonate powders was not independently measured; therefore, particle-related information is reported based on the supplied powder condition and available material description. The available chemical composition and particle-related information of the raw materials are summarised in Table 3.2.

3.4 Preparation of Aqueous H_2CO_3 Solution

3.4.1 Atomization Rig, Sensors, and Operating set-points

Carbonated mixing water was generated using an instrumented gas–liquid atomization rig designed by my co-supervisor, Ts. Dr. Ahmad Hussein Abdul Hamid, which is illustrated and executed as in Figure 3.3 and 3.4 respectively. The apparatus comprises a water line (supply tank, self-priming pump, strainer, manual flow control, inline water-flow and water-pressure sensors, downstream check valve) and a pressurised CO_2 line (30 kg cylinder from AGS, regulator at fixed set pressure, gas-flow and gas-pressure sensors, check valve). Both lines meet at a twin-fluid atomizer. All sensor channels were recorded by a data-acquisition unit, and a high-resolution camera

with speedlight verified a stable spray cone. The CO_2 flow and pressure were maintained as operating set-points during solution preparation, while exposure time was varied until the required pH band was obtained. In this study, the dissolved CO_2 condition was not measured directly using total inorganic carbon analysis. Therefore, the CO_2 concentration in the prepared water was estimated indirectly from the measured pH using carbonate equilibrium assumptions, and the pH value was used as the practical batching indicator for H_2CO_3 solution strength.

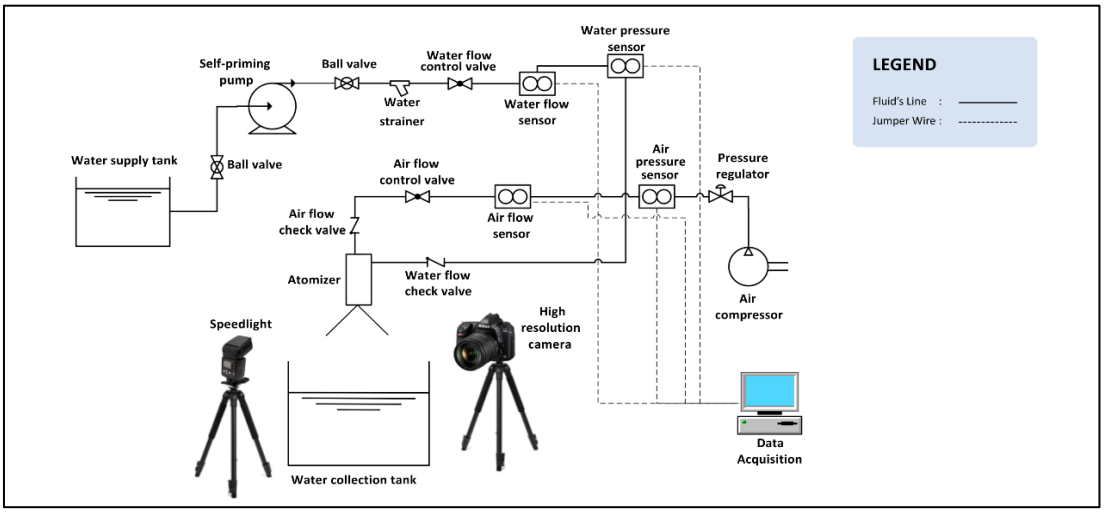


Figure 3.3 Schematic of Gas–Liquid Atomization Rig for H2CO3 Preparation

Production followed a standard protocol. The rig was stabilised at the target setpoints for regulator pressure and liquid and gas flow rates, then samples were withdrawn from the collection tank at one-minute intervals. pH was measured immediately using a bench meter calibrated at 4.0 and 7.0 before each run. Carbonated water was prepared to discrete acidity bands treated as experimental levels: 3.5 to 4.0, 4.0 to 4.50, 4.5 to 5.0, 5.0 to 5.5, and 5.5 to 6.0. Once a sample entered the designated band, it was promptly transferred for mixing at the prescribed water–cement ratio to minimise degassing. Check valves prevented crossflow, and identical setpoints and sampling intervals were used throughout so that any differences in fresh and hardened properties can be attributed to mixing-water acidity and carbonate dosage/type, rather than process variability.

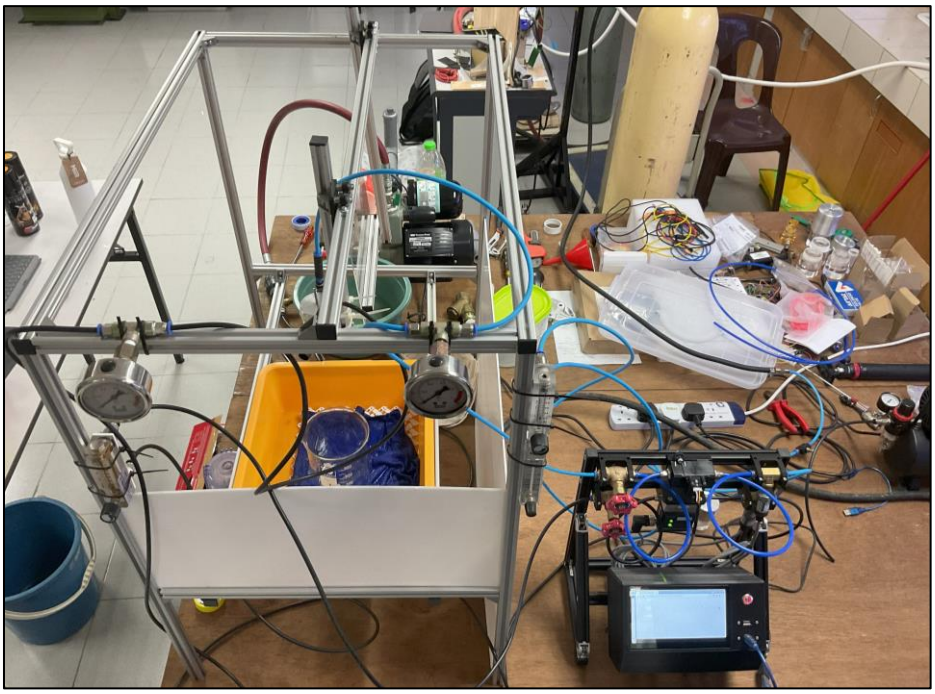


Figure 3.4 Bench-top assembly of the H_2CO_3 preparation rig according to Schematics

The selected pH ranges from 3.5 to 6.0 was chosen to represent the transition from strongly CO_2-conditioned acidic water to weakly acidic near-neutral water. The lower pH bands were included to evaluate the effect of higher dissolved CO_2 condition on early batching behaviour, while the higher pH bands were included to observe whether a less acidic solution reduced the risk of excessive setting delay or strength reduction. This range also allowed the study to identify the practical pH window for H_2CO_3 mixing water before comparing the effect of $CaCO_3$ and $CaMg(CO_3)_2$ precursor replacement.

3.4.2 pH Calibration and Short-Term Stability

pH of the carbonated mixing water was measured using a Hach sensION 378 bench pH meter equipped with automatic temperature compensation and a combination glass electrode as observed in Figure 3.5. The Hach sensION 378 was adopted after a pilot phase with a handheld pen-type meter; drift and response time in the pilot did not meet acceptance criteria, so the handheld device was omitted, and all reported values herein are from the bench system. The meter was calibrated daily using NIST-traceable buffers at pH 4.00, 7.00, and 10.00 at laboratory temperature. Acceptance thresholds were slope from 95 to 105%, offset within ±15 mV, and stability within ±0.01 pH over 30s at the end of calibration. Buffers were poured fresh into single-use cups; the

electrode was rinsed with deionized water and gently blotted between immersions. A mid-run check against the 4.00 buffer was performed after each third batch; if the reading deviated by more than ±0.03 pH, a full recalibration was performed before proceeding.

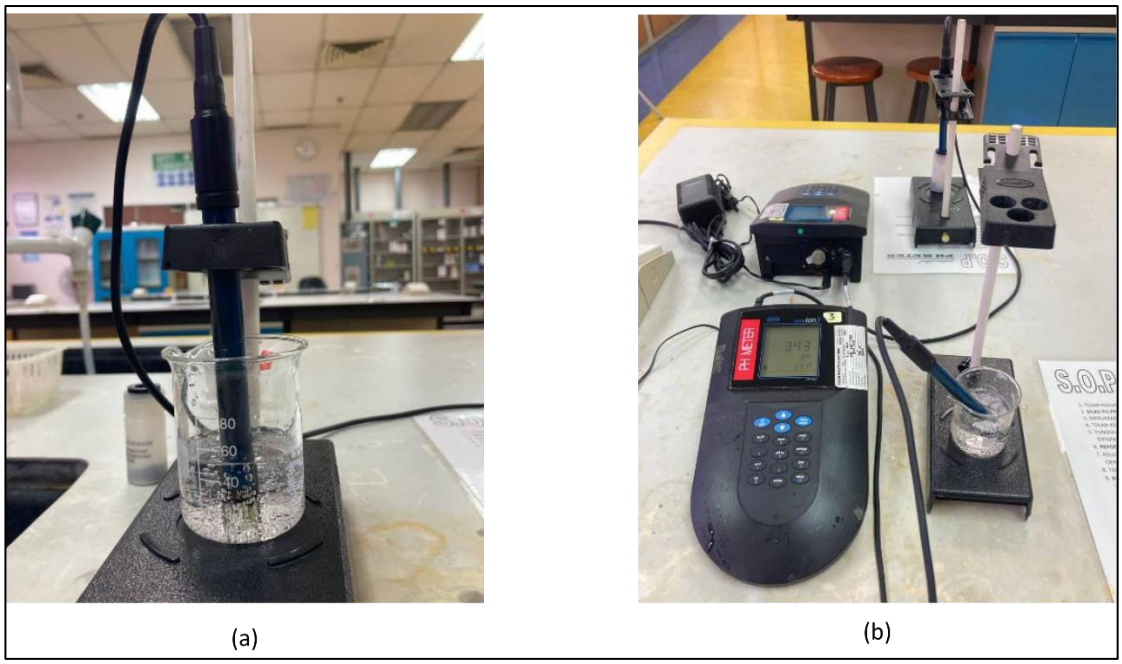


Figure 3.5 pH Measurement of CO_2-Water Using a Hach sensION-378

The apparent dissolved CO_2 concentration was estimated from the measured pH based on the first dissociation equilibrium of carbonic acid. For dilute CO_2-conditioned water, the equilibrium can be expressed as $H_2CO_3 \rightleftharpoons H^+ + HCO_3^-$, where the first dissociation constant, K_{a1}, relates hydrogen ion activity to dissolved carbonic acid species. Under the simplified assumption of dilute water, negligible alkalinity contribution and room-temperature measurement, the apparent H_2CO_3 concentration can be estimated from:

$$H_2CO_3 = \frac{(H+)^2}{K_{a1}} \tag{3.1}$$

where H^+ is obtained from the measured pH. This estimation was used only as an indicative comparison between pH bands, not as a direct carbon-balance measurement. The batching decision was therefore based on measured pH rather than direct CO_2 uptake. The H_2CO_3 solution was used immediately after the target pH band

was confirmed. The time between pH measurement and paste mixing was limited to within 10 minutes to minimise CO_2 loss and pH drift before batching. If the solution was not used within this interval, the pH was rechecked and the solution was accepted only when it remained within the selected pH band.

3.4.3 Mix Design and Batching Protocol

A normal-H_2O control mix was prepared to provide the reference condition for comparison with H_2CO_3-mixed systems. The control consisted of OPC paste prepared with normal tap water, without CO_2 conditioning and without carbonate precursor replacement. This control was used to distinguish the effect of aqueous CO_2 mixing water from the behaviour of the unmodified OPC paste. Where precursor replacement was evaluated, the results were compared against the corresponding OPC-based reference condition at the same water-to-binder ratio.

Batching was designed to isolate the effects of mixing-water acidity and carbonate dosage/type under a fixed proportioning scheme. All proportions were computed on an oven-dry basis with water to cement (w/c) ratio of 0.40 and a constant OPC grade, along with carbonate precursors of $CaCO_3$ or $CaMg(CO_3)_2$, partially replaced cement at 5, 10, 15, 20, and 25% by mass. The factor–level matrix is given in Table 3.3, with full per-batch masses and IDs archived in Appendix A for reproducibility.

Table 3.3
Mix-Design Matrix for OPC Pastes with Aqueous H_2CO_3 Mixed with $CaCO_3$ & $CaMg(CO_3)_2$

pH Range	**3.5 to 4.0**					**4.0 to 4.5**					**4.5 to 5.0**				
$CaCO_3$ / **$CaMg(CO_3)_2$**	5	10	15	20	25	5	10	15	20	25	5	10	15	20	25
w/c Ratio	0.4														

The H_2CO_3 mixing water was produced with the instrumented rig described previously and qualified to a designated pH band which are 3.5 to 4.0, 4.0 to 4.5, 4.5 to 5.0, 5.0 to 5.5, and 5.5 to 6.0, using the bench meter protocol in Section 3.4.2. A batch

was released for mixing only when the median of three (3) readings fell inside the target band and short-term drift under cover was within the acceptance window.

3.5 Specimen Preparation and Curing

Cement paste was cast in 50mm plastic cube moulds prepared with a thin mineral-oil release and verified for flatness as shown in Figure 3.6. Fresh material was placed in two lifts with gentle table vibration to release entrapped air, struck flush with a steel straightedge, and covered immediately to limit evaporative loss. Each mix produced triplicate cubes per target age so later reporting can use mean and standard deviation. The cast cement paste specimens were initially kept covered in the moulds under ambient laboratory condition to minimise early moisture loss. After demoulding, the specimens were stored under ambient laboratory air curing until the selected testing age. No water immersion, carbonation chamber or humidity-controlled curing chamber was used in this study. Therefore, the curing condition is reported as ambient laboratory air curing, with relative humidity not externally controlled.

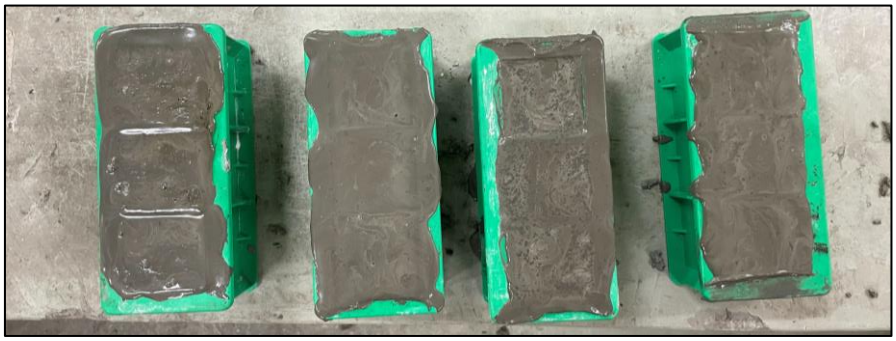


Figure 3.6 Casted Cement Pastes in 50mm Plastic Cube Moulds

Curing ages were selected to resolve both early kinetics and later consolidation. The primary schedule is 3, 7, 14, and 28 days. This window captures the fast response of carbonated mixing water at early age and the approach to the conventional benchmark at 28 days. The choice is consistent with practice reported for aqueous-CO_2 mixing and early carbonation work. Examples include studies that report early and 28-day strengths for carbonated-water mixes and ambient-pressure carbonation or chamber curing for later-age checks, as depicted in Table 3.4. A compact literature matrix is provided for transparency. Cubes from the same batch were reserved for SEM/EDX so micrographs and spot chemistry can be read against the mechanical response without cross-batch confounders.

Table 3.4
Methods and Durations of Compressive Strength Testing From Other Research

Methods									
Hardened-state Compressive strength	Compressive Strength Test (Days)								Reference
	1	3	7	14	28	56	90	180	
✓			✓		✓	✓	✓	✓	(Xiao et al., 2022)
✓									(Meng et al., 2022)
✓			✓		✓		✓		(Russo & Lollini, 2022)
	✓	✓		✓		✓	✓		(Lu et al., 2021)
✓			✓	✓	✓				(Monkman & MacDonald, 2017)
✓	✓				✓				(Xian & Shao, 2021)
✓	✓	✓	✓						(Suescum-Morales et al., 2022)
✓									(Xuan et al., 2016)
✓									(Luo et al., 2018)
✓	✓		✓		✓		✓		(Torrenti et al., 2022)
✓			✓		✓		✓		(Li et al., 2017)
✓		✓	✓		✓				(Lin & Wang, 2021)
✓		✓			✓				(Lu et al., 2022)
✓	✓	✓	✓	✓	✓				(Wu et al., 2022)
✓	✓			✓					(Xian, Zhang, et al., 2022)
✓				✓					(Liang et al., 2020)
✓	✓			✓					(Zhang & Shao, 2016)
✓									(Ahmad et al., 2017)
✓		✓		✓					(Feng et al., 2023)

3.6 Test Methods

The test methods were arranged to evaluate the fresh, mechanical, physical, chemical, phase and thermal behaviour of the modified OPC paste. Unless stated otherwise, each mechanical and physical test was conducted using three specimens for each mix and curing age, and the results were reported as average values. Selected

representative specimens were used for SEM-EDX, XRF, XRD and TGA analyses to support the interpretation of hydration-carbonation behaviour.

3.6.1 Setting Time Test

Setting behaviour of the cement paste was determined with a standard Vicat apparatus conforming to the dimensional and mass tolerances of the relevant standards as observed in Figure 3.7. Both manual and automatic frame for the testing is acceptable. The test quantifies the transition from plastic to rigid paste by periodic needle penetrations under controlled temperature. Initial set is defined at a 25mm penetration criterion; final set is the first reading that does not leave a complete circular impression, verified by two confirmatory penetrations within 90 s, as specified in ASTM C191.

The setting time test was repeated for each selected paste condition to confirm the consistency of the measured initial and final setting behaviour. The reported setting time represents the observed response of the paste under the selected H_2CO_3 mixing-water pH and precursor replacement condition.



Figure 3.7 Vicat Apparatus for Setting Time Evaluation

The paste was prepared using the same liquid mixture and mixed to a fixed water to binder ratio (w/b) of 0.4. This isolates the effect of liquid acidity and carbonate additions from water content. The filled Vicat mould sat on a non-absorptive baseplate in a covered, high-humidity enclosure at 23 ± 2 °C. This enclosure approach is consistent with standard practice for hydraulic cements, ASTM C191 (ASTM, 2008). The needle was zeroed firsthand on the baseplate, while the plunger was gently lowered to contact the paste and released vertically. Penetrations were taken at regular intervals,

each at least 10 mm from the mould rim and from prior imprints; the needle was cleaned between readings. Initial set was recorded at the first time the penetration equalled 25mm. Final set was the first reading that did not leave a complete circular impression, confirmed by two additional penetrations on fresh areas within 90s, and the time from first contact to this endpoint was reported as the Vicat final time of setting.

3.6.2 Compressive Strength

Compressive strength was measured on 50 mm mortar cubes in accordance with ASTM C109/C109M. Figure 3.8 shows the specimens that were casted as in Section 3.6, demoulded after initial set, and cured at laboratory ambient to the scheduled ages. Tests were conducted at the UiTM Concrete Laboratory using a 1000 kN universal testing machine (UTM) fitted with a calibrated load cell and a spherically seated upper platen to accommodate minor misalignment as illustrated in Figure 3.9a. The test schedule prioritised 3, 7, 14, and 28 days, matching the study's early–to–benchmark window. All mixes used the same water-to-cement ratio (0.40) and the same verified mixing-water pH band recorded at batching (Section 3.4.2), so differences in strength reflect liquid chemistry and carbonate type or dose rather than process drift. The load was applied continuously without shock until failure. The loading rate was maintained at approximately 0.9 kN/s, equivalent to the ASTM C109/C109M loading requirement of 900 to 1800 N/s for 50 mm cube specimens. The compressive strength was calculated by dividing the maximum load at failure by the loaded area of the cube.



Figure 3.8 Hardened CO_2 Cured Cement Samples

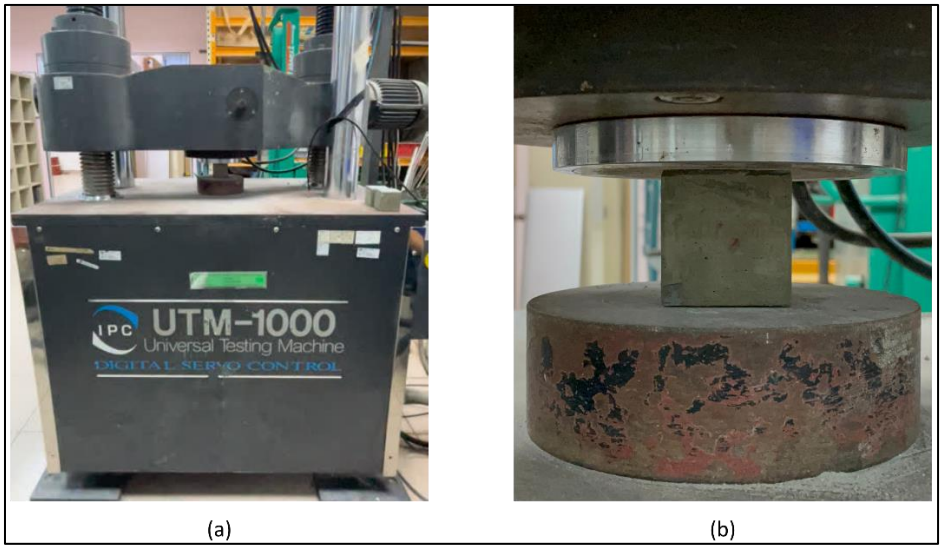


Figure 3.9 (a) UTM for Compressive Testing, (b) Samples in Between UTM Plates

Bearing faces were wiped free of moisture and fines, hence, no capping was applied. Each cube was centred on the lower platen with faces normal to the loading axis, and the upper platen was brought into contact under a minimal seating load as illustrated in Figure 3.9b. Load was then applied at the gradual rate according to ASTM C109, through approximately the first half of the anticipated maximum load, with no further rate adjustments through failure. Maximum load, Pmax, was recorded automatically by the UTM controller.

Strength was computed using the nominal loaded-face area, where A = 2500mm2, for 50 mm cubes and reported in MPa to two decimal places as in by Equation 3.1. For each mix–age cell, triplicate specimens (n = 3) were tested. Results are presented as mean ± standard deviation, with any invalidated specimens such as visible defects, edge spalls before load, or misalignment, was documented in the batch log and excluded with justification, consistent with good laboratory practice under ASTM C109.

$$\text{Compressive strength (Cs)} = \frac{\text{P (Load)}}{\text{A (Area)}} \tag{3.2}$$

3.6.3 Water Absorption

Water absorption behaviour was evaluated to observe the moisture uptake response of hardened OPC paste specimens prepared using different H2CO3 mixing-

water pH conditions. The test was carried out using a simple immersion-based mass response method, where the specimens were exposed to water for a fixed duration and the mass after immersion was recorded. This test was included as a physical indicator because water uptake can provide an indirect indication of pore connectivity, matrix compactness and the ability of water to enter the hardened paste structure.

After the selected curing period, the hardened paste specimens were fully immersed in clean water at room temperature for 14 days. The specimens were placed in a water container to ensure that all surfaces were exposed to water throughout the immersion period. After 14 days, the specimens were removed from the water and surface-wiped using a damp cloth to remove excess water from the outer surface. The specimens were then weighed immediately using a digital weighing balance to obtain the post-immersion mass. The recorded value was used to compare the moisture uptake response between the control paste and the H_2CO_3-mixed paste specimens.

In a standard water absorption calculation, the percentage mass gain is normally calculated using Equation 3.3:

$$\text{Water Absorption (\%)} = \frac{W_{wet} - W_{dry}}{W_{wet}} \text{ x } 100 \qquad (3.3)$$

where W_{wet} is the mass of the specimen after water immersion and W_{dry} is the dry mass before immersion. However, in the present dataset, the absorption response was interpreted based on post-immersion specimen mass because the recorded values were reported as final mass after 14 days of water exposure. Therefore, the result was treated as a comparative moisture uptake indicator rather than a full standard water absorption percentage.

For interpretation, a higher post-immersion mass may indicate greater moisture uptake, which can be associated with a more open or connected pore structure. In contrast, a lower post-immersion mass under the same testing condition may indicate reduced moisture uptake and a denser paste matrix. Therefore, the water absorption result was used as a comparative physical indicator to support the discussion of pore refinement and matrix densification, together with compressive strength and microstructural observations.

3.6.4 Microstructure Overview

Micrographs were obtained on a JEOL JSM-6460LA scanning electron microscope at the Materials Science Laboratory under technician supervision as observed in Figure 3.10. All beam settings and chamber conditions were set and logged by the laboratory technician according to facility SOP. Instrument metadata such as accelerating voltage, working distance, detector, magnification, date or time were recorded with each image for traceability. Working distance in the typical 10 to 15mm range and an accelerating voltage of approximately 15 to 20kV, were used to balance spatial resolution and X-ray yield. Fields of view are acquired across multiple magnifications, including frames with a 10 µm scale bar to standardise ROI selection with the EDX probe.



Figure 3.10 JEOL JSM-6460LA Modelled SEM Machine for Microstructure Analysis

Fragments are taken from M6A and M7A ($CaCO_3$ series) and M10A, M11A, M12C, M15B ($CaMg(CO_3)_2$ series) at the hardened state, along with $CaMg(CO_3)_2$ powder and cement with water, sampling away from visibly cracked zones to avoid artefacts from the compression test as shown in Figure 3.11. Non-conductive fragments of samples were gently cleaned and carbon-coated to suppress charging and stabilise back-scattered contrast prior to SEM imaging. Each piece was mounted on aluminium stubs with conductive carbon adhesive, edges bridged if needed, then coated in a JEOL JFC-600 Auto Fine Coater as shown in Figure 3.12, operated under the laboratory SOP. The sequence was kept simple and repeatable: load stubs, evacuate and argon-purge the

chamber, select the auto cycle, run a short sputter (producing approximately 5 to 10nm Au or Pt/Pd), vent, and unload. Coating parameters such as target, time, chamber pressure, and date were logged with the sample IDs.



Figure 3.11 Sample Fragments for Sputtered Coating and SEM Imaging



Figure 3.12 JEOL JFC-600 Auto Fine Coater for Conductive Sputter Coating Prior to SEM Imaging

For SEM-EDX analysis, representative fractured or prepared surfaces were selected from the hardened paste specimens. The SEM images were used to observe morphology, matrix continuity and visible pore features, while EDX was used to support elemental interpretation at selected analysis points. Since SEM-EDX is localised in nature, the results were interpreted as representative microstructural evidence rather than full quantitative characterisation of the entire specimen.

3.6.5 Chemical Composition

Bulk elemental screening was performed with a handheld energy-dispersive X-ray fluorescence (XRF) analyzer to quantify Ca and Mg in the carbonate powders and to provide rapid checks on selected hardened fragments. XRF does not measure carbon

or oxygen. Results are therefore reported as elemental wt% for Ca and Mg which optionally convertible to CaO or MgO by stoichiometry in later analysis. The method complements SEM–EDX by providing bulk rather than local composition.

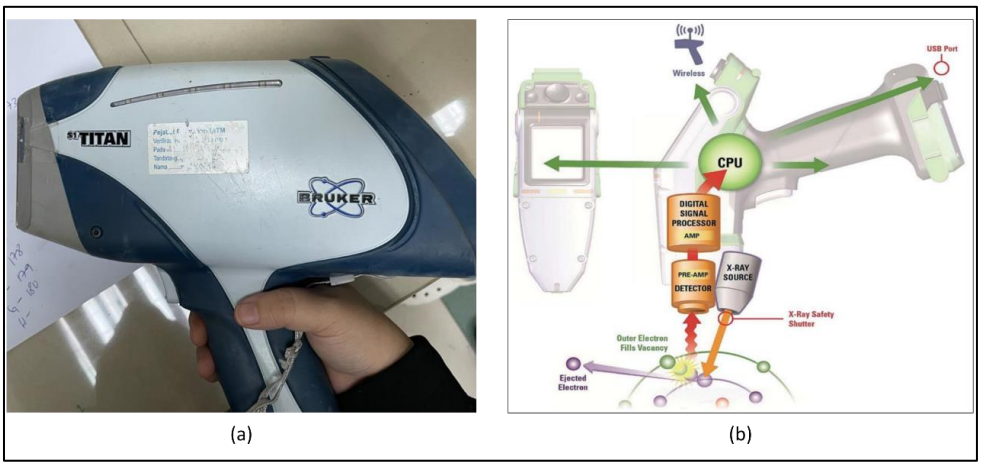


Figure 3.13 (a) XRF Analyzer Machine for Chemical Composition Analysis and (b) The Mechanical Components

Measurements were acquired at the Institute for Infrastructure Engineering and Sustainable Management (IIESM) Laboratory, UiTM Shah Alam using a Bruker S1 TITAN 800 Handheld XRF as shown in Figure 3.13 (a) and (b). The instrument was operated on a benchtop test stand by certified laboratory personnel to ensure fixed geometry and radiation shielding. Figure 3.13 (a) and (b) illustrates th utilized handheld XRF machine, and the mechanical components contained in the XRF analyzer, and its process respectively. Results such as elemental wt% Ca and Mg, were exported to Microsoft Excel and compiled as mean ± SD per specimen. Where needed for comparison with cement standards, elemental values may be reported as oxide equivalents (CaO, MgO) with the conversion noted. Specimen selection and preparation followed a standardised protocol. Powder forms fragments such as $CaCO_3$ and $CaMg(CO_3)_2$ were loaded into disposable sample cups fitted with a thin-film window, tapped gently to obtain a flat, compact surface, and sealed to prevent loss of fines. For hardened fragments, a small planar area was prepared with fine abrasive paper to ensure full contact with the XRF analyzer's nose, and loose dust was removed with a lint-free tissue. All specimens were kept dry and free of visible contamination, as moisture and surface debris can bias the response for light elements.

Chemical composition was analysed using handheld XRF as a rapid comparative method for selected binder systems and precursor material. The results

were used to compare bulk oxide trends between selected mixes. However, handheld XRF analysis of cementitious materials is affected by surface heterogeneity, sample flatness, moisture condition, particle packing and matrix effects. Therefore, the XRF results were interpreted as semi-quantitative comparative data rather than exact absolute oxide composition.

3.6.6 Phase Analysis

Phase identification was performed by X-ray diffraction (XRD) on a Rigaku Ultima IV diffractometer (Bragg–Brentano θ–2θ geometry) equipped with Cu-Kα radiation (λ = 1.5406 Å) which was utilized at Materials Science Laboratory in UiTM Shah Alam as shown in Figure 3.14. The tube was operated at 40 kV, 40 mA with a fixed divergence or receiving slit configuration and sample spinner engaged to improve particle statistics. Diffractograms were collected over 10 to 80° 2θ with a step size of 0.010° 2θ and an effective counting time ~1 s per step (constant step mode). These settings balance angular resolution with throughput for hydrated cement matrices and carbonate phases.



Figure 3.14 Rigaku Ultima IV Diffractometer XRD Pattern Characterization Machine

Hardened material from the designated mixes was gently crushed, passed through a 75 μm sieve, and side-loaded into a low-background holder to minimise preferred orientation. Powders were conditioned at ≤ 50 °C to constant mass before grinding to avoid thermal alteration of hydrates or spurious carbonation. Each holder was cleaned between samples, labelled with the encoded ID, sealed to limit ambient

CO_2 uptake, and delivered to the laboratory with a one-page request sheet specifying: (i) phase targets (portlandite, calcite/aragonite/vaterite, clinker remnants), (ii) preferred scan window, and (iii) file formats requested.

3.6.7 Thermal Properties

Thermal behaviour was assessed by thermogravimetric analysis (TGA) with derivative mass loss (DTG) to resolve bound-water release, portlandite dehydroxylation, and carbonate decarbonation in mixes batched with CO_2-water and calcium-rich precursors. was performed at the Centre for Functional Materials and Nanotechnology (CFMN) in UiTM Shah Alam using a Perkin Elmer Pyris 1 TGA system as shown in Figure 3.15. Operation followed the facility SOP for temperature and mass calibration, baseline correction, and gas handling. Runs were logged with instrument ID, pan type, purge rate, and program file. Hardened material from designated mixes was gently crushed and sieved to less than 75 μm in a covered tray to limit secondary carbonation. Powders were conditioned at less than 50 °C to constant mass and stored in a desiccator until testing. Approximately 20 to 40 mg of powder was weighed into a pre-baked alumina crucible. An empty matched crucible served as the blank for buoyancy or baseline correction. The submission form requested normalization to the initial mass and export of TG and DTG data files.

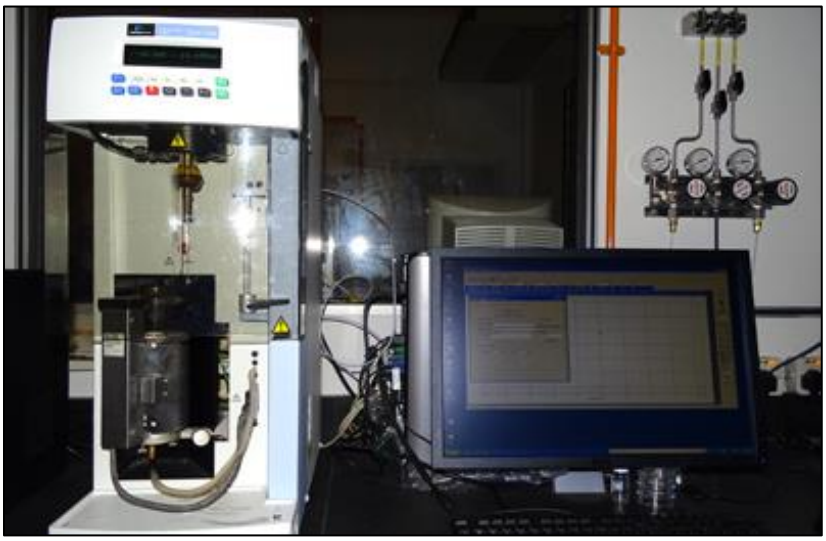


Figure 3.15 Perkin Elmer Pyris 1 TGA Instrument

TGA/DTA was conducted on selected powdered paste samples to evaluate thermal mass loss associated with moisture removal, hydrate decomposition and

carbonate-related decomposition. The test was conducted from room temperature to approximately 1000 °C at a heating rate of 10 °C/min under a nitrogen atmosphere. The mass-loss regions were then interpreted to support discussion of hydration-carbonation behaviour, particularly changes associated with bound water, portlandite decomposition and carbonate decomposition.

CHAPTER 4
RESULTS AND DISCUSSION

4.1 Batching pH and Early-Age Behaviour

The batching pH is treated in this study as an operational boundary condition that defines the short pre-contact window where dissolved CO_2 in the aqueous CO_2 solution can participate in early reactions before the cement pore solution becomes strongly alkaline. In the prepared acidic ranges, dissolved inorganic carbon is initially present mainly as carbonic acid and bicarbonate. Upon contact with OPC, rapid dissolution of alkalis and Ca-bearing phases increases ionic strength and drives the pore solution to high pH within a short time. This rapid alkalinisation changes carbon speciation and reduces the persistence of the initial acidic regime. Therefore, any measurable influence of the aqueous CO_2 solution is expected to be front-loaded, occurring during the brief interval where carbon species remain available in solution while calcium is being released, enabling early precipitation and nucleation events within the fresh paste.

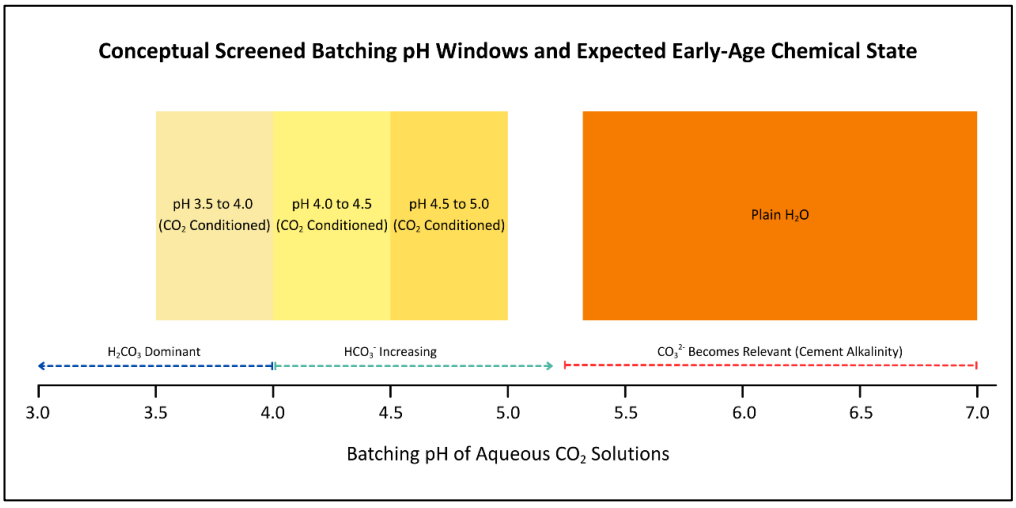


Figure 4.1 Conceptual Screened Batching pH Windows and Expected Early-Age Chemical State

This behaviour is related to the equilibrium of dissolved CO_2 in water. When CO_2 is introduced into water, part of the gas dissolves as aqueous CO_2 and forms carbonic acid, H_2CO_3. The carbonic acid system then dissociates into bicarbonate and carbonate species according to the following equilibrium reactions:

$$CO_{2(g)} \rightleftharpoons CO_{2\,(aq)} \quad (4.1)$$

$$CO_{2\,(aq)} + H_2O \rightleftharpoons H_2CO_3 \quad (4.2)$$

$$H_2CO_3 \rightleftharpoons H^+ + HCO_3^- \quad (4.3)$$

$$HCO_3^- \rightleftharpoons H^+ + CO_3^{2-} \quad (4.4)$$

Therefore, the decrease in pH during CO_2-water preparation reflects the increase in dissolved CO_2 and carbonic-acid-related species in the solution. Before contact with OPC, the lower pH range is expected to contain higher dissolved CO_2, H_2CO_3 and HCO_3^- species, while CO_3^{2-} remains limited. Once the solution contacts the alkaline OPC system, the equilibrium shifts and carbonate species can interact with Ca-bearing phases in the paste. This provides the chemical basis for the conceptual representation shown in Figure 4.1.

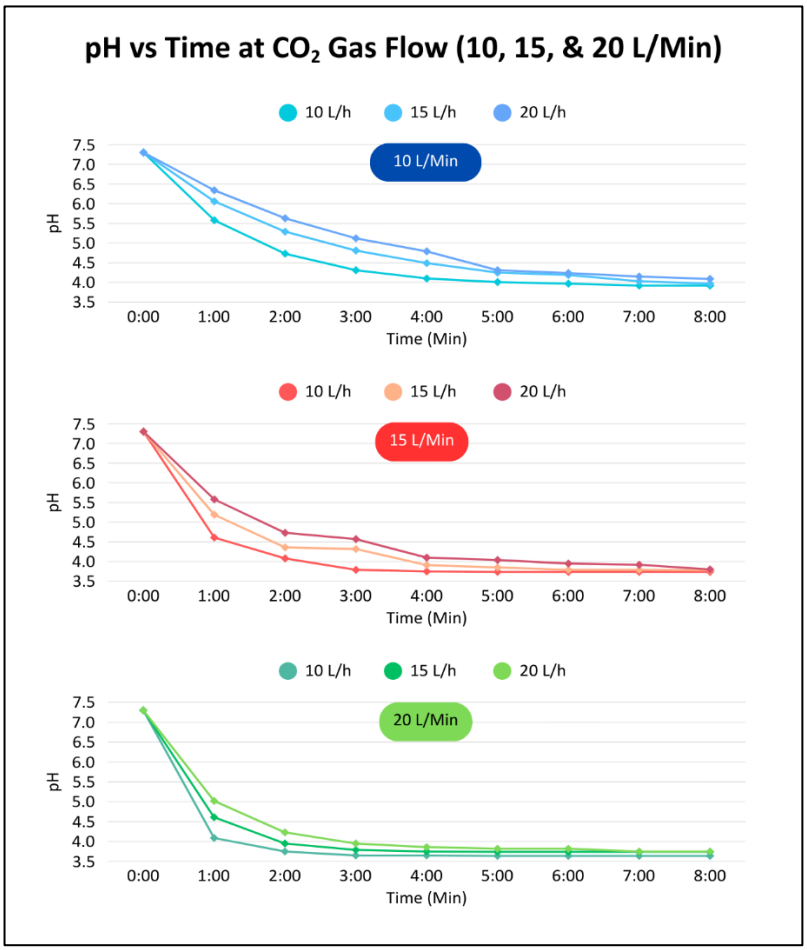


Figure 4.2 pH vs Time (Min) Analysis with Variation of CO_2 Gas Flow (10, 15, and 20 L/Min) and Flowrate of Aqueous CO_2 Solution During Mixing (5, 10, and 15 L/h)

Figure 4.1 summarises this process-window concept and clarifies batching pH as a process window rather than a continuous variable. The acidic windows, namely pH 3.5 to 4.0, 4.0 to 4.5 and 4.5 to 5.0, represent controlled pre-contact states of the mixing liquid where dissolved CO_2 and carbonic-acid-related species strongly influence the solution chemistry. After powder contact, the system transitions through a short mixing regime where carbon species coexist with rising Ca^{2+} concentration and increasing alkalinity, before the chemistry becomes dominated by the typical high-pH cement environment. This framing clarifies why the same nominal preparation condition can still yield different practical outcomes if the liquid experiences different residence time, degassing exposure or flow conditions prior to batching. It also supports the interpretation used later in this chapter, where the role of batching pH is to determine whether the paste experiences a sufficiently long CO_2-active interval at the start of hydration, not to imply that the paste remains acidic during curing.

Table 4.1
pH Evolution (0 to 8 min) of Aqueous CO_2 Solution Under Combined CO_2 Gas Flow (5, 10, 15 L/min) and Water Flow (10, 15, 20 L/h) Operating Conditions

Time	5 L/Min			10 L/Min			15 L/Min		
	10 L/h	15 L/h	20 L/h	10 L/h	15 L/h	20 L/h	10 L/h	15 L/h	20 L/h
0:00	7.30	7.30	7.30	7.30	7.30	7.30	7.30	7.30	7.30
1:00	5.58	6.06	6.34	4.61	5.19	5.58	4.09	4.61	5.02
2:00	4.73	5.29	5.63	4.08	4.36	4.73	3.75	3.95	4.23
3:00	4.31	4.81	5.12	3.79	4.32	4.57	3.65	3.79	3.95
4:00	4.10	4.49	4.79	3.75	3.91	4.10	3.65	3.75	3.86
5:00	4.01	4.25	4.31	3.74	3.85	4.04	3.64	3.74	3.82
6:00	3.97	4.19	4.24	3.74	3.79	3.95	3.64	3.74	3.82
7:00	3.92	4.03	4.15	3.74	3.79	3.92	3.64	3.74	3.75
8:00	3.92	3.97	4.09	3.74	3.78	3.80	3.64	3.74	3.75

Measured pH against time behaviour under various controlled combinations of CO_2 gas flow (L/min) and aqueous CO_2 solution flow (L/h) is depicted in Figure 4.2

and Table 4.1. Across all tested cases, pH decreases rapidly from the initial neutral value to an acidic plateau, but the rate of approach and the plateau pH depend on both flow rates. Increasing CO_2 gas flow accelerates the pH drop and tends to lower the stabilised pH because the gas-liquid mass transfer driving force and CO_2 availability increase. Increasing water flow has the opposite tendency; for a fixed gas flow, a higher water throughput reduces contact time and CO_2 uptake per unit volume, producing a slower decline and a higher pH at a given exposure time. These trends explain the practical observation that achieving a reproducible batching pH is not governed by gas flow alone, but depends on the gas-to-liquid delivery balance that determines how quickly the solution reaches its target acidity and how stable that value remains during handling. To support implementation in batching, the preparation conditions were reduced to three representative pH ranges for subsequent specimen production: pH 3.5 to 4.0 as the primary CO_2-conditioned window, pH 4.0 to 4.5 as a less acidic CO_2-conditioned comparison window, and pH 6.0 to 7.0 as the plain-water baseline. This selection is consistent with the process-window concept in Figure 4.1 and is justified by the observed dynamics in Figure 4.2, where the pH 3.5 to 4.0 window is consistently reachable within minutes under sufficiently high gas delivery, while the plain-water range represents the reference state where the initial carbonic-acid interval is absent. The three-range design also avoids over-fragmentation of batching conditions that are operationally difficult to maintain as distinct bands under practical rig handling.

The pH values presented in Figure 4.2 were used as representative measured values to establish the batching pH windows for paste preparation. The measurements were taken using the same preparation rig and pH measurement procedure to maintain consistency between operating conditions. However, the values are not presented with independent replicate trials, standard deviation or measurement error. Therefore, the interpretation focuses on the relative pH trend and selected batching ranges rather than statistical comparison between individual pH values.

4.2 Setting Behaviour of of H_2CO_3 Mixed OPC Paste with Carbonate Precursor Replacement

Setting times increased as $CaCO_3$ dosage increased under H_2CO_3 mixing-water batching, as shown in Figure 4.3 and tabulated in Table 4.2. The initial set increased from 230 to 270 min between 5% and 25% $CaCO_3$ replacement, while the final set increased from 375 to 480 min over the same dosage range. These values remain within

the normal laboratory envelope for cement paste setting evaluation based on the Vicat method, although the increasing trend indicates a dosage-dependent retardation effect under the H_2CO_3 and $CaCO_3$ condition.

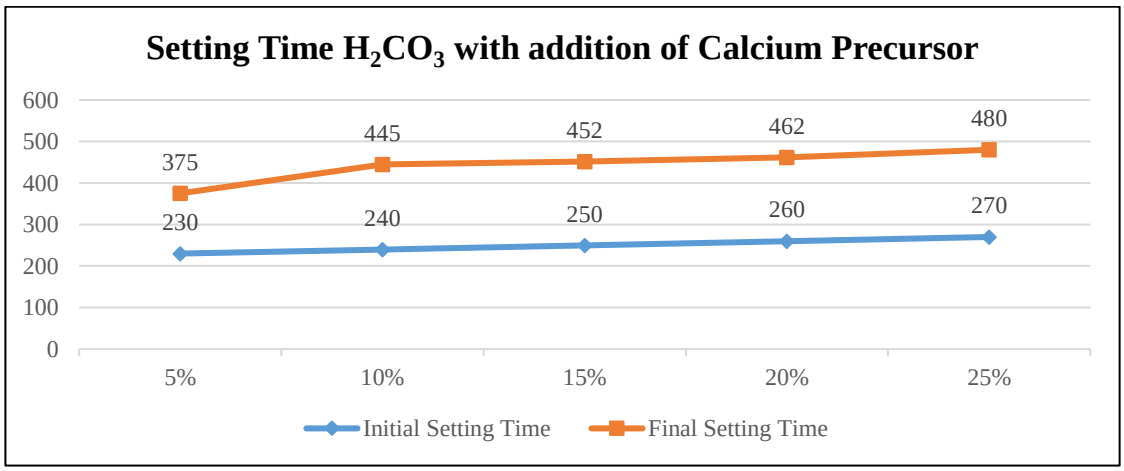


Figure 4.3 Initial and Final Setting Time of H3CO3-Mixed OPC Paste Containing CaCO3 Replacement

The monotonic increase across both initial and final setting times suggests that higher $CaCO_3$ replacement extended the early stiffening period of the paste. This behaviour may be related to the combined influence of carbonate precursor addition and the acidic starting condition of the H_2CO_3 mixing water. In ordinary water systems, limestone or $CaCO_3$ powder can sometimes accelerate early hydration through filler and nucleation effects. However, under H_2CO_3 mixing-water condition, the early ionic environment is different because dissolved CO_2, H_2CO_3 and bicarbonate species are present before the paste rapidly shifts toward the alkaline cement environment. Therefore, the observed setting delay is interpreted as the net effect of carbonate addition, early pH adjustment, dilution of OPC at higher replacement level and possible modification of early hydration reactions.

Setting responses were also sensitive to the chemical starting state defined at batching pH and to the thermal–hygrometric environment of the test. A transient acidic interval produced by aqueous CO_2 solution plausibly shortened the effective induction period at moderate carbonate contents, while higher replacement introduced a counteracting dilution and mild retardation, yielding the observed limestone trend and the dosage peak for dolomite. Small temperature or relative humidity excursions can shift absolute times. Therefore, interpretation focuses on relative changes within the same laboratory conditions rather than cross-laboratory absolutes. The combination of

a controlled batching pH window with standardised Vicat conditions is consistent with early-age studies where CO_2 is introduced during mixing and hydration features advance at moderate availability but slow at excessive acidity.

Table 4.2
Setting Times Measured Through Vicat Testing

System	Dosage (% of Binder)	Initial Set (Min)	Final Set (Min)
$CaCO_3$	5%	230	375
	25%	270	480
$CaMg(CO_3)_2$	5%	232	not reported
	10%	260	405

Table 4.2 also includes the available Vicat setting data for the $CaMg(CO_3)_2$ system. However, part of the $CaMg(CO_3)_2$ final setting-time record could not be retrieved during final data compilation because the electronic data file was corrupted. The missing value was therefore not interpolated or replaced with an estimated result. To avoid misrepresentation of the dataset, the incomplete $CaMg(CO_3)_2$ setting result was excluded from dosage-response trend interpretation. For this reason, the setting behaviour discussion focuses mainly on the complete $CaCO_3$ dataset, while the available $CaMg(CO_3)_2$ values are interpreted cautiously as partial comparative evidence rather than a complete dosage-response trend.

Future work should repeat the $CaMg(CO_3)_2$ setting-time series using a complete replicate matrix, with mean and standard deviation reported under controlled temperature and relative humidity.

4.3 Compressive Strength

Compressive strength is used as the primary performance metric to determine whether the CO_2 conditioned mixing route using H_2CO_3 produces a measurable mechanical response, and to quantify how that response evolves when carbonate precursors are introduced as partial binder replacement. The results are discussed in three layers to separate overlapping effects: (i) a batching pH-window screen that defines the effective chemical boundary condition at the point of mixing, (ii) the dosage response of $CaCO_3$ under the selected aqueous CO_2 batching approach, and (iii) the dosage response of $CaMg(CO_3)_2$ under the same approach. This structure follows the study logic of first identifying a workable CO_2 water condition, then evaluating whether

carbonate additions provide a net benefit through micro-filling and nucleation at low replacement or impose a penalty through reduced reactive binder fraction and disrupted matrix continuity at higher replacement. The figures and tables present the quantitative trends, while the discussion focuses on the governing mechanisms and the consistency of responses across curing ages. The compressive strength values are presented as representative average values from the available test dataset. Since standard deviation and full replicate statistics were not available for all pH bands and replacement levels, the interpretation focuses on relative trends, practical performance windows and consistency between mechanical behaviour and supporting characterisation evidence rather than formal statistical significance.

4.3.1 Effect of CO_2 Conditioned Batching pH on Compressive Strength

The batching pH screen establishes whether the aqueous CO_2 solution produces a measurable compressive strength response relative to the H_2O control and, if so, identifies the workable pH interval for subsequent dosage studies. Table 4.3 and Figure 4.4 show that mixes prepared within the lower pH bands achieved strengths comparable to or slightly above the control, whereas higher pH bands produced a clear reduction. The highest value in the screening set was recorded at pH 3.5 to 4.0 (25.57 MPa), marginally exceeding the control (24.58 MPa), while the pH 4.0 to 4.5 and pH 4.5 to 5.0 bands remained close to this level (24.88 MPa and 25.47 MPa, respectively).

Table 4.3
Compressive Strength by Mixing-Water pH Band (ASTM C109; 50 mm Cubes)

Mixing water pH band	Strength (MPa)	Δ vs neutral (MPa)	%Δ vs neutral
3.5 to 4.0 (H_2O + CO_2)	25.57	+0.99	+4.03%
4.0 to 4.5 (H_2O + CO_2)	24.88	+0.30	+1.22%
4.5 to 5.0 (H_2O + CO_2)	25.47	+0.89	+3.62%
5.0 to 5.5 (H_2O + CO_2)	20.59	−3.99	−16.23%
5.5 to 6.0 (H_2O + CO_2)	22.17	−2.41	−9.80%
6.0 to 7.0 (H_2O - Control)	24.58	0.00	0.00%

In contrast, the response decreased notably at pH 5.0 to 5.5 and pH 5.5 to 6.0 (20.59 MPa and 22.17 MPa), indicating that the benefit associated with CO_2 conditioning is not sustained when the batching liquid approaches less acidic conditions.

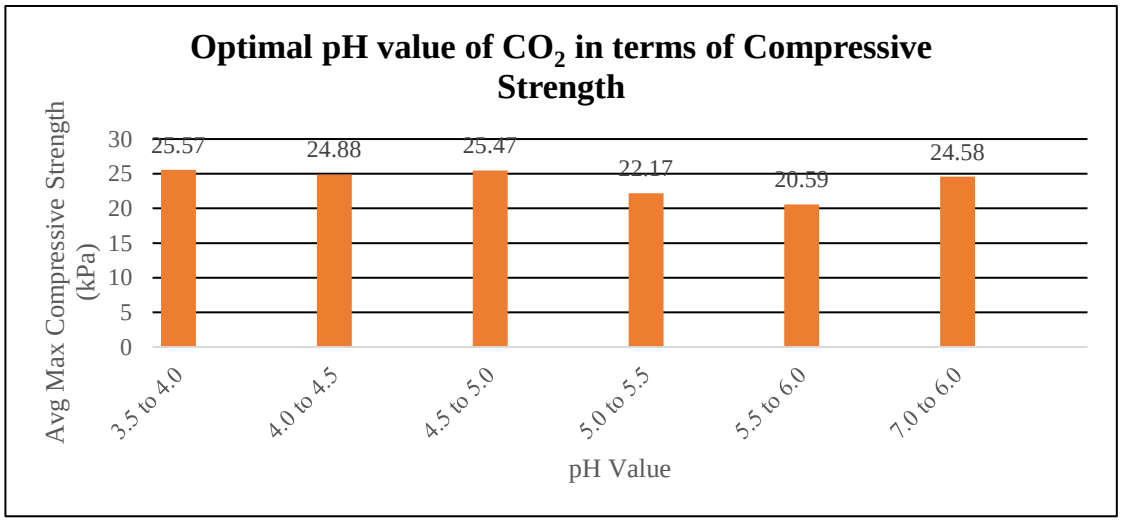


Figure 4.4 Compressive Strength vs. Mixing-Water pH Band Under Liquid-Phase CO_2 Batching

This pattern is consistent with the role of batching pH as a practical indicator of the dissolved CO_2 state immediately prior to cement contact. A lower batching pH reflects a mixing liquid with higher dissolved inorganic carbon availability at the start of mixing, which can support early precipitation and nucleation processes during the short interval before cement alkalinity dominates and shifts the pore solution away from the CO_2 conditioned regime. As batching pH increases, the chemical distinction between aqueous CO_2 solution and ordinary water diminishes due to reduced dissolved CO_2, and the observed strength response converges toward or below the control. The strength decrease at the higher pH bands therefore supports the interpretation that maintaining the aqueous CO_2 solution window at batching is a controlling condition for achieving a measurable mechanical response, rather than treating pH as a secondary parameter. This agrees with previous observations on CO_2-conditioned mixing water and early-age carbonation systems, where controlled CO_2 availability may assist carbonate nucleation and early matrix refinement, but excessive acidity, insufficient CO_2 conditioning or unstable batching conditions can reduce the strength benefit (Lippiatt et al., 2019; Bernal et al., 2024).

Although pH 4.5 to 5.0 recorded a comparable strength value, pH 3.5 to 4.0 was retained as the reference batching condition because it represented the strongest and most consistent CO_2-conditioned mixing-water window obtained during solution preparation. This selection does not imply that lower pH will always produce higher strength. Instead, it identifies the practical batching window where the CO_2-active interval before cement alkalisation was expected to be most pronounced while still producing strength comparable to or slightly higher than the control.

4.3.2 $CaCO_3$ Bearing Systems Under Aqueous CO_2 Solution

The $CaCO_3$ series was used to evaluate how a carbonate precursor behaves under the same aqueous CO_2 solution approach when introduced as partial binder replacement following the batching pH screen. Figure 4.5 presents the compressive strength development of OPC pastes prepared using the aqueous CO_2 solution while varying $CaCO_3$ replacement from 5% to 25% at curing ages of 3, 7, and 28 days.

The response is non-monotonic at early ages, indicating that the role of $CaCO_3$ in this study extends beyond simple dilution of clinker. At 3 days, strengths lie within a narrow band of 20.59 to 26.24 MPa, with the highest value observed at 10% $CaCO_3$ replacement. Increasing $CaCO_3$ above 10% reduced the early strength, reaching 20.59 MPa at 25%, which is consistent with the expectation that higher replacement reduces the early availability of reactive clinker phases and limits rapid formation of a continuous load-bearing hydrate skeleton. At 7 days, the same optimum at 10% remained evident, with 44.23 MPa recorded, whereas higher contents reduced strength relative to this peak, with 33.46 MPa recorded at 25%. This pattern suggests that, up to 7 days, the most effective $CaCO_3$ range is near 10% under the present batching condition, where packing and nucleation contributions appear sufficient to offset the reduction in clinker content. This interpretation is consistent with the known filler and nucleation role of $CaCO_3$ in cementitious binders, where moderate limestone or calcium carbonate addition can provide extra surfaces for early hydrate precipitation, while excessive replacement may reduce the amount of reactive clinker available for strength development.

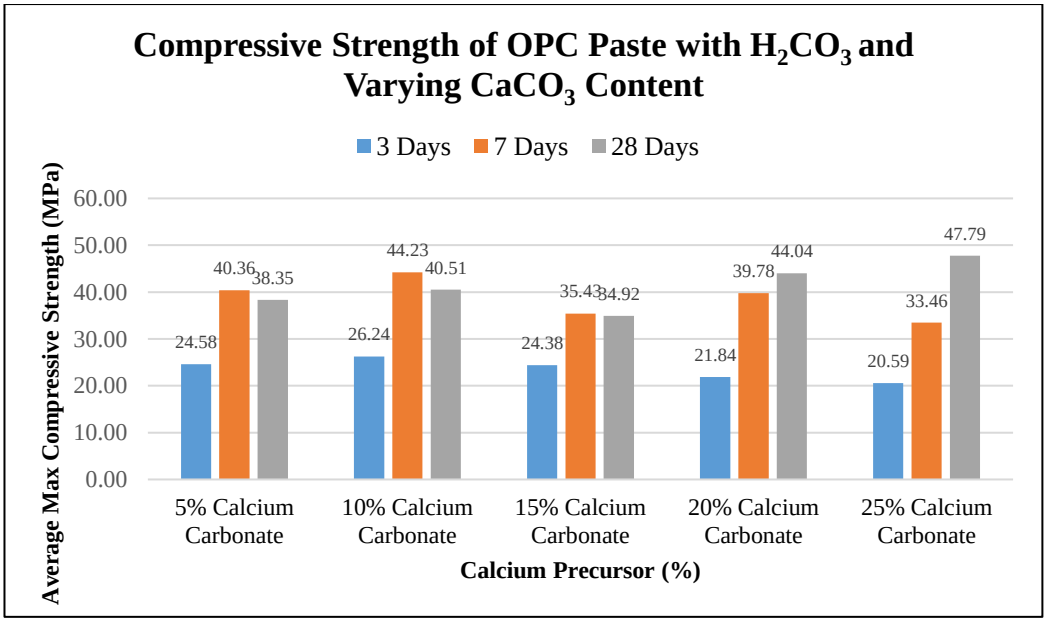


Figure 4.5 Compressive Strength vs CaCO3 Content at 3, 7 and 28 Days with Addition of H_2CO_3

At 28 days, the strength response no longer followed the same early-age pattern. Higher $CaCO_3$ replacement levels showed improved later-age performance, with the 25% $CaCO_3$ mixture recording the highest 28-day strength within the series. This suggests that later-age strength may have benefited from matrix filling, particle packing and gradual densification during curing. However, the lower 3-day and 7-day strengths at higher $CaCO_3$ replacement show that this later-age improvement should not be interpreted as a universal dosage optimum. Therefore, 10% $CaCO_3$ is interpreted in this study as a balanced early-age replacement level rather than the overall optimum for all curing ages. The $CaCO_3$ response should therefore be understood as an age-dependent performance window influenced by replacement percentage, hydration development and paste continuity.

The $CaCO_3$ compressive-strength series was reported at 3, 7 and 28 days to represent early-age, intermediate-age and standard 28-day strength development. A 14-day data point was not included for this series because the $CaCO_3$ compressive-strength programme was compiled using the available scheduled testing ages. No 14-day value was interpolated or estimated.

4.3.3 Compressive Strength Response of $CaCO_3$ Bearing Systems under the Aqueous CO_2 Solution

$CaMg(CO_3)_2$ series was evaluated to determine how a mixed carbonate precursor behaves under the same aqueous CO_2 solution batching condition when introduced as partial binder replacement. Figure 4.6 and Table 4.4 depicts that cement paste mixed $CaMg(CO_3)_2$, does not follow a monotonic strength gain with increasing replacement, but instead exhibits a clear low-dosage optimum and a pronounced penalty at higher dosages.

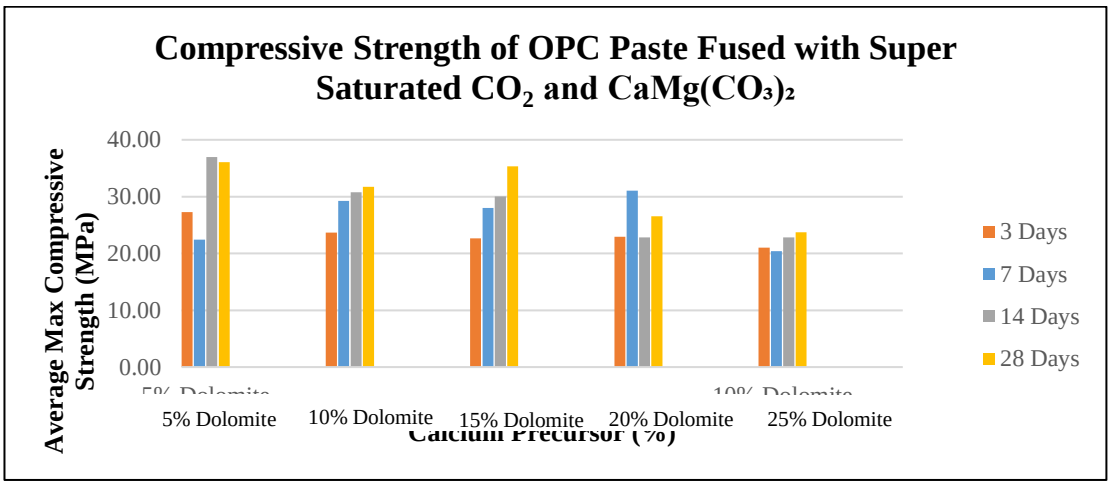


Figure 4.6 Compressive Strength vs $CaMg(CO_3)_2$ Content at 3, 7, 14 and 28 Days with Addition of H_2CO_3

At 28 days, the 5% and 15% mixes retained the highest performance within this series, reaching 36.05 MPa and 35.33 MPa, respectively, while the 10% mix remained moderate at 31.73 MPa. The 20% and 25% mixes however, fell substantially to 26.51 MPa and 23.72 MPa, indicating that once the carbonate replacement exceeds a certain level, the binder skeleton becomes increasingly governed by dilution effects rather than any beneficial particle-mediated densification. The 14-day results reinforce this separation. The 5% mix achieved the highest intermediate-age strength (36.95 MPa), whereas 20 to 25% remained low (22.84 to 22.79 MPa), confirming that the strength divergence is not limited to the 28-day endpoint but is already established by the second week of curing.

Table 4.4
Average Compressive Strength of $CaMg(CO_3)_2$ by Age of Curing

$CaMg(CO_3)_2$ (%)	3 Days	7 Days	14 Days	28 Days
5	27.29	22.45	36.95	36.05
10	23.67	29.27	30.76	31.73
15	22.63	28.01	30.03	35.33
20	22.95	31.03	22.84	26.51
25	21.04	20.38	22.79	23.72

The early-age values between 3 and 7 days fluctuate more irregularly than the 14- and 28-day results. This behaviour may be caused by the sensitivity of early OPC paste strength to local paste continuity, entrapped pores, early hydration progress and the distribution of $CaMg(CO_3)_2$ particles within the matrix. At early age, the paste skeleton is still developing, so small differences in compaction, particle packing, and local water distribution can produce noticeable variation in compressive strength. Therefore, the 3- and 7-day data are interpreted cautiously as early response indicators, while the 14- and 28-day results provide a clearer indication of dosage-dependent strength development. Figure 4.6 is used to show the strength trend visually, while Table 4.4 provides the numerical values used for comparison across curing ages. To avoid repetition, the discussion focuses on the main trend and critical dosage points rather than restating every value in the table. The $CaMg(CO_3)_2$ response suggests that its beneficial range under aqueous CO_2 mixing is narrower than that of $CaCO_3$. Although low to moderate replacement may contribute to particle packing and local densification, higher replacement reduces the proportion of reactive OPC and can interrupt the continuity of the load-bearing hydrate network. The Mg-bearing nature of $CaMg(CO_3)_2$ may also influence the local particle-paste interface differently from $CaCO_3$, making the system more sensitive to replacement level. Therefore, the strength reduction at 20% and 25% replacement is interpreted as the combined effect of dilution, weaker matrix continuity and less favourable particle integration within the cementitious binder skeleton. Overall, the $CaMg(CO_3)_2$ series shows that low to moderate replacement can retain acceptable strength performance, but higher replacement levels are not favourable under the tested aqueous CO_2 mixing condition. The results indicate that $CaMg(CO_3)_2$should be treated as a dosage-sensitive precursor.

4.4 Water Absorption

Water absorption behaviour was assessed to provide an indirect indication of accessible pore connectivity and moisture ingress potential of OPC paste prepared using aqueous CO_2 solution batching. The test procedure was described in Section 3.6.3 as an adapted immersion-based method, with reference to the absorption principle in ASTM C642/C642M. In a standard calculation, water absorption is determined as percentage mass gain using the dry mass before immersion and wet mass after immersion, as shown in Equation 3.x. However, the present dataset was compiled based on the final specimen mass after 14 days of water exposure, while the corresponding pre-immersion dry mass was not available for all specimens during final analysis. Therefore, the results in this section are interpreted as comparative post-immersion mass response rather than complete standard water absorption percentage.

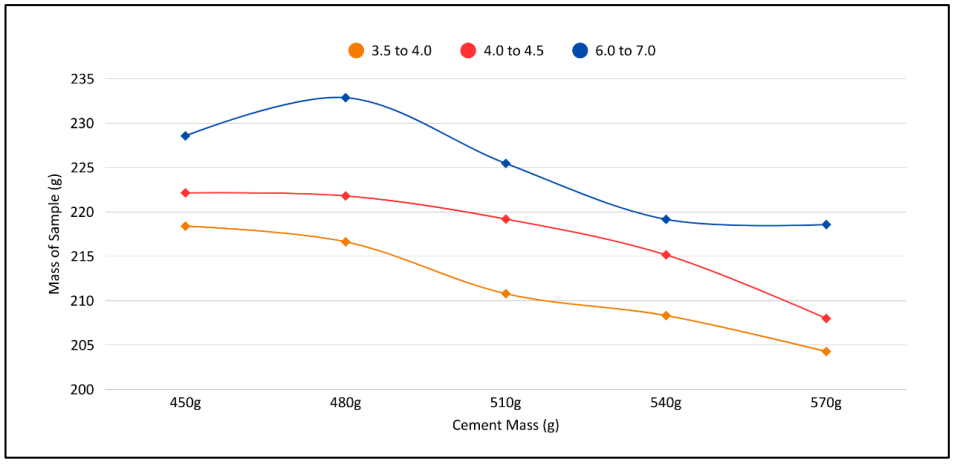


Figure 4.7 Post-Immersion Mass Response of OPC Paste After 14-Day Water Exposure for Selected Aqueous CO_2 Mixing-Water pH Ranges

Three pH ranges were retained for interpretation which were 3.5 to 4.0, 4.0 to 4.5, and 6.0 to 7.0. The selection was intentional to represent (i) the most CO_2 active acidic window targeted for aqueous CO_2 solution preparation, (ii) an adjacent acidic window that reflects partial loss of acidity or buffering, and (iii) a near-neutral condition serving as the practical reference behaviour. Including additional pH bands would increase complexity without strengthening interpretation, particularly where the batching pH variability and limited repeat reads may reduce confidence in fine pH separation; therefore, the dataset was treated as a controlled comparison across three chemically meaningful windows rather than a continuous pH-response mapping. Figure 4.7 and Table 4.5 show a consistent ranking across cement mass levels (450 to 570 g).

Specimens batched at pH 3.5 to 4.0 exhibit the lowest post-exposure specimen mass values, followed by pH 4.0 to 4.5, while pH 6.0 to 7.0 records the highest values throughout. For example, at 450 g, specimen mass is 218.40 g (pH 3.5 to 4.0), 222.15 g (pH 4.0 to 4.5), and 228.57 g (pH 6.0 to 7.0). At 570 g, the corresponding values are 204.27 g, 208.00 g, and 218.58 g, respectively. The persistence of this ordering across all cement mass levels indicates that the pH condition during aqueous CO_2 solution batching exerts a systematic influence on the absorption response rather than producing isolated batch-dependent deviations.

Table 4.5
Final Specimen Mass After 14-day Water Immersion for OPC Paste Prepared with Selected Aqueous CO_2 Mixing-Water pH Ranges

pH Range	**Sample Mass (g)**				
3.5 to 4.0	218.40	216.64	210.79	208.33	204.27
4.0 to 4.5	222.15	221.81	219.20	215.16	208.00
6.0 to 7.0	228.57	232.88	225.47	219.17	218.58

Interpreted in the context of absorption behaviour, the lower post-exposure mass response at pH 3.5 to 4.0 suggests reduced moisture uptake under the same conditioning protocol, consistent with a less permeable pore network or reduced connectivity of accessible pores at 14 days. The intermediate behaviour at pH 4.0 to 4.5 indicates that partial reduction in acidity is associated with a weaker absorption improvement, implying that the benefit is sensitive to the maintained CO_2 water chemistry during batching. The near-neutral condition (pH 6.0 to 7.0) provides the reference response where aqueous CO_2 solution effects are minimal, and the higher post-exposure masses are consistent with comparatively greater water uptake under the same exposure procedure. Overall, the absorption results support the selection of the acidic batching window for subsequent performance interpretation, and they align with the broader premise that aqueous CO_2 solution preparation can influence early pore-structure development in cementitious systems.

Because all specimens were subjected to the same exposure duration, specimen size, handling procedure and weighing method, the final post-immersion mass values were used only for relative comparison between pH conditions. A lower final mass after immersion may indicate lower comparative moisture uptake under the same test

condition, while a higher final mass may indicate greater moisture uptake. However, this interpretation should not be treated as a standardised water absorption percentage. Future testing should record both W_{dry} and W_{wet} for each replicate and report water absorption as percentage mass gain with mean and standard deviation.

4.5 Bulk Chemical Composition by XRF

XRF is used to establish the bulk chemical baseline of the binder systems and to support the interpretation of SEM–EDX by distinguishing specimen-scale composition from localised microstructural domains. Whereas SEM–EDX interrogates specific regions such as matrix, inclusions, and interfaces, XRF provides an averaged chemical signal and is therefore suited to confirming whether the carbonate precursors materially shift the overall Ca–Si balance and whether Mg from $CaMg(CO_3)_2$ is present at specimen scale. For clarity and to avoid repetition, only a representative set of specimens is discussed: a plain OPC paste as a baseline reference, a $CaCO_3$ modified binder prepared under the aqueous CO_2 solution approach (M6A) to represent the Ca carbonate route, a high-replacement $CaMg(CO_3)_2$ mix (M15B) to represent the Mg bearing carbonate route at the upper bound of replacement, and the $CaMg(CO_3)_2$ precursor powder to anchor the carbonate-source signature. This selection is sufficient to verify directionality of chemistry change such as presence or absence of Mg and carbonate contribution. The XRF results are interpreted as semi-quantitative comparative data because oxide totals may be affected by sample heterogeneity, matrix effects, surface condition, moisture condition and normalisation during analysis.

The spectra in Figure 4.8 are dominated by Ca across all paste-containing specimens, consistent with the calcium-rich nature of cementitious binders. The control paste shows the expected coexistence of Ca with Si, Al, and Fe, reflecting the clinker-derived oxide inventory that governs formation of the hydrated binder network. In M6A, the Ca dominant response remains prominent while silicate-associated peaks persist, consistent with a cement-based binder in which $CaCO_3$ contributes additional Ca rich solid content but does not introduce Mg. In M15B, the key discriminating feature is the increased Mg signal relative to the control and $CaCO_3$ modified binder, consistent with incorporation of $CaMg(CO_3)_2$ and aligned with the Mg-bearing domains observed in SEM–EDX for dolomite-containing specimens. The persistence of Si and Al alongside Ca in M15B indicates that the binder remains cement-derived in

chemistry, while the increased Mg signal indicates a compositional shift attributable to the precursor rather than an artefact of local spot selection.

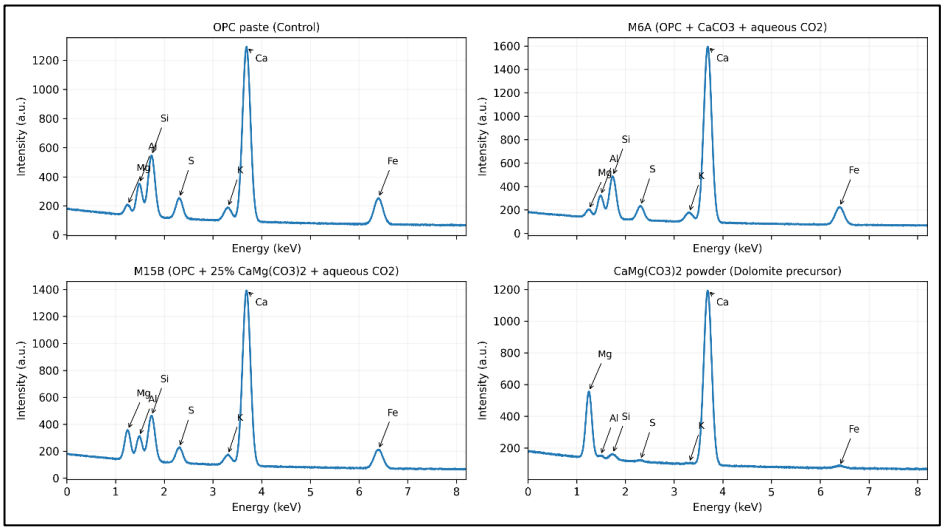


Figure 4.8 XRF Spectra of Selected Binders and Carbonate Precursor, Presented as Separate Panels with Labelled Major Elemental Peaks (Ca, Si, Al, Mg, Fe, S, K)

Table 4.6
Bulk Oxide Composition (wt%) of Selected Binders and $CaMg(CO_3)_2$ Precursor by XRF (SiO_2, Al_2O_3, Fe_2O_3, CaO, MgO, SO_3, Na_2O, K_2O, TiO_2, and LOI)

Sample	SiO_2	Al_2O_3	Fe_2O_3	CaO	MgO	SO_3	Na_2O	K_2O	TiO_2	LOI	Total
OPC Paste (Control)	20.7	5.1	3	63.2	2.3	2.7	0.2	0.7	0.3	2.8	101
$CaMg(CO_3)_2$ Powder	0.6	0.2	0.1	30.5	21.2	0.1	0	0	0	47.3	100
M6A	18.6	4.8	2.8	56.5	2.1	2.5	0.2	0.6	0.3	11.2	99.6
M15B	17.9	4.5	2.7	49	7.8	2.3	0.2	0.6	0.3	14.4	99.7

The oxide totals in Table 4.6 are interpreted within the normal tolerance of semi-quantitative XRF analysis. XRF measures elemental signals and reports them as oxide equivalents; therefore, the total oxide percentage may deviate slightly from 100% due to oxide conversion, rounding, matrix effects, sample heterogeneity, surface condition and moisture-related variation. The control OPC paste recorded a total of 101.0%, which is treated as a small analytical deviation rather than evidence of an additional oxide phase. Hence, the XRF results are used for comparative interpretation of bulk chemical directionality, such as Ca-rich composition, Mg incorporation and carbonate-associated contribution, rather than exact absolute quantification.

Table 4.6 depicts the bulk compositional framing needed to interpret the mechanical response discussed in Section 4.3 and the microstructural evidence discussed in the following sections. The control paste is CaO rich with a substantial silicate fraction (SiO_2) and supporting Al_2O_3 and Fe_2O_3, consistent with a binder controlled by hydration of cement phases. M6A is represented by a higher carbonate-associated volatile fraction (LOI) relative to the control, consistent with the presence of $CaCO_3$ in the bulk system while retaining the cement-derived silicate inventory. M15B shows a markedly higher MgO contribution relative to the control and $CaCO_3$ modified binder, supporting that Mg enters the binder system at specimen scale when $CaMg(CO_3)_2$ is used. In the context of mechanical response, these bulk shifts are interpreted as constraints rather than direct predictors, because compressive strength depends not only on oxide composition but also on hydrate continuity, pore structure, particle distribution and interfacial bonding. This means increasing carbonate contribution and introducing Mg-bearing solids can coexist with early densification features in SEM, but later-age strength is governed by whether the cement-derived hydration network remains sufficiently continuous to bind inclusions and transmit load. Bulk XRF trends are used here to confirm precursor signatures and to provide chemical context for the microstructural discussion, where the spatial distribution of Ca rich paste, Mg-bearing inclusions, and interfacial zones determines whether compositional change translates to beneficial refinement or to discontinuities that penalise strength.

4.6 Microstructural and Elemental Characterisation

4.6.1 SEM Microstructure

Figure 4.9 compiles BSE-SEM fields selected to visualise how the binder skeleton evolves when the mixing liquid carries dissolved CO_2 (as H_2CO_3) and when carbonate precursors are introduced as either $CaCO_3$ (M6A) or $CaMg(CO_3)_2$ (M10A, M12C, and M15B). The annotations were chosen to separate three recurring microstructural domains that control hardened behaviour: (i) the continuous binder matrix (the phase expected to carry most of the load), (ii) discrete inclusions or partially reacted solids embedded in that matrix, and (iii) discontinuities such as voids and micro-cracks that interrupt stress transfer. Compositional contrast assists interpretation: denser, Ca-rich features tend to appear brighter than the surrounding silicate-bearing matrix, enabling the interface between Ca-rich zones. This is particularly relevant to

the present study because the H_2CO_3 route is intended to promote early carbonate precipitation in the fresh system, and any benefit is expected to manifest first as pore refinement and local densification rather than as a wholesale change in bulk morphology. The micrographs therefore serve as the primary morphological evidence that carbonation-related products are localised, and that the binder phase remains continuous in the mixes that performed well in the mechanical programme.

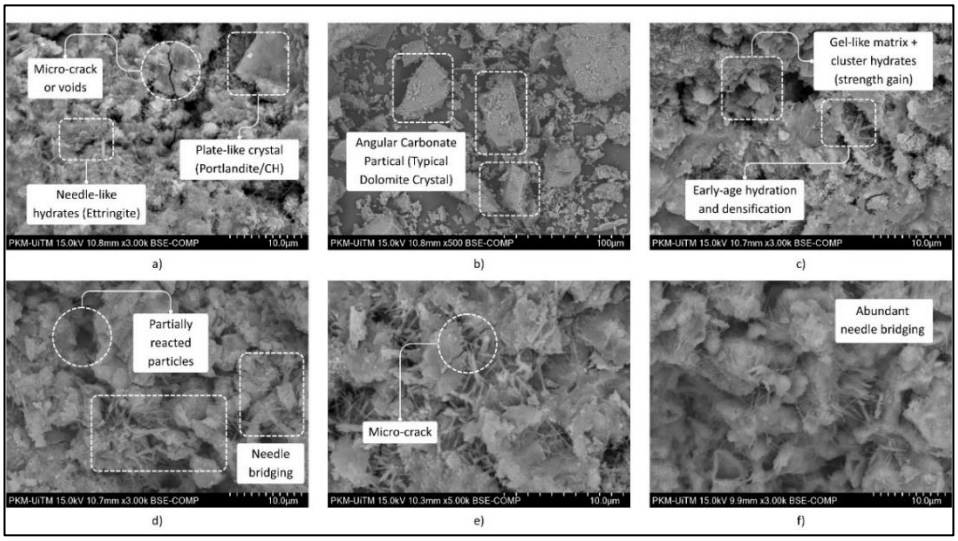


Figure 4.9 SEM Micrographs of Samples: (a) Cement + Water (Control), (b) $CaMg(CO_3)_2$ Powder, H_2CO_3 + $CaCO_3$ Mixed Samples; (c) M6A, and H_2CO_3 + $CaMg(CO_3)_2$ Samples; (d) M10A, (e) M12C and (f) M15B at 7 Days

The control paste in Figure 4.9 (a) is used as the baseline for interpreting the CO_2-conditioned and carbonate-bearing systems. The field is heterogeneous, with hydration products distributed unevenly and interrupted by local discontinuities. Needle-shaped hydrates are visible within the paste matrix, consistent with early-age AFt-type formation that commonly develops into available pore space. Plate-like crystals are also present and are typically associated with portlandite-rich domains in hydrated OPC. These crystalline features coexist with micro-cracks or voids, indicating that the hardened skeleton is not fully continuous at the micro-scale and that pore connectivity remains non-uniform in the selected region. This baseline is important because the role of H_2CO_3 in the present work is not to remove hydration products, but to shift precipitation and nucleation behaviour so that discontinuities are preferentially filled and the matrix becomes more continuous. Figure 4.9 (b) documents the $CaMg(CO_3)_2$ precursor powder morphology to support interpretation of similar features in the blended specimens. The powder consists of angular fragments with sharp edges

and a broad size range, typical of mechanically ground carbonate minerals. This confirms that the precursor is introduced as discrete solids rather than as a phase that forms a continuous binder on its own. Therefore, any microstructural improvement observed later must arise from particle packing, void filling, nucleation sites provided by the carbonate surfaces, and changes at the particle–paste interface, rather than from the formation of an independent carbonate gel network. This explains the carbonate-rich regions in BSE images tend to appear as sharp-edged inclusions, particularly at early ages when reaction rims are expected to be limited in thickness.

Sample M6A shows a comparatively consolidated paste fabric in the selected field as depicted in Figure 4.9 (c). The matrix appears more continuous, with clustered hydrates embedded within a gel-like background and fewer prominent open voids in the viewed area. A clinker remnant is still identifiable, indicating incomplete hydration at the tested age. Although, it is enclosed within the matrix rather than separated by obvious interfacial gaps. The dominant microstructural signal in this panel is improved continuity and local packing around solids, consistent with early densification of the binder phase under CO_2 conditioned mixing. This interprets that H_2CO_3 able to promote matrix development and pore refinement in the $CaCO_3$ series without requiring a distinct change in hydrate morphology.

For the $CaMg(CO_3)_2$ series, the SEM fields indicate a paste system increasingly governed by discrete carbonate inclusions and the extent to which the surrounding binder remains continuous around them. Figure 4.9 (d) depicts partially reacted particles are retained within the matrix, confirming persistence of solid inclusions at the examined age, while needle-like products bridge across adjacent regions, indicating that precipitation has occurred within inter-particle spaces where it can contribute to local connectivity. Figure 4.9 (e) shows that this product formation can coexist with micro-cracking, demonstrating that precipitation alone does not eliminate discontinuities when local stress concentration and interface sensitivity remain present in a particle-rich microstructure. Figure 4.9 (f) presents a denser needle-bridging network interwoven among clustered paste domains, suggesting higher micro-scale linking within the viewed field. The structural benefit of such bridging remains dependent on its spatial context because bridging that develops within a continuous binder matrix supports continuity, whereas bridging confined to isolated pockets between unreacted inclusions does not necessarily imply overall densification. Consequently, the SEM observations for the $CaMg(CO_3)_2$ series are interpreted primarily in terms of matrix

continuity, inclusion retention, and interface integrity, while the elemental signatures required to distinguish paste-rich domains from carbonate-dominated or interfacial regions are addressed in the subsequent EDX subsection.

4.6.2 EDX Elemental Composition

The EDX spectra in Figure 4.10 and Table 4.7 support the SEM interpretation in Figure 4.9 by confirming whether the visually distinct domains are paste-rich (Ca–Si–O dominated), carbonate-rich (Ca–O with elevated C, and Mg where dolomite is present), or mixed interfacial regions. The control OPC paste (cement + water) establishes the baseline elemental envelope expected for hydrated OPC, where Ca and O dominate, and Si and Al appear as secondary constituents associated with the main binding phase. The control selected-area analysis records Ca 41.7 wt%, Si 10.8 wt%, Al 1.3 wt%, Mg 0.4 wt% and O 45.4 wt%, with S at 0 wt% and a minor K signal (0.5 wt%).

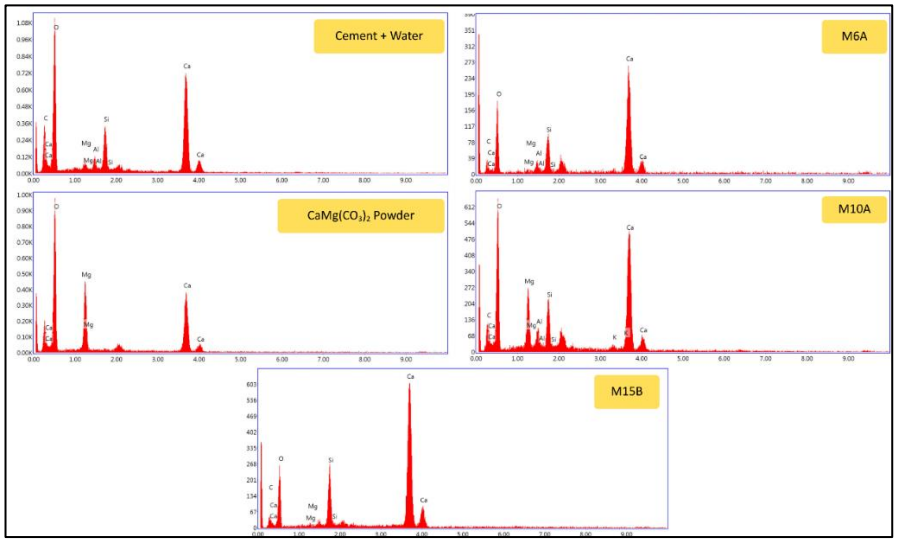


Figure 4.10 EDX Spectra of Selected Samples at 7 Days, Measured from the Selected Area of Each Specimen, Highlighting Relative Changes in Ca, Si, Al, Mg and C/O Related Signals

This Ca–Si–O balance is consistent with a hydrated paste field and provides a direct chemical reference when interpreting the denser and more carbonate-influenced microstructures observed for the H_2CO_3 conditioned systems.

Table 4.7
EDX Elemental Composition (wt%) of Selected Area Analyses of Selected Samples

Sample	Ca wt%	Si wt%	Al wt%	S wt%	Mg wt%	C wt%	O wt%	K wt%
OPC Paste (Control)	41.7	10.8	1.3	0.0	0.4	0.0	45.4	0.5
M6A	63.4	3.8	0.5	0.0	0.3	1.2	30.8	0.0
M7A	37.7	6.1	1.8	1.2	1.0	4.3	47.9	0.0
M10A	43.7	5.9	2.5	0.0	6.7	1.1	38.9	1.3
M11A	47	5.6	0.7	0.0	0.0	0	45.7	1.0
M12C	41.4	11.1	1.5	1.4	0.4	2	42.3	0.0
M15B	54.6	7.6	0.0	0.0	0.0	0.6	37.2	0.0

The EDX results in $CaCO_3$ + H_2CO_3 series, indicate that the analysed regions are predominantly Ca-rich but differ in how the secondary elements are expressed. M6A records a markedly higher Ca content (63.4 wt%) compared with the control, accompanied by lower Si (3.8 wt%) and low Mg (0.3 wt%). This pattern is consistent with the SEM observation of Ca-rich domains embedded in a consolidated matrix within the selected field, indicating that the scanned region intersects a Ca-dominant phase assemblage rather than a silicate-rich matrix. In contrast, M7A shows Ca at 37.7 wt% with higher O (47.9 wt%), measurable Si (6.1 wt%), and detectable minor Al (1.8 wt%), S (1.2 wt%) and Mg (1.0 wt%), together with a higher carbon signal (4.3 wt%) than the other specimens in the table. Within the limits of EDX quantification, this suggests that the scanned area in M7A contains a more mixed binder region rather than an isolated Ca-rich domain, and that the carbonated-water route may have produced carbonate-bearing features within the analysed micro-region. The key point for this subsection is that the $CaCO_3$ + H_2CO_3 specimens do not show a uniform elemental signature across scanned areas, which is consistent with microstructural heterogeneity observed by SEM at the same length scale.

For the $CaMg(CO_3)_2$ series (M10A, M12C, and M15B), the principal question addressed by EDX is whether Mg appears in the analysed micro-regions and whether the Ca–Si balance shifts relative to the control. M10A provides the clearest Mg signal in the dataset, with Mg at 6.7 wt% while Ca remains high at 43.7 wt% and Si is 5.9

wt%, indicating that the analysed area intersects a domain influenced by the dolomite precursor rather than a purely cement-derived binder zone. However, Mg does not appear consistently elevated in the remaining dolomite mixes in the selected Area 1 results. M12C, for example, shows Mg at 0.4 wt% while maintaining a Si content (11.1 wt%) comparable to the control, and M15B records Mg at 0.0 wt% in the analysed region despite the higher dolomite replacement level. This outcome is best interpreted as a field- and location-dependent effect inherent to SEM–EDX: the measured composition reflects the specific phase(s) present under the beam in that scanned area. Where the scan intersects a paste-rich zone dominated by Ca–Si-bearing binder phases, Mg may be low even when dolomite is present elsewhere in the specimen. Conversely, when the scan intersects a carbonate particle or an interface region influenced by the dolomite precursor, Mg can be detected at appreciable levels, as shown by M10A. The $CaMg(CO_3)_2$ series therefore demonstrates that Mg enrichment is not reliably captured by a single spot or area unless the selected region intentionally targets the particle-rich zones identified in SEM. Across the dataset, Ca remains a dominant element in all scanned areas, but its reported wt% varies substantially, from 37.7 wt% in M7A to 63.4 wt% in M6A and 54.6 wt% in M15B. This variability reinforces that EDX should be treated as micro-region evidence rather than bulk composition, and it supports a conservative interpretation strategy. EDX is implicated to confirm which mixes exhibit Ca-rich domains, whether Mg-bearing signatures are detectable in $CaMg(CO_3)_2$ containing systems, and whether the analysed regions are paste-rich or inclusion-influenced. The SEM observations in Figure 4.9 provide the spatial context for the selected EDX measurements shown in Figure 4.10 and Table 4.7, while the combined SEM–EDX interpretation, including how elemental signatures align with the annotated microstructural features, is developed in the subsequent synthesis subsection.

The EDX results in Figure 4.10 and Table 4.7 are interpreted as selected-area elemental measurements rather than full statistical elemental mapping of each specimen. Since EDX analysis is localised to the analysed spot or area, the measured elemental composition may vary depending on whether the beam intersects paste-rich matrix, carbonate-rich inclusions or interfacial regions. Therefore, the EDX data are used to support identification of local chemical domains and are interpreted together with SEM morphology and XRF bulk composition. Multiple EDX points or area scans across each specimen would improve representativeness and are recommended for future work.

4.6.3 SEM-EDX Synthesis

The SEM–EDX correlation in this study is established by treating EDX as a site-specific chemical probe of the microstructural domains identified in SEM, rather than as a bulk compositional measurement. The SEM fields shown in Figure 4.9 consistently resolve three recurring regions: (i) a paste-rich matrix, (ii) discrete carbonate-derived inclusions introduced with $CaCO_3$ or $CaMg(CO_3)_2$, and (iii) interfacial zones where fine precipitates develop and bridge neighbouring solids. The EDX spectra and quantified elemental wt% shown in Figure 4.10 and Table 4.7, respectively, support this domain-based interpretation. Paste-dominant regions are expected to show a Ca–Si–O signal attributable to hydration products and Ca-rich phases, whereas inclusion-dominant regions shift toward Ca–O with measurable C, reflecting carbonate-bearing particles. Mg becomes pronounced only when the analysed area intersects dolomite fragments or their reaction rims. This explains why Mg can appear modest or variable in $CaMg(CO_3)_2$ mixtures even at higher replacement levels, as the EDX response is highly dependent on the analysed micro-area and the relative contribution of matrix versus inclusion within the interaction volume. Consequently, SEM descriptors such as needle-like bridging or apparent densification are interpreted as structurally meaningful only when their paired EDX signature indicates formation within paste-rich or interfacial regions that contribute to a continuous binder skeleton. Similar morphologies confined to carbonate-rich pockets may reflect local precipitation without proportional improvement in overall matrix continuity.

These microstructural observations help explain the mechanical trends reported in Section 4.3. The $CaCO_3$ mixes showed a performance window because moderate replacement can contribute to matrix filling, nucleation and local densification, while excessive replacement reduces the amount of reactive OPC and may weaken the continuity of the hydrated binder skeleton. For $CaMg(CO_3)_2$, the presence of Mg-bearing or carbonate-rich regions confirms precursor incorporation, but these regions do not necessarily improve strength unless they are well integrated into the paste matrix. Therefore, higher carbonate or Mg-bearing signatures should not be interpreted as direct evidence of higher compressive strength. Strength improvement depends on whether the observed carbonate-related products and precursor particles contribute to a continuous, dense and well-bonded matrix capable of transferring load. This supports

the earlier interpretation that compressive strength is governed by the combined effect of carbonate formation, pore refinement, particle distribution, matrix continuity and interfacial bonding.

4.7 Thermogravimetric Analysis (TGA)

Distinct mass-loss regimes that separate the bound-water reactions typical of hydrated OPC from the high-temperature decomposition of carbonate-bearing systems as depicted in Figure 4.11. The OPC paste (pH 6.0 to 7.0) exhibits the largest cumulative loss across the low- to mid-temperature range, dropping from approximately 100% to 90.27% by 200 °C and further to 79.51% by 600 °C, before approaching a final residue of 75.72% at 1000 °C. This behaviour is consistent with substantial evaporable water removal and dehydration of early hydrates at low temperature, followed by progressive loss associated with chemically bound water at higher temperatures. In contrast, all OPC + $CaCO_3$ mixes retain markedly higher mass up to 600 °C, typically around 93 to 96%, indicating that the dominant mass-loss processes below 600 °C are reduced relative to the plain paste. The main drop is instead shifted to the high-temperature region where carbonate decomposition becomes active. This separation is important for interpretation because when the major mass loss occurs above approximately 600 °C, the curve mainly reflects carbonate stability and decomposition rather than only the amount of hydrates or free water present in the paste.

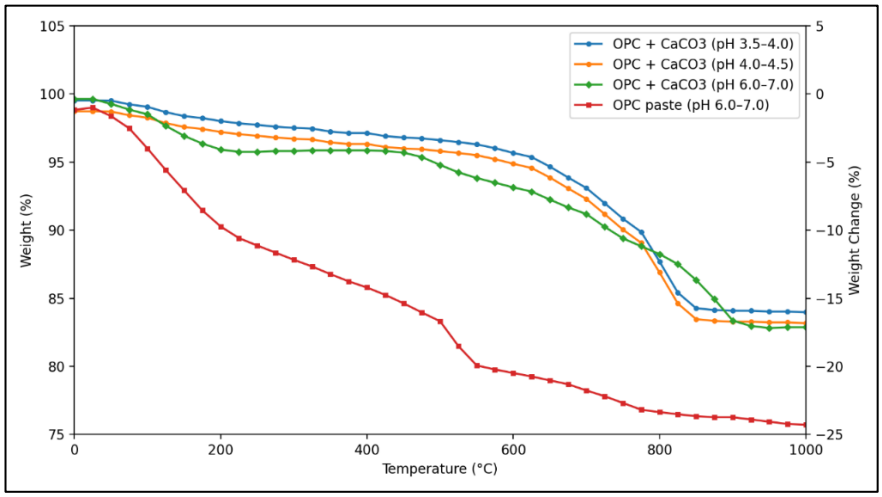


Figure 4.11 TG Curves of OPC Paste and OPC Mixed CaCO3 Pastes Prepared Under Different Mixing-Water pH Conditions

DTG curves were not generated as separate output during the final compilation of the TGA dataset. Therefore, the thermal interpretation in this study was based on the

TG mass-loss curves in Figure 4.11 and the partitioned mass-loss ranges summarised in Table 4.8. The temperature windows were selected to approximate the main thermal events in hydrated cement paste, where the low-temperature region represents evaporable water and dehydration of hydration products, the mid-temperature region is associated with portlandite decomposition, and the high-temperature region is associated mainly with carbonate decomposition. Although DTG curves would provide clearer peak identification, the mass-loss partition still allows comparative interpretation of hydrate-related and carbonate-related thermal response. The mass-loss values in Table 4.8 were rechecked against the TG residual-mass readings and are interpreted as temperature-window partitions rather than direct phase quantification. Future work should include DTG curves to identify the peak temperature of portlandite and carbonate decomposition more precisely.

A clearer comparison emerges by reading the curves in temperature windows. Between ~30 to 200 °C, the OPC paste loses ~8.73%, whereas the carbonate-bearing mixes lose substantially less at approximately ~1.51% for pH 3.5 to 4.0 and pH 4.0 to 4.5, and ~3.72% for pH 6.0 to 7.0. Between 200 to 600 °C, the OPC paste continues to lose ~10.76%, while the OPC + $CaCO_3$ mixes show smaller additional losses approximately ~2.33% for pH 3.5 to 4.0 and pH 4.0 to 4.5, and ~2.77% for pH 6.0 to 7.0). The dominant distinction is then concentrated in the 600 to 800 °C range whereby the OPC paste shows only ~2.87% loss, whereas the carbonate-bearing mixes lose ~4.90% (pH 6.0 to 7.0) up to ~7.98% (pH 3.5 to 4.5). This is the characteristic zone where carbonate decomposition governs the mass change, and the sharper high-temperature step in the $CaCO_3$ systems is therefore interpreted as direct evidence of a larger carbonate contribution to the thermal response. Above 800 °C, the $CaCO_3$ mixes continue to decline at an additional ~3.72 to 5.37% to 1000 °C, while the OPC paste changes only slightly of ~0.92%, reinforcing that the late-stage response is carbonate-driven rather than hydrate-driven. The clearest divergence occurs in the high-temperature region associated with carbonate decarbonation. $CaCO_3$ containing mixes undergo a pronounced step drop starting around ~650 to 700°C and stabilising by ~850 to 900°C, where the mass decreases from roughly ~93 to 96% to ~83 to 85% accumulating around 10 to 12% loss). This high-temperature step is markedly smaller for the OPC control, dropping only a few percent over the same interval, consistent with a lower carbonate inventory in the control paste compared with $CaCO_3$ containing systems. Among the $CaCO_3$ mixes, the pH 6.0 to 7.0 curve trends to a slightly lower

final residual mass (~83%) compared with the pH 3.5 to 4.5 curves (~84 to 85%), indicating a marginally higher net high-temperature decomposable fraction under the near-neutral mixing condition. Importantly, this difference in carbonate-associated loss should be interpreted together with strength and SEM observations; a larger carbonate-related mass loss does not automatically translate to improved mechanical performance if carbonate formation is localised and disrupts matrix continuity rather than contributing to a uniformly load-bearing microstructure.

Table 4.8
Summary of TG Residual Mass and Mass-Loss Partition by Temperature Windows

Sample Mix	Weight				Loss			
	200 °C (%)	600 °C (%)	800 °C (%)	1000 °C (%)	30 to 200 °C (%)	200 to 600 °C (%)	600 to 800 °C (%)	800 to 1000 °C (%)
OPC paste (pH 6.0 to 7.0)	90.27	79.51	76.64	75.72	8.73	10.76	2.87	0.92
OPC + $CaCO_3$ (pH 3.5 to 4.0)	98.49	96.16	88.18	84.46	1.51	2.33	7.98	3.72
OPC + $CaCO_3$ (pH 4.0 to 4.5)	98.49	96.16	88.18	84.46	1.51	2.33	7.98	3.72
OPC + $CaCO_3$ (pH 6.0 to 7.0)	96.28	93.51	88.61	83.24	3.72	2.77	4.90	5.37

The quantitative mass-loss breakdown in Table 4.8 confirms that the CO_2 conditioned mixing route shifts the dominant thermal response of the $CaCO_3$ systems away from low–mid temperature dehydration and toward high-temperature carbonate decomposition. The OPC paste shows the greatest cumulative loss below 600 °C, decreasing to ~90.3% by 200 °C and ~79.5% by 600 °C, consistent with substantial evaporable-water removal and hydrate dehydration. In contrast, all OPC + $CaCO_3$ mixes retain higher mass up to 600 °C (~93 to 96%) and exhibit markedly smaller losses in the 30 to 200 °C and 200 to 600 °C windows, indicating reduced water-associated mass loss relative to the control. The clearest divergence occurs between 600 to 800 °C, where the OPC paste shows only ~2.87% loss while the $CaCO_3$ mixes lose ~4.90 to 7.98%, confirming that decarbonation governs the principal mass-loss event in the

carbonate-bearing systems. Differences between the pH conditions suggest that batching-water chemistry influences the partitioning between early dehydration-related loss and the magnitude of the decarbonation step. However, carbonate-associated loss should be interpreted together with strength and microstructural evidence, because a larger decarbonation signal does not necessarily indicate improved performance unless carbonate formation contributes to a more continuous load-bearing matrix.

A limitation of the present thermogravimetric dataset is that TGA was conducted only for the OPC and OPC + $CaCO_3$ systems, while the $CaMg(CO_3)_2$ series was not tested. This decision was driven by (i) practical constraints in instrument access and run allocation, and (ii) the need to prioritise a chemically simpler system where the high-temperature mass-loss step can be interpreted with higher confidence as carbonate decarbonation. In $CaMg(CO_3)_2$ containing mixes, thermal mass loss is expected to reflect overlapping decomposition reactions associated with Ca–Mg carbonate domains and their interfacial products, which would require higher-resolution DTG peak separation and a larger replicate set to support defensible phase attribution. As a result, the present discussion for the dolomite series relies primarily on microstructural (SEM–EDX) evidence and mechanical trends, while quantitative thermal confirmation of carbonate partitioning in $CaMg(CO_3)_2$ mixes remains a recommendation for future work.

4.8 Correlation of Degree of Reaction with Physico-Mechanical Performance

Correlation in this study is assessed by checking whether independent datasets describe the same change in the hardened system under aqueous CO_2 solution batching. Strength is treated as the primary indicator of load-bearing continuity, water absorption as an indicator of connected pore structure, TG as evidence of how the solid inventory is partitioned between hydrate-dominated reactions and carbonate decomposition, and SEM–EDX as the spatial check that distinguishes a continuous paste network from inclusion- or defect-dominated regions. The correlation statements below are therefore based on agreement between trend direction and mechanism consistency across methods, with explicit acknowledgement when datasets are not paired densely enough to support statistical inference.

The TG partitioning provides the clearest confirmation that carbonate-bearing mixes develop a different reaction signature from the OPC control. As shown in Figure

4.12, the OPC paste exhibits the largest mass loss in the low-to-mid temperature windows (0 to 200 °C = 8.73% and 200 to 600 °C = 10.76%), which is consistent with dehydration of hydrates and loss of bound water dominating the thermal response below 600 °C. In contrast, both $CaCO_3$ mixes prepared with aqueous CO_2 solution show substantially smaller low-to-mid temperature losses (0–200 °C = 1.51% and 200–600 °C = 2.33%), while their principal loss is concentrated in the high-temperature decomposition regime (600 to 800 °C = 7.98% and 800–1000 °C = 3.72%). The separation is not subtle where the control is dehydration-dominant, while the $CaCO_3$ systems are decarbonation-dominant. This window-based interpretation supports the degree-of-reaction requirement by demonstrating that the carbonate contribution is thermally significant and is expressed primarily through the 600 to 1000 °C region rather than by increasing dehydration-related loss below 600 °C.

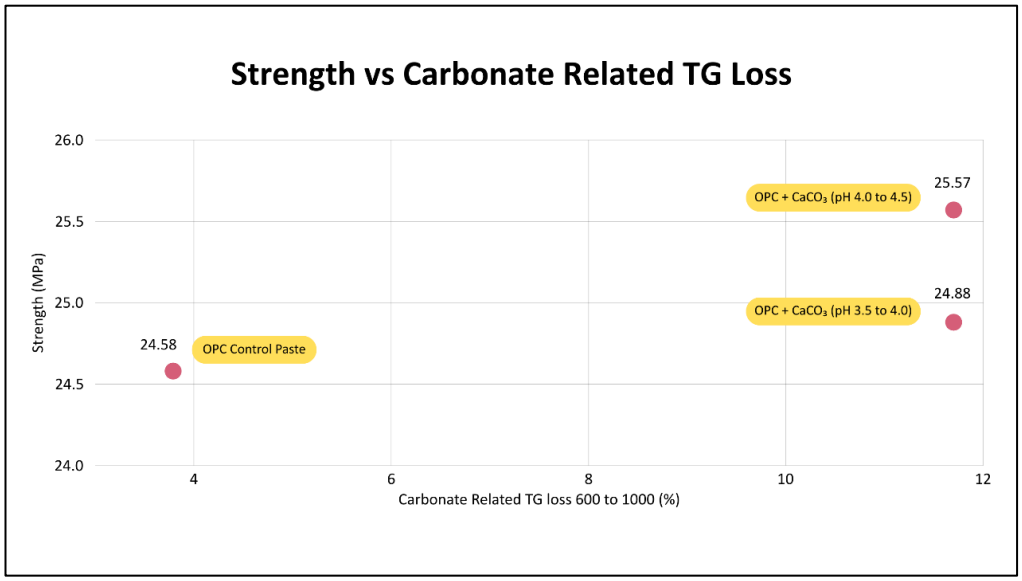


Figure 4.12 TG Mass-Loss Partition by Temperature Window for Selected Mixes (Control and Representative $CaCO_3$ Pastes) to Distinguish Dehydration-Dominated Loss (<600 °C) from Carbonate Decomposition (600 To 1000 °C)

Figure 4.13 then tests whether the carbonate-related TG indicator translates into measurable strength differences. The carbonate-related TG loss is defined by the combined 600–800 °C and 800–1000 °C windows, and it increases from 3.79% in the OPC control (2.87% + 0.92%) to 11.70% in the $CaCO_3$ mixes (7.98% + 3.72%). Mechanistically, this confirms a larger decomposable carbonate fraction in the $CaCO_3$ systems. However, the compressive strengths remain clustered within a narrow band: 24.58 MPa (control), 24.88 MPa (pH 3.5–4.0 $CaCO_3$), and 25.57 MPa (pH 4.0–4.5

$CaCO_3$). Two $CaCO_3$ conditions share the same carbonate-related TG loss (11.70%) but do not share identical strengths, indicating that carbonate inventory at specimen scale does not operate as a stand-alone predictor of mechanical performance within the present dataset. The correct interpretation is that TG confirms the presence and magnitude of carbonate contribution, while strength reflects whether that contribution improves the continuity of the load-bearing network rather than forming localised deposits or discrete inclusions that do not increase effective load transfer. For this reason, the fitted line in Figure 4.10 is included as a visual guide only, and the relationship is treated as descriptive rather than predictive.

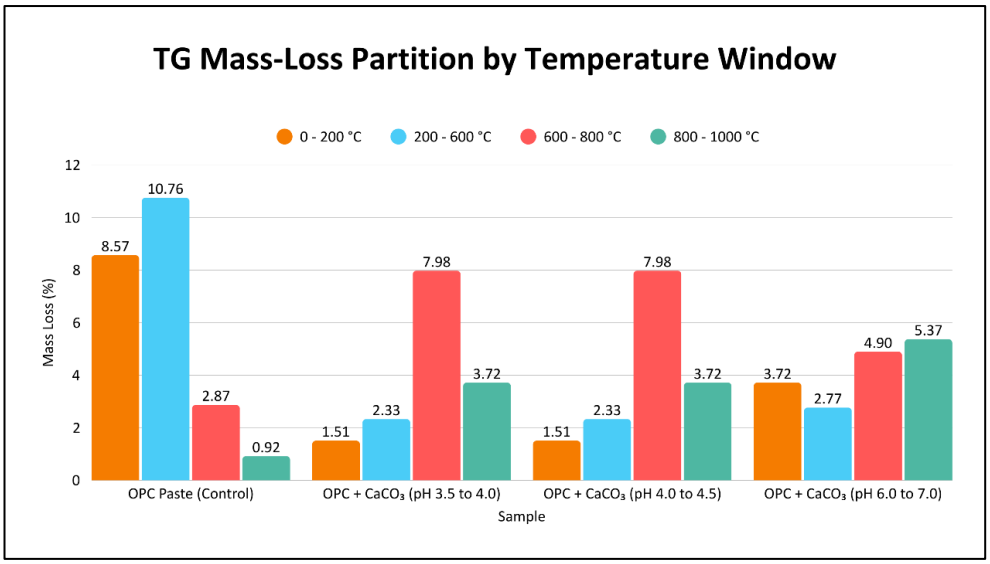


Figure 4.13 Compressive Strength Versus Carbonate-Related TG Loss (600 to 1000°C)

The role of SEM–EDX is to resolve this apparent mismatch between a strong TG carbonate signature and a modest strength separation. TG is a bulk measurement that confirms carbonate decomposition behaviour, but it does not indicate where carbonates and hydrates are located within the microstructure. SEM identifies whether the matrix is continuous or interrupted by pores, micro-cracks, and clustered solids, while EDX supports whether the observed domains are paste-rich regions (Ca–Si–O dominated) or carbonate-/inclusion-rich zones (Ca-dominant and/or Mg-bearing in dolomite-containing systems). Within this framework, correlation with physico-mechanical response is expected to be strongest when carbonate-associated precipitation contributes to matrix densification and reduces pore connectivity, which would align with reduced water absorption and improved strength. Where carbonate

contribution is present but is concentrated in discrete domains or poorly bonded interfaces, TG may still show elevated carbonate-related loss while strength does not increase proportionally, because continuity of the paste skeleton remains the governing factor. Accordingly, the correlated outcome from this study is that the aqueous CO_2 solution route produces a clear thermal shift toward carbonate-driven behaviour in $CaCO_3$ systems, but the physico-mechanical benefit is controlled by microstructural continuity rather than carbonate quantity alone.

CHAPTER 5
CONCLUSION

5.1 Summary of Study

This thesis evaluated supersaturated aqueous CO2 solution batching as an early-stage chemical control and examined how carbonate precursors influence fresh and hardened behaviour when used as partial binder replacement. The results show that the treatment effect is governed by a short initial chemical window at mixing and by whether the hardened network remains paste-continuous when carbonate solids are introduced. The main findings are summarised according to the research objectives, beginning with H2CO3 solution behaviour, followed by physico-mechanical performance, reaction indicators and the correlation between reaction evidence and material behaviour.

a) For Objective 1, the narrow batching pH window governs whether the aqueous CO_2 solution produces a measurable performance response. Within the tested bands, pH 3.5 to 4.0 produced the highest compressive strength response in the pH-screen dataset compared with higher pH CO_2 bands and the neutral-water control, indicating that the treatment effect is realised only when dissolved carbon species remain sufficiently active during the short pre-alkalinisation interval after mixing

b) For Objective 2, increasing $CaCO_3$ replacement under the aqueous CO_2 solution condition delayed setting across the tested endpoints. Initial set shifted from approximately 230 min at 5% $CaCO_3$ toward 270 min at 25%, while final set extended from approximately 375 min toward 480 min. The trend indicates that, under the present batching approach, higher carbonate replacement does not accelerate rigidification and instead prolongs the time required to develop a stable solid network.

c) The $CaCO_3$ mixes displayed an age-dependent strength response rather than a single universal optimum. At early age, 10% $CaCO_3$ produced the strongest response within the tested series, with 26.24 MPa at 3 days and 44.23 MPa at 7 days. However, the 28-day trend changed, where the highest 28-day strength was recorded at 25% $CaCO_3$ with 47.79 MPa, followed by 20% $CaCO_3$ with 44.04 MPa. Therefore, 10% $CaCO_3$ is interpreted as a balanced early-age replacement level, while higher $CaCO_3$ replacement may contribute to later-age densification when matrix continuity is maintained. This confirms that the $CaCO_3$ response should be interpreted as a performance window governed by curing age, replacement level

and paste continuity, rather than as a fixed optimum dosage. The corrected Chapter 4 data support this age-dependent interpretation, where 10% is strongest at 3 and 7 days, while 25% is highest at 28 days.

d) The $CaMg(CO_3)_2$ mixes exhibited a non-linear response and were sensitive to replacement level. At 28 days, 5% and 15% $CaMg(CO_3)_2$ achieved the highest performance (36.05 MPa and 35.33 MPa), while 20–25% replacement produced marked reductions. The 14-day results indicate that divergence is already established by the second week, confirming that high replacement is detrimental under the present method when compressive strength is the primary metric.

e) The water exposure result provided a comparative physical response rather than a full standard water absorption percentage. Specimens prepared within the lower pH aqueous CO_2 condition showed lower post-immersion mass response compared with the near-neutral control condition, suggesting reduced comparative moisture uptake under the same exposure procedure. This supports the interpretation that the selected CO_2-conditioned batching window may contribute to a denser or less connected pore structure, although the result should be treated as comparative because complete dry-mass and wet-mass data were not available for all specimens.

f) For Objective 3, microstructural and chemical evidence supports continuity-controlled behaviour. SEM fields from higher-performing mixes show a more continuous paste matrix in the analysed regions, whereas poorer-performing mixes show more frequent discontinuities and inclusion-dominated domains. EDX spot compositions support the presence of silica-bearing matrix regions with localised Ca-rich domains rather than uniform carbonate-dominated fields at low replacement; at higher replacement, the increased prevalence of Ca-rich islands and fewer uniform matrix fields is consistent with reduced strength through interruption of a continuous C–S–H-dominated skeleton and increased interface-controlled behaviour.

g) For Objective 4, thermogravimetric partitioning confirms a shift in phase balance between the control and carbonate-bearing systems, although it does not directly predict mechanical performance. The treated mixes show reduced low-to-mid temperature mass loss and increased high-temperature decomposition contribution relative to the OPC control, consistent with hydrate–carbonate balance modification. However, within the limited paired TG–strength dataset, carbonate-related mass loss did not scale proportionally with compressive strength, indicating that carbonate inventory is not a stand-alone predictor; performance depends on spatial distribution and matrix continuity.

h) From an application perspective, the findings support controlled use of carbonate replacement under aqueous CO_2 solution batching where a defined strength class is targeted. Although high replacement levels were not consistently favourable for

compressive strength, the approach may remain technically relevant for product-oriented, non-structural cementitious applications if future work verifies surface integrity, transport behaviour, dimensional stability and durability. Therefore, product-oriented optimisation should evaluate physical performance and durability indicators alongside the target strength class rather than relying on compressive strength alone.

5.2 Limitations

The study was designed to establish an operating window for supersaturated aqueous CO_2 solution batching and to benchmark the response of carbonate precursor replacement under that window. Several limitations constrain the extent to which the findings can be generalised or statistically parameterised.

a) Uneven replication and incomplete pairing across datasets.

Not all pH bands, replacement levels, and precursor systems were populated with equivalent replication density, and several characterisation methods were applied to representative conditions due to scheduling and instrument capacity constraints. Compressive strength testing was conducted using three 50mm cube specimens for each available mix and curing age, where complete mix-age datasets were available. However, the pH-screening data, setting-time data, water absorption data and characterisation datasets were more limited in replication. The pH evolution results were treated as representative measured profiles, while Vicat setting time was conducted for selected mixtures rather than a complete pH-by-dosage matrix. The $CaMg(CO_3)_2$ setting-time dataset was one of the most affected because part of the final setting record was unavailable during final compilation. Water absorption was also limited because the available dataset was based on post-immersion mass response rather than a complete dry-mass and wet-mass record for all specimens. SEM-EDX, XRF and TGA were conducted on selected representative specimens, with TGA limited to the OPC and OPC + $CaCO_3$ systems. As a result, the findings are most defensible as comparative regime behaviour, such as low versus high replacement and control versus CO_2-conditioned batching, rather than as a complete response surface with robust interaction terms and tight confidence intervals. Strength-to-thermal and strength-to-microstructure correlation is limited by the number of conditions for which datasets are fully paired.

b) Microstructural evidence is representative but not statistically quantified.

SEM/EDX analysis provides clear qualitative support for continuity-controlled behaviour; however, cement paste heterogeneity means that additional field coverage and repeated sampling across multiple locations per mix would improve robustness. Quantitative descriptors such as Ca-rich area fraction, pore-feature statistics, or replicated EDX spot distributions were not implemented, and therefore microstructural conclusions are presented as supporting evidence aligned with mechanical trends rather than statistically resolved microstructural metrics.

c) Thermal interpretation benefits from complementary phase confirmation.

TG partitioning provides strong comparative evidence of dehydration and decarbonation regimes, but peak attribution and phase quantification are strengthened when supported by complementary phase identification protocols such as XRD, DTG and baseline-corrected quantification. In the absence of full phase confirmation across all mixes, TG results in this thesis primarily support comparative interpretation of phase-balance shifts rather than providing definitive phase content breakdown for each system. The $CaMg(CO_3)_2$ series was not included in the TGA programme, which limits direct thermal comparison between $CaCO_3$- and $CaMg(CO_3)_2$-bearing systems.

d) Durability and long-term performance were outside the present scope.

The present work emphasised strength, setting, transport screening via water absorption at a single age, and microstructural or thermal signatures under the selected curing regime. Durability-relevant behaviour such as permeability, permeability proxies, chloride penetration, sulphate resistance, carbonation depth, shrinkage and volumetric stability are sensitive to pore connectivity and interface quality and may not track strength directly. Therefore, conclusions are confined to mechanical, physical and early-age behaviour under the studied regime and should not be extended to service durability without dedicated long-term testing. Future durability testing should include

chloride penetration, sulphate resistance and carbonation depth to strengthen the practical relevance of the aqueous CO_2 mixing route, especially if the method is later extended from paste-scale specimens to mortar or concrete applications.

5.3 Recommendations for Future Works

Based on the findings and limitations of this study, future work should first improve the replication and statistical reporting of the experimental programme. The selected pH bands, precursor types and replacement levels should be repeated using a more complete replicate matrix, especially for setting time, compressive strength and water absorption. At least three specimens should be tested for each mix and curing age, and the results should be reported using mean values with standard deviation. This would allow the observed trends to be interpreted with stronger statistical confidence rather than mainly as comparative regime behaviour. The water absorption procedure should also be repeated using a complete standard mass-gain method. In future testing, both the dry mass before immersion and the wet mass after immersion should be recorded for every specimen so that water absorption can be calculated as percentage mass gain. Additional transport-related tests such as sorptivity, permeability and chloride penetration are also recommended to determine whether the moisture uptake behaviour observed in this study is related to actual pore refinement and durability performance.

Long-term durability evaluation is necessary before the aqueous H_2CO_3 mixing-water route can be considered for practical application. Future studies should include chloride penetration, sulphate resistance, carbonation depth, shrinkage and wet-dry exposure testing. These tests are important because short-term compressive strength and water exposure response do not fully represent service performance. The long-term behaviour of H_2CO_3-mixed binders should therefore be verified under exposure conditions that are closer to actual mortar or concrete applications.

Further microstructural and elemental analysis should be conducted to improve the representativeness of SEM-EDX interpretation. Future SEM-EDX work should include multiple analysis points or area scans for each specimen instead of relying only on selected local measurements. Quantitative image analysis, such as pore-feature distribution, Ca-rich area fraction and carbonate-rich domain mapping, would help explain the relationship between particle distribution, matrix continuity and

compressive strength. This is particularly important for $CaMg(CO_3)_2$ mixes because Mg-bearing regions may not be uniformly distributed within the paste.

Thermal and phase analysis should also be expanded. Future TGA work should include both TG and DTG curves to allow clearer identification of portlandite decomposition and carbonate decomposition peaks. The $CaMg(CO_3)_2$ series should also be included in the thermal analysis so that its behaviour can be compared directly with the $CaCO_3$ series. Additional XRD analysis with clearer phase identification would strengthen the interpretation of carbonate-related phases and hydration-carbonation behaviour. sFuture work should also include direct quantification of dissolved CO_2 in the H_2CO_3 mixing water. Measurement of dissolved inorganic carbon or total inorganic carbon would allow batching pH to be related more directly to actual dissolved CO_2 content. A simple carbon-balance assessment is also recommended before the method is described as a verified CO_2 reduction technology, because the present study only evaluated material performance and reaction indicators rather than net CO_2 uptake.

Finally, the most promising pH and precursor replacement windows identified in this study should be extended from paste-scale testing to mortar and concrete systems. This is necessary to evaluate the effect of aggregates, workability, compaction, interfacial transition zone behaviour and practical batching conditions. Scale-up testing would determine whether the aqueous H_2CO_3 mixing-water route can remain effective beyond OPC paste and whether it can be developed into a practical cementitious material technology.

REFERENCES

Ahmad, S., Assaggaf, R. A., Maslehuddin, M., Al-Amoudi, O. S. B., Adekunle, S. K., & Ali, S. I. (2017). Effects of carbonation pressure and duration on strength evolution of concrete subjected to accelerated carbonation curing. Construction and Building Materials, 136, 565-573.

Ahmed, O., Ahmad, S., & Adekunle, S. K. (2024). Carbon dioxide sequestration in cementitious materials: A review of techniques, material performance, and environmental impact. Journal of CO2 Utilization, 83, 102812.

Akhil, N., Kumar, B. N., Sai, M. M., Bhargav, E. S., & Pavan, T. S. (2024). Development of sustainable standard grade concrete with inclusion of dolomite material as a high-performance mineral admixture. Discover Civil Engineering, 1(1), 128.

Alibeigibeni, A., Stochino, F., & Zucca, M. (2025). Enhancing concrete sustainability: a critical review of the performance of recycled concrete aggregates (RCAs) in structural concrete. Buildings, 15(8), 1-25.

André, J. (2017). Mixing cement with carbon dioxide–effect on early hydration.

Andrew, R. M. (2018). Global CO 2 emissions from cement production, 1928–2017. Earth System Science Data, 10(4), 2213-2239.

Arasteh-Khoshbin, O., Seyedpour, S. M., & Ricken, T. (2022). A comparative study on the effect of rice husk ash, nano-SiO2, and nano-Al2O3 on the mechanicalproperties and durability of concrete: A case study of Caspian seawater curing condition.

Arias, B., A. Criado, Y., Pañeda, B., & Abanades, J. (2022). Carbonation kinetics of Ca (OH) 2 under conditions of entrained reactors to capture CO2. Industrial & engineering chemistry research, 61(9), 3272-3277.

Ashraf, W., & Olek, J. (2016). Carbonation behavior of hydraulic and non-hydraulic calcium silicates: potential of utilizing low-lime calcium silicates in cement-based materials. Journal of materials science, 51(13), 6173-6191.

ASTM. (2013). Standard test method for compressive strength of hydraulic cement mortars (using 2-in. or [50-mm] cube specimens). Annual Book of ASTM StandardsAnnual Book of ASTM Standards, 4(1), 1-9.

ASTM, C.-. (2008). Standard test methods for time of setting of hydraulic cement by Vicat needle. West Conshohocken, PA: ASTM International, C191-08.

Azdarpour, A., Asadullah, M., Mohammadian, E., Hamidi, H., Junin, R., & Karaei, M. A. (2015). A review on carbon dioxide mineral carbonation through pH-swing process. Chemical Engineering Journal, 279, 615-630.

Baras, A., Li, J., Ni, W., Hussain, Z., & Hitch, M. (2023). Evaluation of potential factors affecting steel slag carbonation. Processes, 11(9), 2590.

Benjeddou, O., Alwetaishi, M., Tounsi, M., Alyousef, R., & Alabduljabbar, H. (2021). Effects of limestone filler fineness on the rheological behavior of cement–Limestone filler grouts. Ain Shams Engineering Journal, 12(4), 3569-3578.

Bergmans, J., Kazemi Kamyab, H., Ghosh, D., Van Mierloo, P., Carens, H., & Nielsen, P. (2024). Carbonation of recycled concrete aggregates for new concrete and concrete fines to make cement-free hollow blocks. Sustainability, 16(8), 3494.

Bernal, S. A., Dhandapani, Y., Elakneswaran, Y., Gluth, G. J., Gruyaert, E., Juenger, M. C., Lothenbach, B., Olonade, K. A., Sakoparnig, M., & Shi, Z. (2024). Report of RILEM TC 281-CCC: A critical review of the standardised testing methods to determine carbonation resistance of concrete. Materials and Structures, 57(8), 173.

Bertos, M. F., Simons, S., Hills, C., & Carey, P. (2004). A review of accelerated carbonation technology in the treatment of cement-based materials and sequestration of CO2. Journal of hazardous materials, 112(3), 193-205.

Biava, G., Depero, L. E., & Bontempi, E. (2024). Accelerated carbonation of steel slag and their valorisation in cement products: a review. Spanish Journal of Soil Science, 14, 12908.

Bilek Jr, V., Švec, J., Másilko, J., Sedlačík, M., Materak, K., Wieczorek, A., Koniorczyk, M., Hajzler, J., & Kucharczyková, B. (2025). Comparison of thermogravimetry response of alkali-activated slag and Portland cement pastes after stopping their hydration using solvent exchange method. Journal of Thermal Analysis and Calorimetry, 150(2), 1013-1037.

Bonfante, F., Humbert, P., Tulliani, J.-M., Palmero, P., & Ferrara, G. (2024). CO2 uptake of cement by-pass dust via direct aqueous carbonation: an experimental design for time and temperature optimisation. Materials and Structures, 57(8), 181.

Boualleg, S., Bencheikh, M., Belagraa, L., Daoudi, A., & Chikouche, M. A. (2017). The combined effect of the initial cure and the type of cement on the natural

carbonation, the portlandite content, and nonevaporable water in blended cement. Advances in Materials Science and Engineering, 2017.

Bui, H., Delattre, F., & Levacher, D. (2023). Experimental methods to evaluate the carbonation degree in concrete—state of the art review. Applied Sciences, 13(4), 2533.

Campagiorni, L., Tonelli, M., & Ridi, F. (2025). Synergistic effect of limestone and supplementary cementitious materials in ternary blended cements. Current Opinion in Colloid & Interface Science, 75, 101885.

Chang, X., He, T., Niu, M., Zhao, L., Wang, L., & Wang, Y. (2024). Influence of limestone powder mixing method on properties of manufactured sand concrete. Case Studies in Construction Materials, 20, e02996.

Chen, T., Bai, M., & Gao, X. (2021). Carbonation curing of cement mortars incorporating carbonated fly ash for performance improvement and CO2 sequestration. Journal of CO2 Utilization, 51, 101633.

Chen, T., & Gao, X. (2019). Effect of carbonation curing regime on strength and microstructure of Portland cement paste. Journal of CO2 Utilization, 34, 74-86.

Chen, X., Chen, H., Chen, Q., Lawi, A. S., & Chen, J. (2022). Effect of partial substitution of cement with Dolomite powder on Glass-Fiber-Reinforced mortar. Construction and Building Materials, 344, 128201.

Chen, X., Li, S., Hu, M., Geng, Y., Meng, S., Jin, L., Hu, Q., & Han, S. (2024). Early age accelerated carbonation of cementitious materials surface in low CO2 concentration condition. Construction and Building Materials, 445, 137975.

Chen, Z., Zhang, T., Wu, Y., Madsen, I., Ma, J., Sagoe-Crentsil, K., Neild, A., & Duan, W. (2025). In-situ XRD study of the effects of amino acids on the carbonation kinetics of cementitious calcium silicates. Cement and Concrete Research, 193, 107879.

Cheng, D., Reiner, D. M., Yang, F., Cui, C., Meng, J., Shan, Y., Liu, Y., Tao, S., & Guan, D. (2023). Projecting future carbon emissions from cement production in developing countries. Nature communications, 14(1), 8213.

Choi, H.-J., Kim, J. K., Yeo, W., Lee, N., Moon, H., Park, J.-J., & Yoo, D.-Y. (2024). Effect of nanobubble water on the mechanical properties and carbon sequestration efficiency of concrete cured under various conditions. Case Studies in Construction Materials, 21, e03596.

Davolio, M., Muciaccia, G., & Ferrara, L. (2025). Concrete carbon mixing–A systematic review on the processes and their effects on the material performance. Cleaner Materials, 100292.

De Weerdt, K., Haha, M. B., Le Saout, G., Kjellsen, K. O., Justnes, H., & Lothenbach, B. (2011). Hydration mechanisms of ternary Portland cements containing limestone powder and fly ash. Cement and Concrete Research, 41(3), 279-291.

DiGiovanni, C., Hisseine, O. A., & Awolayo, A. N. (2024). Carbon dioxide sequestration through steel slag carbonation: review of mechanisms, process parameters, and cleaner upcycling pathways. Journal of CO2 Utilization, 81, 102736.

Divekar, R. S., & Sawant, R. (2023). Dolomite powder in concrete: a review of mechanical properties and microstructural characterization. Civil Eng Archit, 11, 3314-3321.

Eloneva, S., Teir, S., Salminen, J., Fogelholm, C.-J., & Zevenhoven, R. (2008). Steel converter slag as a raw material for precipitation of pure calcium carbonate. Industrial & engineering chemistry research, 47(18), 7104-7111.

EN, N. (2011). 197-1; Cement: composition, specifications and conformity criteria for common cements. British Standards Institute.

EN, N. (2021). 197-5; Portland Composite Cement CEMII CM and Composite Cement CEMVI. AFNOR Editions: La Plaine Saint-Denis, France.

European Committee for Standardization. (2009). Methods of testing cement—part 3: determination of setting times and soundness. In Prüfverfahren für Zement-Teil 3: Bestimmung der Erstarrungszeiten und der Raumbeständigkeit (pp. 17). Beuth-Verlag Berlin, Germany.

Feng, C., Cui, B., Guo, H., Zhang, W., & Zhu, J. (2023). Study on the effect of reinforced recycled aggregates on the performance of recycled concrete--synergistic effect of cement slurry-carbonation. Journal of Building Engineering, 64, 105700.

Ferrara, G., Humbert, P., Garufi, D., & Palmero, P. (2024). Evolution of CO2 Uptake Degree of Ordinary Portland Cement During Accelerated Aqueous Mineralisation. Ceramics, 7(4), 1711-1726.

Friedlingstein, P., O'sullivan, M., Jones, M. W., Andrew, R. M., Hauck, J., Landschützer, P., Le Quéré, C., Li, H., Luijkx, I. T., & Olsen, A. (2024). Global carbon budget 2024. Earth System Science Data Discussions, 2024, 1-133.

Fu, X., Guerini, A., Zampini, D., & Rotta Loria, A. F. (2024). Storing CO2 while strengthening concrete by carbonating its cement in suspension. Communications Materials, 5(1), 109.

Gao, Y., Wang, J., Wei, B., Abudoureheman, M., Chen, L., Liu, K., & Li, X. (2025). Understanding the mechanism of CO2 mineralization and carbon sequestration performance in carbide slag: Effects of liquid-solid ratio and gas flow rate. Journal of Environmental Management, 390, 126246.

Gardeh, M. G., Kistanov, A. A., Nguyen, H., Manzano, H., Cao, W., & Kinnunen, P. (2022). Exploring mechanisms of hydration and carbonation of MgO and Mg (OH) 2 in reactive magnesium oxide-based cements. The Journal of Physical Chemistry C, 126(14), 6196-6206.

Gasós, A., Gall, L., & Mazzotti, M. (2025). Recycling solvent and managing impurities: Screening industrial wastes for cyclic operation in indirect mineral carbonation. Journal of Environmental Chemical Engineering, 118006.

Gasós, A., Meijssen, M., & Mazzotti, M. (2024). Indirect mineral carbonation of recycled concrete aggregate: Enhancing calcium extraction using a packed bed reactor. Journal of Cleaner Production, 449, 141745.

Gasos, A., Tschurtschenthaler, L., Tiefenthaler, J., & Mazzotti, M. (2024). Industrial demonstration of indirect mineralization at 100 kg of CO2 per hour scale: process operation and performance using various industrial feedstocks. Available at SSRN 5016491.

GCCA. (2021). The GCCA 2050 cement and concrete industry roadmap for net zero concrete. Concrete Roadmap Full Document GCCA Concrete Future-Roadmap to Net Zero.

Gonçalves, B., Exposito, C., Ishikawa, T. T., & Koga, G. Y. (2023). X-ray diffraction study of the early hydration of Portland cements containing calcium carbonate by in-situ and ex-situ approaches. Construction and Building Materials, 365, 129947.

Guleria, H., Sharma, D., & Goyal, S. (2024). Long term performance of concrete using accelerated carbonation curing: an effective CCUS technique. European Journal of Environmental and Civil Engineering, 28(9), 2138-2159.

Gupta, S., Kashani, A., & Mahmood, A. H. (2022). Carbon sequestration in engineered lightweight foamed mortar–Effect on rheology, mechanical and durability properties. Construction and Building Materials, 322, 126383.

Gusain, P., Sharma, S., Debarma, S., Sharma, A. K., Mishra, N., & Dahale, P. P. (2023). Study of concrete mix by adding dolomite in conventional concrete as partial replacement with cement. Mater. Today Proc, 73, 163-166.

Hadjari, M., Marouf, H., Dahou, Z., & Maherzi, W. (2025). Investigation of the Mechanical and Fracture Properties of Recycled Aggregate Concrete. Buildings, 15(7), 1155.

He, Z., Li, Z., & Shao, Y. (2017). Effect of carbonation mixing on CO 2 uptake and strength gain in concrete. Journal of Materials in Civil Engineering, 29(10), 04017176.

He, Z., Shao, X., & Chen, X. (2023). Effect of carbonation treatment on the strength and CO2 uptake rate of composite cementitious material with a high steel slag powder content. Materials, 16(18), 6204.

Hernández-Rodríguez, A., Orlando, A., Montegrossi, G., Huet, B., Virgili, G., & Vaselli, O. (2021). Experimental analysis on the carbonation rate of Portland cement at room temperature and CO2 partial pressure from 1 to 51 bar. Cement and Concrete Composites, 124, 104271.

Ho, H.-J., & Iizuka, A. (2025). Chemical-Free Pressure-Swing Carbonation of Blast Furnace Slag for CO2 Utilization and Sequestration. ACS Sustainable Chemistry & Engineering, 13(10), 3842-3852.

Ho, H.-J., Iizuka, A., Shibata, E., Tomita, H., Takano, K., & Endo, T. (2020). CO2 utilization via direct aqueous carbonation of synthesized concrete fines under atmospheric pressure. ACS omega, 5(26), 15877-15890.

Hu, H., Yao, W., Wei, Y., & She, A. (2024). Evolution of early hydration in mortar by using waste dolomite powder as a micro-aggregate. Construction and Building Materials, 438, 137158.

Huang, H., Wang, T., Kolosz, B., Andresen, J., Garcia, S., Fang, M., & Maroto-Valer, M. M. (2019). Life-cycle assessment of emerging CO2 mineral carbonation-cured concrete blocks: Comparative analysis of CO2 reduction potential and optimization of environmental impacts. Journal of Cleaner Production, 241, 118359.

Hudson, R., de Graaf, R., Strandoo Rodin, M., Ohno, A., Lane, N., McGlynn, S. E., Yamada, Y. M., Nakamura, R., Barge, L. M., & Braun, D. (2020). CO2 reduction driven by a pH gradient. Proceedings of the national academy of sciences, 117(37), 22873-22879.

Huijgen, W. J., Witkamp, G.-J., & Comans, R. N. (2005). Mineral CO2 sequestration by steel slag carbonation. Environmental science & technology, 39(24), 9676-9682.

IEA. (2021). Global cement production in the Net Zero Scenario, 2010-2030. IEA. Retrieved 29 August from https://www.iea.org/data-and-statistics/charts/global-cement-production-in-the-net-zero-scenario-2010-2030

IEA. (2024). World Energy Outlook 2024. I. E. A. (IEA). https://www.iea.org/reports/world-energy-outlook-2024

Izoret, L., Pernin, T., Potier, J.-M., & Torrenti, J.-M. (2023). Impact of industrial application of fast carbonation of recycled concrete aggregates. Applied Sciences, 13(2), 849.

Jaschik, J., Jaschik, M., & Warmuzinski, K. (2014). The Use of Alkaline Industrial Waste in the Capture of Carbon Dioxide 7th International Scientific Conference on Energy and Climate Change, Athens, Greece.

Kaddah, F., Ranaivomanana, H., Amiri, O., & Rozière, E. (2022). Accelerated carbonation of recycled concrete aggregates: Investigation on the microstructure and transport properties at cement paste and mortar scales. Journal of CO2 Utilization, 57, 101885.

Kalkreuth, J., Ullrich, A., Garbev, K., Merz, D., Stemmermann, P., & Stapf, D. (2024). Accelerated carbonation of hardened cement paste: quantification of calcium carbonate via ATR infrared spectroscopy. Journal of the American Ceramic Society, 107(4), 2627-2640.

Kang, I., Shin, S., & Kim, J. (2024). Optimal Limestone Content on Hydration Properties of Ordinary Portland Cement with 5% Ground Granulated Blast-Furnace Slag. Materials, 17(13), 3255.

Kim, G., Cho, S., Moon, J., Suh, H., Her, S., Sim, S., & Bae, S. (2024). Investigation of the hydrate formation and mechanical performance of limestone calcined clay cement paste incorporating nano-CaCO3 and nano-SiO2 as partial limestone substitutes. Construction and Building Materials, 418, 135335.

Kim, Y.-J., Sim, S.-R., & Ryu, D.-W. (2023). Experimental study on effects of CO2 curing conditions on mechanical properties of cement paste containing CO2 reactive hardening calcium silicate cement. Materials, 16(22), 7107.

Kohitlhetse, I. C., Manono, M. S., Motsetse, C. K., & Mendonidis, P. M. (2024). A Step Towards CO2 Sequestration through Mineral Carbonation: Using Ammonium

Based Lixiviants for the Dissolution of Calcium from Iron Making Blast Furnace Slag.

Kong, Y., Song, Y., Kurumisawa, K., Wang, T., Yan, D., Zeng, Q., Zhou, X., & Ruan, S. (2022). Use of hydrated cement pastes (HCP) as a CO2 sponge. Journal of CO2 Utilization, 55, 101804.

Kumar, R. V., & Prabagharb, A. (2023). Evaluation of strength of self-compacting concrete having dolomite powder as partial replacement for cement.

Kusin, F. M., Hasan, S. N. M. S., Hassim, M. A., & Molahid, V. L. M. (2020a). Mineral carbonation of sedimentary mine waste for carbon sequestration and potential reutilization as cementitious material. Environmental Science and Pollution Research, 27, 12767-12780.

Kusin, F. M., Hasan, S. N. M. S., Hassim, M. A., & Molahid, V. L. M. (2020b). Mineral carbonation of sedimentary mine waste for carbon sequestration and potential reutilization as cementitious material. Environmental Science and Pollution Research, 27(11), 12767-12780.

Kusin, F. M., Hasan, S. N. M. S., Molahid, V. L. M., Yusuff, F. M., & Jusop, S. (2023). Carbon dioxide sequestration of iron ore mining waste under low-reaction condition of a direct mineral carbonation process. Environmental Science and Pollution Research, 30(9), 22188-22210.

Kwasny, J., Basheer, P., Russell, M. I., Doherty, W., Owens, K., & Ward, N. (2014). CO2 sequestration in cement-based materials during mixing process using carbonated water and gaseous CO2.

Li, B., Tian, Y., Zhang, G., Liu, Y., Feng, H., Jin, N., Jin, X., Wu, H., Shao, Y., & Yan, D. (2023). Comparison of detection methods for carbonation depth of concrete. Scientific Reports, 13(1), 19980.

Li, L., Poon, C. S., Xiao, J., & Xuan, D. (2017). Effect of carbonated recycled coarse aggregate on the dynamic compressive behavior of recycled aggregate concrete. Construction and Building Materials, 151, 52-62.

Li, L., & Wu, M. (2022). An overview of utilizing CO2 for accelerated carbonation treatment in the concrete industry. Journal of CO2 Utilization, 60, 102000.

Li, N., Mo, L., & Unluer, C. (2022). Emerging CO2 utilization technologies for construction materials: A review. Journal of CO2 Utilization, 65, 102237.

Li, W., Wang, H., Liu, Z., Li, N., Zhao, S., & Hu, S. (2024). Steel slag accelerated carbonation curing for high-carbonation precast concrete development. Materials, 17(12), 2968.

Li, X., & Cao, M. (2024). Recent developments on the effects of Micro-and Nano-Limestone on the hydration process, products, and kinetics of cement. Materials, 17(9), 2133.

Li, X., & Ling, T.-C. (2020). Instant CO2 curing for dry-mix pressed cement pastes: Consideration of CO2 concentrations coupled with further water curing. Journal of CO2 Utilization, 38, 348-354.

Li, Z., He, Z., & Chen, X. (2019). The performance of carbonation-cured concrete. Materials, 12(22), 3729.

Liang, C., Li, B., Guo, M.-Z., Hou, S., Wang, S., Gao, Y., & Wang, X. (2024). Effects of early-age carbonation curing on the properties of cement-based materials: a review. Journal of Building Engineering, 84, 108495.

Liang, C., Lu, N., Ma, H., Ma, Z., & Duan, Z. (2020). Carbonation behavior of recycled concrete with CO2-curing recycled aggregate under various environments. Journal of CO2 Utilization, 39, 101185.

Lim, T., Ellis, B. R., & Skerlos, S. J. (2019). Mitigating CO2 emissions of concrete manufacturing through CO2-enabled binder reduction. Environmental Research Letters, 14(11), 114014.

Lin, R.-S., & Wang, X.-Y. (2021). Effects of cement types and addition of quartz and limestone on the normal and carbonation curing of cement paste. Construction and Building Materials, 305, 124799.

Lippiatt, N., & Ling, T.-C. (2020). Rapid hydration mechanism of carbonic acid and cement. Journal of Building Engineering, 31, 101357.

Lippiatt, N., Ling, T.-C., & Eggermont, S. (2019). Combining hydration and carbonation of cement using super-saturated aqueous CO2 solution. Construction and Building Materials, 229, 116825.

Lippiatt, N., Ling, T.-C., & Pan, S.-Y. (2020). Towards carbon-neutral construction materials: Carbonation of cement-based materials and the future perspective. Journal of Building Engineering, 28, 101062.

Liu, L., Gan, M., Fan, X., Gao, Z., Sun, Z., Ji, Z., Wei, J., & Ma, S. (2024). Mechanism of ultrasonic enhanced acetic acid efficiently leaching of steel slag and synthesis

of calcium carbonate whiskers. Separation and Purification Technology, 339, 126615.

Liu, L., Liu, Y., Tian, X., & Chen, X. (2022). Superior CO2 uptake and enhanced compressive strength for carbonation curing of cement-based materials via flue gas. Construction and Building Materials, 346, 128364.

Liu, X., Wu, P., Liu, X., Zhang, Z., & Ai, X. (2024). The utilization of carbonated steel slag as a supplementary cementitious material in cement. Materials, 17(18), 4574.

Liu, Z., & Meng, W. (2021). Fundamental understanding of carbonation curing and durability of carbonation-cured cement-based composites: A review. Journal of CO2 Utilization, 44, 101428.

Liyew, G., Lee, N., Park, S., Lee, H. K., Park, J.-J., & Kim, H.-K. (2024). Understanding mechanism on carbonation curing for Portland cement through phase profiling via QXRD analysis and thermodynamic modeling. Journal of CO2 Utilization, 87, 102919.

Lu, B., He, P., Liu, J., Peng, Z., Song, B., & Hu, X. (2021). Microstructure of Portland cement paste subjected to different CO2 concentrations and further water curing. Journal of CO2 Utilization, 53, 101714.

Lu, Z., Tan, Q., Lin, J., & Wang, D. (2022). Properties investigation of recycled aggregates and concrete modified by accelerated carbonation through increased temperature. Construction and Building Materials, 341, 127813.

Luo, S., Ye, S., Xiao, J., Zheng, J., & Zhu, Y. (2018). Carbonated recycled coarse aggregate and uniaxial compressive stress-strain relation of recycled aggregate concrete. Construction and Building Materials, 188, 956-965.

Maia Neto, F., & Skibsted, J. (2025). Characterization of aqueous carbonated cement-based materials by multinuclear solid-state NMR spectroscopy. Journal of Sustainable Cement-Based Materials, 14(6), 1191-1206.

Mazzella, A., Errico, M., & Spiga, D. (2016). CO2 uptake capacity of coal fly ash: Influence of pressure and temperature on direct gas-solid carbonation. Journal of Environmental Chemical Engineering, 4(4), 4120-4128.

Mehta, P. K., & Monteiro, P. J. (2014). Concrete: microstructure, properties, and materials. McGraw-Hill Education.

Meng, D., Unluer, C., Yang, E.-H., & Qian, S. (2022). Carbon sequestration and utilization in cement-based materials and potential impacts on durability of structural concrete. Construction and Building Materials, 361, 129610.

Merah, A. (2024). Methods of concrete accelerated carbonation test: a review. Discover Civil Engineering, 1(1), 53.

Merino-Lechuga, A. M., González-Caro, Á., Fernández-Ledesma, E., Jiménez, J. R., Fernández-Rodríguez, J. M., & Suescum-Morales, D. (2023). Accelerated carbonation of vibro-compacted porous concrete for eco-friendly precast elements. Materials, 16(8), 2995.

Millero, F. J., Pierrot, D., Lee, K., Wanninkhof, R., Feely, R., Sabine, C. L., Key, R. M., & Takahashi, T. (2002). Dissociation constants for carbonic acid determined from field measurements. Deep Sea Research Part I: Oceanographic Research Papers, 49(10), 1705-1723.

Mo, L., Yang, S., Huang, B., Xu, L., Feng, S., & Deng, M. (2020). Preparation, microstructure and property of carbonated artificial steel slag aggregate used in concrete. Cement and Concrete Composites, 113, 103715.

Molahid, V. L. M., Kusin, F. M., Kamal, N. M. A., Hasan, S. N. M. S., Ramli, N. A. A., Abdullah, A. M., & Ashaari, Z. H. (2021). Carbon sequestration of limestone mine waste through mineral carbonation and utilization as supplementary cementitious material. International Journal of Integrated Engineering, 13(1), 311-320.

Molina, W. M., Guzman, E. A., Garcia, H. C., Gomez, C. L., Valdez, F. G., Lopez, T. P., Trujeque, J. R., Zapata, J. T., Quiroz, J. P., & Barrios, H. H. (2015). Analysis of Carbonation in Mortars made with Solid Waste as a Substitute for Cement. 2015 International Conference on Structural, Mechanical and Material Engineering,

Monkman, S., Hanmore, A., & Thomas, M. (2022). Sustainability and durability of concrete produced with CO2 beneficiated reclaimed water. Materials and Structures, 55(7), 170.

Monkman, S., & MacDonald, M. (2017). On carbon dioxide utilization as a means to improve the sustainability of ready-mixed concrete. Journal of Cleaner Production, 167, 365-375.

Namiki, K., Yamashita, K., Tabara, K., & Noda, S. (2025). Comparison and reliability assessment of CO2 quantification methods for carbonated cementitious materials. Journal of CO2 Utilization, 97, 103140.

Nath, S. K., & Dutta, R. K. (2010). Fluoride removal from water using crushed limestone.

National Academies of Sciences, Engineering, & Medicine, a. (2019). Gaseous carbon waste streams utilization: Status and research needs. National Academies Press.

Neville, A. M. (1995). Properties of concrete (Vol. 4). Longman London.

Oh, D., Kitagaki, R., Masuo, T., & Kuroda, Y. (2024). Development of CO2 absorption evaluating device for building materials. Energy Reports, 11, 4008-4014.

Ouyang, J., Zhang, Z., Zhao, H., & Liu, J. (2025). Prepare nano-CaCO3 by secondary carbonation of steel slag for carbon capture utilization and storage. Construction and Building Materials, 492, 142892.

Owais, M., Järvinen, M., Taskinen, P., & Said, A. (2019). Experimental study on the extraction of calcium, magnesium, vanadium and silicon from steelmaking slags for improved mineral carbonation of CO2. Journal of CO2 Utilization, 31, 1-7.

Pacheco-Torgal, F., Shi, C., & Palomo, A. (2018). Carbon dioxide sequestration in cementitious construction materials. Woodhead Publishing.

Padmalal, A., Kulkarni, K. S., Rawat, P., & Sugandhini, H. (2024). Efficacy of Accelerated Carbonation Curing and Its Influence on the Strength Development of Concrete. Buildings, 14(8), 2573.

Page, M. J., McKenzie, J. E., Bossuyt, P. M., Boutron, I., Hoffmann, T. C., Mulrow, C. D., Shamseer, L., Tetzlaff, J. M., Akl, E. A., & Brennan, S. E. (2021). The PRISMA 2020 statement: an updated guideline for reporting systematic reviews. bmj, 372.

Pan, X., Shi, C., Farzadnia, N., Hu, X., & Zheng, J. (2019). Properties and microstructure of CO2 surface treated cement mortars with subsequent lime-saturated water curing. Cement and Concrete Composites, 99, 89-99.

Pan, X., Shi, C., Hu, X., & Ou, Z. (2017). Effects of CO2 surface treatment on strength and permeability of one-day-aged cement mortar. Construction and Building Materials, 154, 1087-1095.

Phan, T. D., Noh, H. W., Lee, S. Y., & Kim, D. J. (2025). Effects of high-volume limestone powder substitution on hydration and mechanical–microstructural

development of low-carbon cement pastes: Simulation and experiment. Construction and Building Materials, 471, 140710.

Photong, C., & Pragot, W. (2022). Effect of adding monohydrocalcite on the microstructural change in cement hydration. ACS omega, 7(41), 36318-36329.

Phung, Q. T., Maes, N., & Seetharam, S. (2019). Pitfalls in the use and interpretation of TGA and MIP techniques for Ca-leached cementitious materials. Materials & Design, 182, 108041.

Pu, Y., Li, L., Shi, X., Wang, Q., & Abomohra, A. (2023). Recent advances in accelerated carbonation for improving cement-based materials and CO2 mitigation from a life cycle perspective. Construction and Building Materials, 388, 131695.

Qian, X. (2017). In-situ production of calcium carbonate nanoparticles in fresh concrete using pre-carbonation method. The University of Alabama.

Qin, L., Gao, X., & Chen, T. (2019). Influence of mineral admixtures on carbonation curing of cement paste. Construction and Building Materials, 212, 653-662.

Qin, L., Gao, X., & Li, Q. (2018). Upcycling carbon dioxide to improve mechanical strength of Portland cement. Journal of Cleaner Production, 196, 726-738.

Qiu, J., Lyu, J. W., Yang, J. L., Cui, K. B., Liu, H. Z., Wang, G. F., & Liu, X. (2024). Review on Preparation, Modification and Application of Nano-Calcium Carbonate. Particle & Particle Systems Characterization, 41(11), 2400097.

Quaghebeur, M., Nielsen, P., Horckmans, L., & Van Mechelen, D. (2015). Accelerated carbonation of steel slag compacts: development of high-strength construction materials. Frontiers in Energy Research, 3, 52.

Ravikumar, D., Zhang, D., Keoleian, G., Miller, S., Sick, V., & Li, V. (2021). Carbon dioxide utilization in concrete curing or mixing might not produce a net climate benefit. Nature communications, 12(1), 855.

Ren, P., Ling, T.-C., & Mo, K. H. (2021). Recent advances in artificial aggregate production. Journal of Cleaner Production, 291, 125215.

Romanov, V., Soong, Y., Carney, C., Rush, G. E., Nielsen, B., & O'Connor, W. (2015). Mineralization of carbon dioxide: a literature review. ChemBioEng Reviews, 2(4), 231-256.

Rostami, V., Shao, Y., Boyd, A. J., & He, Z. (2012). Microstructure of cement paste subject to early carbonation curing. Cement and Concrete Research, 42(1), 186-193.

Ruiying, W., Tao, Q., Hongfeng, J., Gang, D., Canhua, L., Shujing, Z., Jiamao, L., & Chen, Z. (2025). Study on preparation technology and properties of calcium based CO2 absorbent from acid leaching steel slag. Green Energy and Resources, 100140.

Russo, N., & Lollini, F. (2022). Effect of carbonated recycled coarse aggregates on the mechanical and durability properties of concrete. Journal of Building Engineering, 51, 104290.

Ryu, H.-k., Heo, S.-s., & Kim, S.-c. (2017). Effect of carbonated water manufactured by a soda carbonator on etched or sealed enamel. The Korean Journal of Orthodontics, 48(1), 48-56.

Salehi, S., Khattak, M., Ali, N., & Rizvi, H. (2016). Development of geopolymer-based cement slurries with enhanced thickening time, compressive and shear bond strength and durability. IADC/SPE Drilling Conference and Exhibition,

Sander, R. (2023). Compilation of Henry's law constants (version 5.0. 0) for water as solvent. Atmospheric Chemistry & Physics, 23(19).

Sanna, A., Uibu, M., Caramanna, G., Kuusik, R., & Maroto-Valer, M. (2014). A review of mineral carbonation technologies to sequester CO 2. Chemical Society Reviews, 43(23), 8049-8080.

Šavija, B., & Luković, M. (2016). Carbonation of cement paste: Understanding, challenges, and opportunities. Construction and Building Materials, 117, 285-301.

Scrivener, K. L., John, V. M., & Gartner, E. M. E., UN. (2018). Eco-efficient cements: Potential economically viable solutions for a low-CO2 cement-based materials industry. Cement and Concrete Research, 114, 2-26.

Shao, Z., Cao, M., & Zheng, X. (2024). Limestone particle sizes and sulfate impact on the early hydration of limestone calcined clay cement. Journal of Building Engineering, 97, 110848.

Shuvo, A. K., Sarker, P. K., Shaikh, F. U. A., & Rajayogan, V. (2024). Improvement of crushed returned concrete aggregates by wet carbonation. Construction and Building Materials, 448, 138253.

Shuvo, A. K., Sarker, P. K., Shaikh, F. U. A., & Rajayogan, V. (2025). Enhancement of Attached Mortar in Recycled Aggregates of Returned Concrete by Wet Carbonation. Journal of Materials in Civil Engineering, 37(11), 04025414.

Silva, A., Nogueira, R., Bogas, A., Abrantes, J., Wawrzyńczak, D., Ściubidło, A., & Majchrzak-Kucęba, I. (2022). Valorisation of recycled cement paste: feasibility of a short-duration carbonation process. Materials, 15(17), 6001.

Soares, E. G., & Castro-Gomes, J. (2022). The role of biomass bottom ash in Carbonated Reactive Magnesia Cement (CRMC) for CO2 mineralisation. Journal of Cleaner Production, 135092.

Song, B., Shi, C., Hu, X., Ouyang, K., Ding, Y., & Ke, G. (2021). Effect of early CO2 curing on the chloride transport and binding behaviors of fly ash-blended Portland cement. Construction and Building Materials, 288, 123113.

Standardization, E. C. f. (2011). Cement: composition, specifications and conformity criteria for common cements. British Standards Institute.

Suescum-Morales, D., Fernández-Rodríguez, J. M., & Jiménez, J. R. (2022). Use of carbonated water to improve the mechanical properties and reduce the carbon footprint of cement-based materials with recycled aggregates. Journal of CO2 Utilization, 57, 101886.

Sun, X., Xu, H., Manickam, S., Gupta, R. K., Cravotto, G., Yoon, J. Y., Wang, B., Wang, W., & Sun, D. (2025). Innovative mineral carbonation techniques: A comprehensive review of ultrasound-assisted processing, mechanistic insights, optimization strategies, and environmental impacts. Carbon Capture Science & Technology, 100469.

Takahashi, H., & Maruyama, I. (2024). Quantification of CO2 in cement pastes with different degrees of carbonation. Journal of Advanced Concrete Technology, 22(11), 706-715.

Tang, B., Fan, M., Yang, Z., Sun, Y., & Yuan, L. (2023). A comparison study of aggregate carbonation and concrete carbonation for the enhancement of recycled aggregate pervious concrete. Construction and Building Materials, 371, 130797.

Tennis, P., Thomas, M., & Weiss, W. (2011). State-of-the-Art Report on Use of Limestone in Cements at Levels of up to 15%. PCA R&D SN3148, Portland Cement Association, Skokie, IL.

Torrenti, J. M., Amiri, O., Barnes-Davin, L., Bougrain, F., Braymand, S., Cazacliu, B., Colin, J., Cudeville, A., Dangla, P., & Djerbi, A. (2022). The FastCarb project: Taking advantage of the accelerated carbonation of recycled concrete aggregates. Case Studies in Construction Materials, 17, e01349.

Tranfield, D., Denyer, D., & Smart, P. (2003). Towards a methodology for developing evidence-informed management knowledge by means of systematic review. British journal of management, 14(3), 207-222.

Vollpracht, A., Gluth, G. J., Rogiers, B., Uwanuakwa, I. D., Phung, Q. T., Villagran Zaccardi, Y., Thiel, C., Vanoutrive, H., Etcheverry, J. M., & Gruyaert, E. (2024). Report of RILEM TC 281-CCC: insights into factors affecting the carbonation rate of concrete with SCMs revealed from data mining and machine learning approaches. Materials and Structures, 57(9), 206.

Wang, C., Chazallon, C., Braymand, S., & Hornych, P. (2024). Thermogravimetric analysis (TGA) for characterization of self-cementation of recycled concrete aggregates in pavement. Thermochimica Acta, 733, 179680.

Wang, F., Dreisinger, D., Jarvis, M., & Hitchins, T. (2021). Kinetic evaluation of mineral carbonation of natural silicate samples. Chemical Engineering Journal, 404, 126522.

Wang, S., Wang, M., Liu, F., Song, Q., Deng, Y., Ye, W., Ni, J., Si, X., & Wang, C. (2024). A review on the carbonation of steel slag: properties, mechanism, and application. Materials, 17(9), 2066.

Wang, T., Yi, Z., Song, J., Zhao, C., Guo, R., & Gao, X. (2022). An industrial demonstration study on CO2 mineralization curing for concrete. IScience, 25(5).

Wang, W.-C., Lee, M.-G., Deng, J.-L., Wang, Y.-C., Chuo, S.-F., Pei-Chi, H., & Jen-Wei, S. (2024). Study on carbon sequestration and CO2 mixing of fresh cement mortar. Case Studies in Construction Materials, 21, e03813.

Wang, X., Ni, W., Li, J., Zhang, S., & Li, K. (2021). Study on mineral compositions of direct carbonated steel slag by QXRD, TG, FTIR, and XPS. Energies, 14(15), 4489.

Wang, Z., Zhou, H., Lian, S., Meng, T., Yu, H., Zhou, X., Wang, S., & Ruan, S. (2025). Hydration behaviors, workability, and strength variations in direct aqueous carbonation (DAC) of Portland cement paste. Scientific Reports, 15(1), 5517.

Winnefeld, F., Leemann, A., German, A., & Lothenbach, B. (2022a). CO2 storage in cement and concrete by mineral carbonation. Current Opinion in Green and Sustainable Chemistry, 100672.

Winnefeld, F., Leemann, A., German, A., & Lothenbach, B. (2022b). CO2 storage in cement and concrete by mineral carbonation. Current Opinion in Green and Sustainable Chemistry, 38, 100672.

Wu, Y., Mehdizadeh, H., Mo, K. H., & Ling, T.-C. (2022). High-temperature CO2 for accelerating the carbonation of recycled concrete fines. Journal of Building Engineering, 52, 104526.

Xia, J., Li, C., Ma, H., & Ren, Q. (2025). Mix Design-Driven Control of Carbonation and Hydration in CO2-Mixed Cement Pastes: Effects of Water, Slag, and Surfactant. Buildings, 15(12), 2116.

Xian, X., Logan, C., & Shao, Y. (2022). Dimensional stability of cement paste and concrete subject to early-age carbonation curing. Materials and Structures, 55(3), 94.

Xian, X., & Shao, Y. (2021). Carbonation curing of concretes in a flexible enclosure under ambient pressure. Journal of Materials in Civil Engineering, 33(4), 04021025.

Xian, X., Zhang, D., Lin, H., & Shao, Y. (2022). Ambient pressure carbonation curing of reinforced concrete for CO2 utilization and corrosion resistance. Journal of CO2 Utilization, 56, 101861.

Xiao, J., Zhang, H., Tang, Y., Deng, Q., Wang, D., & Poon, C.-s. (2022). Fully utilizing carbonated recycled aggregates in concrete: Strength, drying shrinkage and carbon emissions analysis. Journal of Cleaner Production, 377, 134520.

Xu, J., Lu, D., & Xu, Z. (2024). Reaction Behaviour of Dolomite Powder in Portland Cement Pastes Cured at Different Conditions. In.

Xuan, D., Zhan, B., & Poon, C. S. (2016). Assessment of mechanical properties of concrete incorporating carbonated recycled concrete aggregates. Cement and Concrete Composites, 65, 67-74.

Yang, H., He, z., & Shao, Y. (2015). Early carbonation behavior of high-volume dolomite powder-cement based materials. Journal of Wuhan University of Technology-Mater. Sci. Ed., 30(3), 541-549.

Yang, M., Zhang, S., Wang, Y., Li, Z., Wen, J., Quan, X., & Lu, C. (2024). A cleaner-sustainable process for recovering valuable elements from steel slag with acetic acid: leaching studies and multi-value-added products. Journal of Environmental Chemical Engineering, 12(3), 112825.

Yao, Y., Wang, L., Li, J., De Belie, N., Shi, X., Van Den Heede, P., Zhang, C., Liu, Z., Talakokula, V., & Jin, Z. (2023). Recommendation of RILEM TC 281-CCC: Test method to determine the effect of uniaxial compression load and uniaxial tension load on concrete carbonation depth. Materials and Structures, 56(7), 121.

Yu, J. (2025). Achieving Net Zero in the Cement Industry Duke University].

Zajac, M., Skibsted, J., Bullerjahn, F., & Skocek, J. (2022). Semi-dry carbonation of recycled concrete paste. Journal of CO2 Utilization, 63, 102111.

Zhang, D., Cai, X., & Jaworska, B. (2020). Effect of pre-carbonation hydration on long-term hydration of carbonation-cured cement-based materials. Construction and Building Materials, 231, 117122.

Zhang, D., Ghouleh, Z., & Shao, Y. (2017). Review on carbonation curing of cement-based materials. Journal of CO2 Utilization, 21, 119-131.

Zhang, D., Li, V. C., & Ellis, B. R. (2018). Optimal pre-hydration age for CO2 sequestration through portland cement carbonation. ACS Sustainable Chemistry & Engineering, 6(12), 15976-15981.

Zhang, D., & Shao, Y. (2016). Early age carbonation curing for precast reinforced concretes. Construction and Building Materials, 113, 134-143.

Zhang, J., Chen, H., Jia, Y., Zhuoma, P., & Lv, M. (2024). The Effects of Dolomite Powder Content and Type on the Yield Stress Relationship between Self-Compacting Mortar and Paste. Buildings, 14(8), 2557.

Zhang, N. (2020). Rapid aqueous mineralisation of carbon dioxide in a scalable process with brines Newcastle University].

Zhang, X., Luo, Y., & Yao, W. (2022). Research on the carbonation resistance of concretes containing dolomite powder. Fullerenes, Nanotubes and Carbon Nanostructures, 30(12), 1221-1232.

Zhang, X., Zhao, J., Liu, Y., & Li, J. (2024). Use of steel slag as carbonation material: A review of carbonation methods and evaluation, environmental factors and carbon conversion process. Journal of CO2 Utilization, 88, 102947.

Zhang, Z., Angst, U., Troian, V., Guo, B., & Zeng, Q. (2025). Durability performance of concrete incorporating carbonated recycled coarse aggregates: a review. npj Materials Sustainability, 3(1), 27.

Zhao, Q., Liu, C., Mei, X., Saxén, H., & Zevenhoven, R. (2025). Research progress of steel slag-based carbon sequestration. Fundamental Research, 5(1), 282-287.

Zhong, W., Wang, P., Ye, N., Shu, K., Dai, R., Ba, M., & Fang, X. (2025). Effects of Different Carbonation Treatment Methods for Recycled Concrete Aggregate. Buildings, 15(17), 3054.

AUTHOR'S PROFILE



Zulhaziq Khan Bin Zuljar is a postgraduate student at the Faculty of Civil Engineering, Universiti Teknologi MARA (UiTM). He completed his Bachelor of Engineering in Civil Engineering before pursuing his Master of Science in the field of civil engineering materials and sustainable cementitious systems. His research focuses on the physico-mechanical properties and reaction behaviour of carbonic acid incorporated cementitious binders through aqueous carbon dioxide integration. The study involves the use of carbon dioxide-conditioned mixing water and calcium-based carbonate precursors, particularly calcium carbonate and dolomite, to evaluate their effects on setting behaviour, compressive strength, water absorption, chemical composition, thermal response and microstructural development of ordinary Portland cement paste. Throughout his postgraduate study, he gained experience in cementitious material preparation, laboratory testing, data analysis, microstructural characterisation and academic writing. His research interests include sustainable construction materials, low-carbon cement technology, carbonation-related reactions and practical material innovation for the construction industry.

LIST OF PUBLICATIONS

Zuljar, Z. K., Zailani, W. W. A., Apandi, N. M., Simarani, K., & Ibrahim, N. M. (2024). Review on the potential co-application of aqueous CO_2 solution in cementitious material. *Jurnal Kejuruteraan, 36*(4), 1657–1675.

UNIVERSITI TEKNOLOGI MARA

PERPUSTAKAAN TUN ABDUL RAZAK
BAHAGIAN SUMBER RUJUKAN UNIVERSITI (BSRU)

BORANG PENYERAHAN BAHAN HARTA INTELEK UiTM

UiTM's Intellectual Property Submission Form

Nama (*Name*) : ZULHAZIQ KHAN BIN ZULJAR

No. Telefon(Pejabat/Hp) : *Telephone No.(Office / handphone)* 0197886147

Fakulti/Pusat Akademik/Bahagian : *Faculty / Academic Centres / Department* KOLEJ PENGAJIAN KEJURUTERAAN

E-mel *(E-mail)* : 2023589797@student.uitm.edu.my

Tarikh *(Date)* : 11-08-2026

Pihak Fakulti / Pusat Akademik / Bahagian / Saya bersetuju bahawa dokumen dan tajuk yang disenaraikan untuk dimasukkan ke dalam Repositori Institusi UiTM.
The Faculty / Academic Centres / Department / I agree that the document and titles listed below to be placed in the UiTM Institutional Repository.

JENIS BAHAN (Sila nyatakan) : *Types of Material (Please specify)* Theses

Types of Material: Article / Book / Theses / Bulletin / Seminar / Image / Entrepreneurship / Student Project / Research Report / Industrial Training / Annual Report / Manual / Oral History / Exam Paper / Speech / Dataset / Audio / Video / Others

MAKLUMAT BAHAN ***(Information of Materials)*:**

Bil. *No*	JUDUL BAHAN *Title*	HARDCOPY (✓)	SOFTCOPY (✓)
1.	Physico-Mechanical Properties And Reaction Kinetics of H2CO3 Incorporated Cementitious Binders Via Aqueous		✔

* Sila sediakan lampiran sekiranya ruangan yang disediakan tidak mencukupi *(Please provide attachment if necessary)*

TUJUAN PENYERAHAN BAHAN (Sila tandakan √):

Purpose (Please mark √):

1. **Bahan untuk dimuat naik ke dalam Repositori Institusi UiTM**.
   (Materials for uploading into the UiTM Institutional Repository (UiTM IR)):
   Fakulti / Pusat Akademik / Bahagian / Saya perlu memastikan bahawa setiap dokumen telah dibuat semakan terlebih dahulu dan tidak mengandungi sebarang maklumat sulit sebelum diserahkan kepada pihak PTAR. ✔
   The Faculty / Academic Centres / Department must ensure that each document has been reviewed in advance and does not contain any confidential information before being submitted to PTAR.
2. **Bahan mengandungi maklumat TERHAD yang telah ditentukan oleh organisasi / badan di mana penyelidikan dijalankan:**.
   (Materials consisting of RESTRICTED information which has been determined by the organisation/body where the research was conducted):
   Sila nyatakan tarikh tamat embargo (jika ada):
   (Please indicate the embargo expiry date (if any)):
   Embargo expiry date: Day: Month: Year: ☐
   Nota: Embargo Expiry Date adalah tarikh tamat tempoh yang ditetapkan oleh penulis di mana pada atau selepas tarikh ini, bahan tersebut akan dipaparkan secara langsung di Repositori Institusi UiTM dan ianya boleh diakses.
   Note: Embargo Expiry Date is the date that an author or a publisher imposed embargo expires. On and after this date, this document will be accessible in UiTM Institutional Repository.
3. **Bahan boleh diakses secara teks penuh dan terbuka.** ✔
   (Materials can be accessed in full text via open access).
4. **Bahan dipinjamkan sementara untuk tujuan pendigitalan dan akan dikembalikan semula kepada pemilik.** ☐
   (Materials are on temporary loan for digitization and will be returned to the owner).

Pemberitahuan: Jika Repositori Institusi UiTM menerima bukti pelanggaran hak cipta, bahan yang berkaitan akan dikeluarkan serta-merta.
(Notification: If UiTM Institutional Repository receives proof of copyright violation, the relevant item will be removed immediately).

PERAKUAN :
Declaration:
Saya / kami akan bertanggungjawab ke atas bahan yang diserahkan untuk pendigitalan dan muat naik ke dalam Repositori Institusi UiTM.
I/ we will be responsible for the materials submitted for digitization and uploaded into UiTM Institutional Repository.

Tandatangan Pemohon
Applicant Signature
Tarikh (*Date*): 11 OGOS 2026

DR WARID WAZIEN AHMAD ZAILANI
Pensyarah Kanan
Pengajian Kejuruteraan Awam
Kolej Pengajian Kejuruteraan
Universiti Teknologi MARA
40450 Shah Alam, Selangor

Tandatangan dan Cop Ketua Jabatan / Bahagian / Penyelia
Head of Division / Department / Supervisor Signature and stamp
Tarikh (*Date*): 13 OGOS 2026

UNTUK KEGUNAAN PEJABAT (*For office use*)

DITERIMA OLEH / *Received By* :
TANDATANGAN / *Signature* :
TARIKH (*Date*):

DISAHKAN OLEH / *Certified By* :
TANDATANGAN / *Signature* :
TARIKH (*Date*):